SKB

TECHNICAL REPORT 94-12

Research on corrosion aspects of the Advanced Cold Process Canister

D J Blackwood, A R Hoch, C C Naish, A Rance,
S M Sharland

AEA Technology, Harwell Laboratory, Didcot,
Oxfordshire, UK

January 1994

SVENSK KÄRNBRÄNSLEHANTERING AB
SWEDISH NUCLEAR FUEL AND WASTE MANAGEMENT CO

BOX 5864 S-102 40 STOCKHOLM

TEL. 08-665 28 00 TELEX 13108 SKB S
TELEFAX 08-661 57 19

RESEARCH ON CORROSION ASPECTS OF THE ADVANCED COLD PROCESS CANISTER

D J Blackwood, A R Hoch, C C Naish, A Rance, S M Sharland

AEA Technology, Harwell Laboratory, Didcot, Oxfordshire, UK

January 1994

RESEARCH ON CORROSION ASPECTS OF THE ADVANCED COLD PROCESS CANISTER

D J Blackwood, A R Hoch, C C Naish, A Rance and S M Sharland

AEA Technology, Harwell Laboratory, Didcot, Oxfordshire, UK

January 1994

Keywords: corrosion, hydrogen, modelling

AEA-D&W-0684

Research on Corrosion Aspects of the Advanced Cold Process Canister

D J Blackwood, A R Hoch, C C Naish, A Rance and S M Sharland

Abstract

The Advanced Cold Process Canister (ACPC) is a waste canister being developed jointly by SKB and TVO for the disposal of spent nuclear fuel. It comprises an outer copper canister, with a carbon steel canister inside. A concern regarding the use of the ACPC is that, in the unlikely event that the outer copper canister is penetrated, the anaerobic corrosion of the carbon steel container may result in the formation of hydrogen gas bubbles. These bubbles could disrupt the backfill, and thus increase water flow through the near field and the flux of radionuclides to the host geology.

A number of factors that influence the rate at which hydrogen evolves as a result of the anaerobic corrosion of carbon steel in artificial granitic groundwaters have been investigated. A previously observed, time-dependent decline in the hydrogen evolution rate has been confirmed as being due to the production of a magnetite film. Once the magnetite film is about 0.7-1.0 μm thick, the rate of hydrogen evolution reaches a steady state value. The pH and the ionic strength of the groundwater were both found to influence the long-term hydrogen evolution rate. The results of the experimental programme were used to update a model of the corrosion behaviour and hydrogen production from the Advanced Cold Process Canister.

AEA Technology
Harwell Laboratory
Didcot
Oxfordshire

January 1994

Abstract (Swedish)

The Advanced Cold Process Canister (ACPC) är en avfallskapsel för slutförvaring av använt bränsle som utvecklas gemensamt av SKB och TVO. Den består av en yttre kopparkapsel med en stålkapsel inuti. Av intresse vid användandet av ACPC är att, för det osannolika fallet av genombrott på den yttre kopparkapseln, den anaeroba korrosionen av kolstålkapseln kan tänkas resultera i bildandet av vätgasbubblor. Dessa bubblor skulle kunna riva upp bufferten och därigenom öka vattenflödet genom närområdet och utsläppet av radionuklider till den omgivande berget.

Ett antal faktorer som påverkar hastigheten vätgasen bildas med genom anaerob korrosion av kolstål i artificiellt granitiskt grundvatten har studerats. En tidigare observerad, tidsberoende nedgång i hastigheten för vätgasbildning har fastställts bero på bildandet av ett magnetitskikt. När magnetitskiktet är ungefär 0,7-1,0 μm tjockt, når hastigheten för vätgasbildning ett stabilt värde. pH och grundvattnets jonstyrka befanns båda påverka hastigheten för vätgasbildning i det långa perspektivet. Resultaten från den experimentella programmet användes för att uppdatera en modell för korrosionsbeteendet och vätgasproduktionen från ACPC.

EXECUTIVE SUMMARY

The Advanced Cold Process Canister (ACPC) is a waste container being developed jointly by SKB and TVO for the disposal of spent nuclear fuel. It comprises an outer copper canister, with a carbon steel container inside. A concern regarding the use of the ACPC as part of a deep geological disposal concept is that, in the unlikely event that the outer copper canister is penetrated, the anaerobic corrosion of the carbon steel container may result in the formation of hydrogen gas bubbles. These bubbles could disrupt the backfill, and thus increase water flow through the near field and the flux of radionuclides to the host geology.

This report presents the results of a series of investigations into aspects of the corrosion behaviour of the ACPC, which AEA Technology have carried out for SKB and TVO. The rate at which hydrogen evolves due to the corrosion of carbon steel was determined experimentally. This data was used to update calculations of the rate of hydrogen production from the ACPC, following a breach in the ACPC outer canister.

The experimental measurements investigated the rate at which hydrogen evolves from the corrosion of carbon steel wires in the anaerobic granitic groundwaters likely to be found in the waste repository. Particular emphasis was placed on the following aspects:

i) High humidity conditions are likely to be encountered by the carbon steel immediately after penetration of the outer copper canister, but before the internal annulus has flooded. Experiments showed that the long-term hydrogen evolution rate from carbon steel in a high humidity anaerobic atmosphere was less than 0.5 dm^3 (STP) m^{-2} $year^{-1}$. However, the time to reach such low rates was observed to be considerably longer if the carbon steel was partially-submerged in the groundwater, which may be a more realistic model of the conditions in a penetrated ACPC.

ii) The nature and effectiveness of the protective layers that form on carbon steel in artificial granitic groundwaters and restrict the rate of hydrogen evolution was investigated. Magnetite was shown to be more protective than iron(II) carbonate, with a thickness of 0.5 - 1.0 μm being sufficient to reduce the long-term rate of hydrogen production to around 0.5 dm^3 (STP) m^{-2} $year^{-1}$.

iii) The effect of soluble iron(II) species on the rate of formation of the protective magnetite layers was investigated. No link was established.

iv) The effect of radiolysis product on the hydrogen evolution rate was investigated. The concentrations of ammonia and nitrate likely to be generated within the ACPC were found to have no significant effect on rate of hydrogen production.

v) The effect of the ionic strength of the groundwater was investigated. Increasing the ionic strength of the groundwater 10-fold was found to increase the observed hydrogen evolution rate after 5000 hours by almost an order of magnitude.

Calculations of the hydrogen production rate from the ACPC following a breach in the outer canister were updated using the experimental results. The main difference to previous calculations was that a much lower corrosion rate was assumed, which reduced the rate of production of hydrogen gas and the maximum pressure achieved in the canister. Corrosion is assumed to stop when the pore space inside the canister is filled with corrosion product. As a result of the lower corrosion rate, corrosion was calculated to continue over a much longer timescale.

TABLE OF CONTENTS

1 INTRODUCTION

One of the primary requirements for the safe encapsulation of spent nuclear fuel for geological disposal is a container that is resistant to corrosion in the environment likely to be encountered in the repository. The Advanced Cold Process Canister (ACPC) is a new concept for the encapsulation of spent nuclear fuel for geological disposal, which is presently being evaluated by TVO of Finland and SKB of Sweden. Two options are under consideration for the design of the ACPC; the first involves a 60 mm copper wall thickness over a 55 mm thickness of carbon steel, and the second a 50 mm thickness of both copper and steel. The internal volumes of both packages is similar at around 1150 dm^3 and both have a 2 mm annular gap between the copper and steel canisters.

Once the repository has been sealed, it will eventually become flooded with groundwater. Since deep groundwaters tend to have low concentrations of oxygen, the available oxygen supply will be limited to that trapped in the repository upon sealing. In time, the corrosion of the outer copper canister will consume all the oxygen[1]. Under the resulting anaerobic conditions, the copper canister should, on thermodynamic grounds, be immune to further corrosion[2]. Thus, it represents the primary barrier between the waste and the external groundwater environment in the repository. The role of the internal carbon steel container is to provide mechanical strength to the overall package, as well as acting as a secondary barrier. The intention is to use the ACPC packed with either BWR or PWR fuel, in a type KBS 3 repository.

One of the concerns regarding the use of the ACPC in deep geological disposal sites is that, in the unlikely event that the outer copper canister is penetrated, the anaerobic corrosion of the carbon steel container may result in the formation of hydrogen gas. Bubbles of such gas could disrupt the backfill, and thus increase water flow through the near field and the flux of radionuclides to the host geometry. The likelihood of hydrogen bubble formation depends on the rate of hydrogen production and the rate of its transport away from the container's surface. Therefore factors which influence the rate of anaerobic corrosion of the carbon steel container will affect both the performance of the individual canisters, and the overall performance of the repository.

AEA Technology has previously provided SKB and TVO with experimental data and predictions from computer models relating to the expected corrosion behaviour of the ACPC. This work focused on the unlikely scenario that the outer copper case was breached after a relatively short period of time[3,4]. It considered the generation of hydrogen from corrosion of the carbon steel container. This report describes more recent work. Four areas where further corrosion experiments would improve the accuracy of the predictive models were considered. These were:

Task 1 Corrosion Rate Under Conditions of High Humidity

After an initial penetration of the outer copper canister, but before the complete flooding of the inner carbon steel fuel container, there may be a period in which the carbon steel will be corroding in a high humidity anaerobic atmosphere. In the modelling of Marsh[3] and Henshaw et al[4] on gas generation inside the ACPC, it was assumed that the rate of anaerobic corrosion in high humidity conditions is the same as that under saturated ones. The aim of this task was to determine the likely corrosion rate of carbon steel under high humidity conditions.

Task 2 Magnetite Retardation of Corrosion Reaction

The modelling work of Henshaw et al[4] considered the effect of the assumption that the corrosion rate decreases with corrosion product film thickness and that mass transport through the solid corrosion product reduces the rate of corrosion to negligible levels. The model indicated that this process could have a significant effect on the corrosion behaviour of the canister and the overall rate of hydrogen production. However, no directly relevant data were available. The aims of this task were (i) to provide relevant data for the model and (ii) to compare the effectiveness of different types of possible corrosion products in curtailing the rate of hydrogen production.

Task 3 Ferrous Ion Retardation of Corrosion Rate

During active corrosion, soluble species are usually produced in competition with solid corrosion product formation. In the case of iron in solutions of pH less than 9.0, Fe^{2+} is the major soluble ion produced. Initially, the rate-determining step is believed to be the second electron transfer process[5]. However, as the electrolyte becomes saturated in Fe^{2+}, the rate-determining step switches to the dissolution/desorption of the Fe^{2+} ions from the corroding surface[5]. This has the effect of reducing the dissolution rate of the film. Inside the restricted volume of the annulus and the internal void of the inner carbon steel container, it is likely that ferrous ion saturation will occur at some stage during the storage period. The aim of this task was to determine whether the concentration of soluble iron species in the groundwater has a significant effect on either the rate of formation of the film or the degree of corrosion protection afforded by this layer.

Task 4 Effect of Ionic Strength, NH_3 and NO_3^- on Corrosion Rate

Under anaerobic conditions, the cathodic process associated with corrosion is the evolution of hydrogen. This involves the loss of water from the system. If the resultant corrosion product is soluble in the local environment, an increase in the hydroxide concentration will occur:

$$Fe + 2H_2O \rightarrow Fe^{2+} + 2OH^- + H_2\uparrow \qquad [1]$$

If mass transport from the bulk is impeded, for example, if the original crack in the copper canister of the ACPC is blocked by precipitated corrosion product, both the pH and the ionic strength of the solution trapped in the annulus/container would increase. Any increase in the pH of the groundwater from hydrogen evolution is not expected to increase the corrosion rate, since the pH can not rise above 10.6, at which point the hydroxide consuming $HFeO_2^-$ complex becomes the thermodynamically most favourable Fe(II) species[6]. The effect of increasing the ionic strengths of the groundwater on the hydrogen production/rate of corrosion is not clear. Both NH_3 and NO_3^-, which are expected to be produced by radiolysis reactions, could influence the corrosion rate[7]. The latter can also provide the additional cathodic process of NO_3^- to NO_2^-. The aim of this task was to determine whether changes in ionic strength and the stable chemical products formed following radiolysis reduction would have a significant influence on the corrosion behaviour of carbon steel in simulated granitic groundwaters.

Task 5 Update of Previous Modelling Study

The results from these tasks have been brought together to update the previous modelling studies of hydrogen production and corrosion behaviour.

2 EXPERIMENTAL

The anaerobic corrosion rates of carbon steel in a range of granitic groundwaters were measured using a hydrogen gas evolution displacement test. In these experiments, the amount of hydrogen gas generated from the anaerobic corrosion of the carbon steel is determined by the pressure it exerts within a closed system. The pressure build-up is calculated from the height that a low vapour pressure liquid is displaced up a precision bore glass tube. Using the barometric cell design shown in Figure 1, with a 1.6 mm diameter precision bore tubing and di-n-butyl phthalate as the low vapour pressure liquid to be displaced, hydrogen gas evolution rates from a total carbon steel surface area of $0.1 m^2$ could be determined to within ± 0.5 dm^3 (STP) m^{-2} $year^{-1}$. Complete experimental details of the gas evolution liquid displacement technique have been described elsewhere[8,9].

In order to obtain estimates of the maximum likely hydrogen evolution rates from the carbon steel wire samples, any air-formed oxide film was removed prior to their placement into the barometric cells. The procedure for this was to degrease the wires with alcohol, then to pickle them in 10% HCl for 5 minutes, followed by three washings in clean, doubly distilled water before a final rinse with absolute ethanol[8].

The composition of the standard artificial groundwater used in all the experiments was provided by SKB[10] and is shown in Table 1. All experiments were carried out at a

temperature of 50°C. All chemicals used were of AnalaR grade or equivalent and solutions were made up using deoxygenated doubly distilled water.

3 EXPERIMENTAL RESULTS AND DISCUSSION

3.1 INTRODUCTION

In an earlier study for SKB[8], the hydrogen evolution and corrosion rates for carbon steel wires in the standard SKB artificial groundwater were determined (Tables 2 & 3). These data were used as a control against which all the results generated for this report were evaluated.

As mentioned above, in all the experiments in the current study, the hydrogen evolution rate was observed to fall with time, reaching an equilibrium rate within 5000 hours. This trend is characteristic of the corrosion behaviour of carbon steel in anaerobic groundwaters and is associated with the formation of a protective layer[8,9]. At the same time that this protective layer formed, a precipitate of magnetite also appeared at the base of all the experimental cells. Figure 2 shows the profile of hydrogen evolution rate versus time, obtained in reference [8], while Figures 3 to 9 show the corresponding profiles for all the tests carried out for this report.

3.2 TASK 1. CORROSION RATE UNDER CONDITIONS OF HIGH HUMIDITY

Three hydrogen evolution cells were prepared for this task, these contained:

i) carbon steel wires positioned completely clear of a reservoir of artificial groundwater;

ii) carbon steel wires dipped into the groundwater so that approximately 20% of their surface area was in direct contact with the solution;

iii) no carbon steel (control cell).

3.2.1 Carbon Steel with no Contact with the Groundwater

After 5000 hours both the production rate and the total amount of hydrogen produced in the first cell, (in which the carbon steel was completely clear of the groundwater), were similar to that recorded from a cell containing completely immersed samples[8] (Tables 2 & 4). Differences were observed in the initial hydrogen production rates and in the time required to form the protective magnetite layers, (as indicated by the rate of decline in the hydrogen production rate): After 100 hours, the rate of hydrogen production recorded from the humidity cell was 70 dm^3 (STP) m^{-2} $year^{-1}$ compared to 51 dm^3 (STP) m^{-2} $year^{-1}$ from the immersed carbon steel wires (Table 2). Between 100 and 500 hours; the rate of hydrogen

production in the high humidity cell fell by almost 95%, whereas it only dropped by 66% under totally immersed conditions (Figures 2 and 3).

These differences are probably due to the fact that any vapour which condensed out on the carbon steel would have had a lower pH than the bulk groundwater, as most of the salts will not exist in the vapour phase. A lower pH is expected to produce a higher corrosion rate. However, there may be a more rapid build-up of the magnetite which forms the protective film. In the humid conditions, it is not possible for any of the corrosion product to diffuse into a bulk solution, as soluble Fe^{2+} ions, leading to more rapid film formation. The degree of protection offered by the magnetite film may also vary with pH.

3.2.2 Carbon Steel Partially-Submerged in Groundwater

The hydrogen production rate from the cell containing the partially-submerged carbon steel wires was initially less than that from both the cell in which the samples were completely clear of the groundwater and the cell which contained totally submerged wires (Table 2). The partially-submerged cell also exhibited a much slower rate of decline in its hydrogen production rate. Rates in excess of 10 dm^3 (STP) m^{-2} $year^{-1}$ were recorded after 1000 hours, despite the fact that by this time a black magnetite film was clearly visible over most of the surface.

As mentioned above, vapour which has condensed out onto the surface of the carbon steel will have a lower pH than that found in the bulk solution, therefore a pH gradient will be produced along the surface of the partially immersed specimens. This could result in a form of galvanic coupling, with increased hydrogen production in the low pH vapour regions and increased magnetite formation in the high pH submerged regions. Therefore the magnetite might be expected to spread slowly up the wires, from the submerged ends, giving rise to the observed gradual decrease in the hydrogen production rate.

The total amount of hydrogen produced after 5000 hours was only about 10% larger than from the standard artificial groundwater control cell[8]. This suggests that the final thicknesses of the protective magnetite layer are probably similar.

3.2.3 Control Cell

The control cell revealed background internal pressure changes of less than 0.25 dm^3 (STP) m^{-2} $year^{-1}$, which is within the experimental error.

3.3 TASK 2. CORROSION RATE RETARDATION BY FILM GROWTH

In order to confirm that the formation of solid corrosion products is responsible for the observed decline in the corrosion rate and to provide data to support the gas generation model[4], hydrogen evolution tests were carried out using carbon steel wires with pre-formed films of either iron(II) carbonate or magnetite on their surfaces. The magnetite films were grown by placing the carbon steel wires in a boiling mixture of 25% w/w NaOH and 25% w/w $NaNO_3$ using the method described by Nomura and Ujihira[11]. The carbonate films were formed by placing the carbon steel in a solution of the artificial groundwater which was continuously purged with carbon dioxide for one or thirty days and maintained at 50°C. Two thicknesses of both types of films were used, these were approximately 50 nm and 500 nm[11].

It should be noted that the properties of the chemically formed films used in this task may be different from those of the true corrosion products. However, attempts to grow corrosion films at accelerated rates by electrochemical methods proved to be unsatisfactory due to the formation of FeO(OH). The presence of Fe(III) oxides in a corrosion product would allow the Fe(III) → Fe(II) reduction reaction to act as an alternative cathodic process to hydrogen evolution.

The results from the current study show that both types of film are able to reduce the initial burst in the hydrogen production rate that is observed on bare metal surfaces, with the order of increasing effectiveness being: thin carbonate < thin magnetite < thick carbonate < thick magnetite (Table 2). These findings support the conclusion that it is the formation of the magnetite/carbonate film which causes the decrease in the corrosion rate, which is observed during the first 1500 hours with unfilmed carbon steel samples, as discussed in the previous sections. The final equilibrium corrosion rates for all of the pre-coated specimens were similar to the unfilmed samples (Table 3), although the thin carbonate film did result in a slightly higher value. This suggests that magnetite is the more protective of the two types of corrosion products.

The thick magnetite film specimens showed very little corrosion, with an apparent negative rate of hydrogen production during the first 100 hours. For the next 1000 hours, the hydrogen production rate was observed to slowly increase before it again declined. However, at all times the rates were below those measured on unfilmed specimens at comparable times (Table 2). This result can be explained if the corrosion rate of carbon steel samples covered with a thick magnetite film is so slow, that corrosion is initially supported by the residual oxygen left in all the cells during assembly. The atmosphere inside the glove box in which the cells were constructed had an oxygen content of approximately 2 ppm.

The rate of hydrogen production from the carbon steel wires pre-filmed with the thick, 500 nm, magnetite layer was at no time greater than 1.0 dm^3 (STP) m^{-2} $year^{-1}$. When this is compared to final production rates from all the samples, approximately 0.5 dm^3 (STP) m^{-2} $year^{-1}$ (Table 2), it can be estimated that the final thickness of the protective films is probably of the order of 700 - 1000 nm.

As the protective films thickened the rate of hydrogen production continued to decline steadily. This suggests that these protective films did not become stressed and crack as they thickened, since such behaviour would have resulted in bursts of hydrogen production.

Marsh[3] stated that hydrogen production is likely to continue until the entire carbon steel container is filled with corrosion product. It is highly probable that the majority of this material will have become detached from the walls of the container and it will be made up of a mixture of solid $Fe(OH)_2$, Fe_3O_4 and $FeCO_3$. In order to investigate whether such a powdered material could act as an effective barrier to mass transport processes, and thus be capable of significantly reducing or even halting the rate of hydrogen evolution, carbon steel wires were buried in an artificial corrosion product layer consisting of a mixture of iron carbonate and magnetite powder. Artificial groundwater was subsequently poured over the mixture. At the same time a control cell containing just the groundwater and the mixture of iron carbonate and magnetite powders, i.e. without any carbon steel, was set up.

Unexpectedly large amounts of hydrogen were evolved from both the control and test cells for more than 1000 hours. This was most likely due to traces of unoxidised iron in the magnetite powder used to represent the corrosion product. Since the hydrogen evolution on the powder completely masked out that from the carbon steel wires in the vital first 1000 hours period, no conclusions could be drawn from the data on the ability of loose corrosion products to act as a mass transport barrier.

3.4 Task 3. Ferrous Ion Retardation of Corrosion Rate

Previous work[8,9], now supported by the results of Task 2, indicated that the long-term corrosion rate of carbon steel under anaerobic conditions is restricted by the formation of a protective film, predominantly made up of magnetite. It was further postulated that the rate at which this magnetite film forms could depend on the concentration of Fe^{2+} ions in the surrounding solution. Thus, if this was initially at a high level, magnetite formation would be expected to occur much earlier. In order to investigate this theory, hydrogen evolution tests were conducted with carbon steel wires immersed in artificial groundwaters that contained, in addition to the components in the standard groundwater recipe (Table 1), either 0.1M $FeSO_4$ or 0.1M K_2SO_4. K_2SO_4 was used in order to distinguish the effects of Fe^{2+} from SO_4^{2-}.

The results of the experiments failed to confirm the above hypothesis. The addition of 0.1M $FeSO_4$ resulted in greatly increased long-term corrosion rates (Table 3). Additionally, there appeared to be very little formation of the expected magnetite film; a black precipitate was observed on the bottom of the cell instead. It is possible that an unprotective layer of $FeSO_4$ may have formed on the surface of the wires, and that this prevented the adherence of the protective magnetite. Alternatively, it is possible that the addition of iron sulphate caused iron carbonate to precipitate out of solution, thus leading to a decrease in the pH and a more aggressive corrosion environment. At the end of the experiment it was found that the solution in the cell was at pH 7.3. The initial solution of 0.1M $FeSO_4$ in the SKB artificial groundwater had an pH of 6.5; the rise in pH in the experiment is caused by reaction [1]. These values are less than the final pH in the standard groundwater cell Table 5). It therefore appears that the increase in corrosion rate observed in these experiments was largely due to a shift in the pH towards more aggressive conditions. However, a control cell, which contained 0.1M K_2SO_4 instead of the iron sulphate, also showed a larger than expected long-term corrosion rate, although almost an order of magnitude less than that with the $FeSO_4$. The pH of this control solution was found to be pH 8.9 at the end of the experiment. This would suggest that sulphate can cause an increase in the long-term corrosion rate without a decrease in pH.

An alternative explanation for the long-term increase in hydrogen production with sulphate may be that it simply increased the ionic strength of the groundwater. The section describing the results obtained in Task 4 discusses how increased ionic strength could lead to both a short term decrease and a long-term increase in the observed corrosion rates of carbon steel in anaerobic granitic groundwaters.

To overcome problems of salt precipitation and the accompanying pH shifts, the experiment was repeated using SKB artificial groundwater saturated with $FeCO_3$. The low solubility constant of $FeCO_3$ meant that Fe^{2+} saturation was achieved without the precipitation of any of the components of the standard granitic groundwater (Table 1), so that the pH was not perturbed. (It is worth noting here that in both the SKB and TVO repositories carbonate is likely to be the dominant anion, so this experiment probably represented more realistic Fe^{2+} concentrations than the iron sulphate experiment). The results from this cell indicated rates of hydrogen production and corrosion similar to those observed in the absence of the $FeCO_3$ (Table 2 & 3). This suggests that the concentration of Fe^{2+} ions in the repository groundwater will not significantly affect the rate at which the protective magnetite films are formed. Therefore the rate of hydrogen production can be assumed to be independent of the soluble iron(II) concentration.

A possible explanation for why Fe^{2+} ions do not affect the rate of hydrogen production is that two types of magnetite films are believed to form[12], as inner and outer layers. The outer is a precipitation layer, and therefore its rate of growth should be expected to depend on Fe^{2+} concentration. However, the majority of the corrosion protection is believed to be provided by the hard inner film which forms directly on to the surface of the steel by an electrochemical mechanism, without going through a Fe^{2+} intermediate stage, and therefore its development is less likely to be affected by the Fe^{2+} concentration.

3.5 Task 4. Effect of Ionic Strength, NH_3 and NO_3^- on Corrosion Rate

3.5.1 Effect of Ammonia and Nitric Acid

Ammonia and nitric acid are possible products of the radiolysis of trapped water vapour and nitrogen gas. The maximum quantities of ammonia and nitric acid that can be expected to be produced in the lifetime of the ACPC have previously been calculated by Henshaw et al[4], and would give rise to concentrations of 9 mM NH_3 and 3 mM HNO_3 when dissolved in a volume of solution that is equal to that within the space in the internal void[3].

Carbon steel wires were exposed to SKB artificial groundwater with additions of either 9 mM NH_3 or 3 mM HNO_3. The additions were found to have only a minor effect on the rates at which hydrogen gas evolved. In both cases, the additions apparently reduced the initial corrosion rate (Table 3), as a consequence of which the total volumes of hydrogen produced were less than that evolved in the standard artificial groundwater cell[8] (Table 4). The long-term hydrogen evolution rates were unaffected by either the ammonia or nitric acid additions.

The reduction in the initial corrosion rate of the carbon steel can be explained by the increase in pH the addition of ammonia would have induced in the groundwater (Table 5).

The addition of the 3 mM HNO_3 should have caused the pH to fall considerably, perhaps down to pH 3, and therefore was expected to increase the corrosion rate. It is unclear why a decrease in the initial rate of hydrogen production was observed. One possible explanation is that the present experimental technique can not monitor the hydrogen that is evolved in the first 48 hours after the carbon steel is placed in the groundwater. If the corrosion rate is very high during this period the nitric acid may be completely consumed before any observations can be taken.

One possible explanation for the lack of any long-term influence of the nitric acid, is that when it reacts with carbon steel soluble ferrous ions are produced.

$$Fe + 2HNO_3 \rightarrow Fe^{2+} + 2NO_3^- + H_2\uparrow \qquad [2]$$

When all the nitric acid is consumed this reaction should revert back to reaction [1], which is the dominant reaction for iron in anaerobic conditions over the pH range pH 7 - 10.5. Thus the long-term corrosion mechanism, and hence the long-term corrosion rate, is independent of the initial nitric acid concentration. Reaction [1] is the reason why the final pH values for nearly all the groundwaters shifted from an original value of pH 8.1 to about pH 9 during the course of the experiments (Table 5).

The total volume of groundwater in the test cell was about 150 cm^3, thus the 3 mM HNO_3 represented only 4.5 $x10^{-4}$ moles of H^+: this quantity could produce only an additional 5 cm^3 of hydrogen gas before the supply of nitric acid would have been exhausted. When it is noted that in excess of 100 cm^3 of hydrogen are produced in the first 500 hours of the experiments (Table 4), it is not surprising that the 3 mM nitric acid had only a marginal effect on the long-term corrosion behaviour of the carbon steel.

The cathodic process of reduction of NO_3^- to NO_2^- could also have occurred in competition with the hydrogen evolution reaction[13]; although the low concentration of nitrate means that it is unlikely to have had a significant long-term effect.

At this point, it is perhaps useful to reconsider the results obtained from the barometric cell containing carbon steel wires in a solution of standard granitic groundwater with an additional 0.1M $FeSO_4$, that were presented under Task 3. In this case, the continued high rate of hydrogen production was attributed to lower pH in the experiment than that with no $FeSO_4$, (Table 5). However, it is not clear why the pH did not fully recover in that case. It is probable that the high concentration of Fe^{2+} already present in the groundwater, near saturation level, meant that any corrosion products produced immediately precipitated out, effectively buffering the groundwater, and thus no overall change in pH would occur from the corrosion reaction;

$$Fe + 2H_2O \rightarrow Fe(OH)_2 + H_2\uparrow. \qquad [3]$$

3.5.2 Effect of Ionic Strength

In order to investigate the effect of the ionic strength of the solution on the corrosion rate of carbon steel, the rate of hydrogen evolution was monitored from carbon steel exposed to a solution containing 10 times the amount of all the components of standard SKB artificial groundwater, except for the HCl, which was used to obtain the desired pH 8.1. This gave a new total anion content of around 3 $x10^{-2}$M.

It was found that increasing the ionic strength of the solution 10-fold caused a decrease in the normally high hydrogen production rates observed in the more dilute groundwaters during the first 500 hours (Table 2). However, the final equilibrium value for the corrosion rate, after the

protective magnetite film had formed, (after 1000 hours), was approximately an order of magnitude greater than in the dilute groundwater (Table 3).

The ionic strength of 0.1M K_2SO_4 is approximately 3 times that of the 10-fold strength groundwater, yet the two solutions yielded virtually identical results with respect to hydrogen evolution, (see the data from Task 3). This suggests that the dependence of the hydrogen evolution rate on ionic strength is restricted to a domain below a threshold value, (somewhere between that of the standard and 10-fold strength groundwaters). Above this limit, further increases in the ionic strength of the groundwater are not expected to affect the hydrogen evolution process.

A possible explanation for the observed higher long-term hydrogen evolution rates in high ionic strength groundwaters is that, since no initial burst of corrosion was observed, the time required to form a thick protective magnetite film can be expected to be longer. This idea is partly supported by the visual observation that the black film on the carbon steel wires did not appear to be as coherent as in the dilute solutions. However, this explanation was not supported by the hydrogen evolution rates, which were observed to be reasonably constant from about 500 hours through to the end of the experiment, 5000 hours. This behaviour is inconsistent with the idea of a steady thickening of the protective film.

At the present time, there is no satisfactory explanation for the higher hydrogen evolution rates observed in the high ionic strength solutions, although some possibilities are:

i) increased competition between magnetite film formation and other less protective iron salts, i.e. $FeCO_3$ or $FeSO_4$ films;

ii) increased availability of anions to form more soluble corrosion products, i.e. $FeCl_2$ instead of $Fe(OH)_2$ and hence a reduction in the ability to form a protective magnetite film;

iii) incorporation of ions in the magnetite film, which increases its conductivity, and possibly increases its effectiveness as a hydrogen electrode;

iv) local buffering of the pH. Magnetite is more thermodynamically favoured at high pHs, therefore the protective hard inner film[12] may only form when the pH at the carbon steel/groundwater interface is significantly higher than the pH 8.1 of the bulk solution;

v) increased conductivity may enable more efficient electron transfer to occur between the carbon steel and the water reduced to form the hydrogen.

The visual observation that the black magnetite films formed tended to be less coherent in the more concentrated groundwaters tends to support the first explanation, i.e. magnetite is formed in competition with other less protective films. However, this is not fully supported by the conclusions from Task 2.

The similarity between the results from the 0.1M K_2SO_4 and the 10-fold ionic strength groundwaters supports the idea of increased electron transfer efficiency in the more conductive solutions. Once sufficient conductivity has been reached it is likely that the particular electron transfer process involved would no longer be the rate limiting step.

A film was not visually detectable on the carbon steel until approximately 1000 hours, i.e. about the same time scale as in the normal dilute groundwater. However the film did not appear to be as coherent in this case. It is possible that the film could include less protective ferrous sulphate or carbonate which would explain the higher long-term corrosion rates.

3.6 SUMMARY OF RESULTS

The hydrogen evolution process on carbon steel in anaerobic groundwaters can be divided into two regions (Figure 2). In the short-term, (<1500 hours), the rate at which hydrogen evolves is initially high, but then rapidly declines. In the long-term, the hydrogen evolution rate attains a steady state value.

The present study involved varying a number of experimental parameters. A brief description of the resulting effects on the hydrogen evolution process is given in the following two sub-sections. Table 2 shows the approximate hydrogen gas evolution rates. The corrosion rates calculated from these production rates and the total volumes of hydrogen produced during the 5000 hours of the experimental programme are shown in Tables 3 and 4 respectively.

3.6.1 Short-Term Hydrogen Evolution Rates on Carbon Steel

The initial hydrogen evolution rate on carbon steel in standard SKB artificial groundwater has been found to be of the order of 50 dm^3 (STP) m^{-2} $year^{-1}$, (Rate at 100 hours; Table 2)[8]. This rate declines by >95% during the first 1500 hours. This short-term process was observed to:

i) occur at an initially slightly higher rate and to decline more rapidly when the carbon steel was in high humidity conditions, but not in contact with the groundwater;

ii) occur at an initially slower rate and to decline more slowly when the carbon steel was only partially-submerged in the groundwater;

iii) be virtually eliminated if the carbon steel was pre-coated with a layer of magnetite or iron carbonate. The order of increasing effectiveness was thin carbonate < thin magnetite < thick carbonate < thick magnetite (Thin ≈ 50 nm; Thick ≈ 500 nm);

iv) no longer sharply decline if an addition of 0.1M $FeSO_4$ was made to the groundwater;

v) occur at an initially slower rate if an addition of 0.1M K_2SO_4 was made to the groundwater;

vi) to be virtually unaffected if the groundwater was saturated with $FeCO_3$;

vii) occur at an initially slightly slower rate when an addition of 9 mM NH_3 was introduced to the groundwater;

viii) occur at an initially slightly slower rate when an addition of 3 mM HNO_3 was introduced to the groundwater;

ix) occur at an initially slower rate when the ionic strength of the groundwater was increased 10-fold.

3.6.2 Long-Term Hydrogen Evolution Rates on Carbon Steel

The long-term hydrogen evolution rate on carbon steel in standard SKB groundwater was found to be <0.5 dm^3 (STP) m^{-2} $year^{-1}$. This long-term rate was found to:

i) be independent of whether the carbon steel was in high humidity or completely submerged conditions;

ii) require the prior formation of an approximately 700 - 1000 nm thick magnetite film on the carbon steel;

iii) to increase by a factor of 50 with the addition of 0.1M $FeSO_4$ to the groundwater;

iv) to increase by an order of magnitude with the addition of 0.1M K_2SO_4 to the groundwater;

v) be independent of the concentration of $FeCO_3$ in the groundwater;

vi) to be unaffected by an addition of 9 mM NH_3 to the groundwater;

vii) to be unaffected by an addition of 3 mM HNO_3 to the groundwater;

viii) to increase by an order of magnitude when the ionic strength of the groundwater was increased 10-fold.

4 MODELLING OF HYDROGEN PRODUCTION

4.1 SUMMARY OF MODEL

In the model, the ACPC is represented by a 50 mm thick copper canister of height 4.5 m and radius 0.4 m covering a 50 mm thick carbon steel canister of height 4.4 m and radius 0.35 m (Figure 10). The canisters are separated by a 2 mm fitting gap. The inner steel canister is filled with packing materials, leaving a void volume of 0.4 m^3. There is assumed to be a single circumferential crack in each, at a height h_1 in the inner canister and height h_2 in the outer. It is intended that the ACPC will be placed in a hole drilled into the floor of a tunnel cut into granite rock. The hole will be backfilled with compacted sodium bentonite. After water saturation of the repository, the external pressure will reach a value of 15MPa, resulting from a hydrostatic pressure of 5MPa and a bentonite swelling pressure of 10MPa.

The model then considers the following processes:-

i) Ingress of water into the annulus between the canisters, until the height of water reaches h_1. Depending on the relative positions of the cracks, this stage may be affected by the generation of hydrogen by the corrosion reactions.

ii) Filling of the inner canister. Clearly if the water in the annulus reaches height h_1, then it will enter the inner canister. This stage will be affected by the increase in hydrogen pressure, and will continue until the gas pressure in the canister equals the hydrostatic pressure at the outer crack.

iii) Emptying the annulus. As the pressure inside the canister exceeds that outside, then water above the outer crack will be forced out of the annulus.

iv) Enhanced corrosion up to the height of the water in the annulus on the outer surface of the steel due to galvanic contact. The stages described in 1-3 may be affected by a corrosion rate which varies with water height in the annulus.

v) Consumption of water remaining in the inner canister by the anaerobic corrosion reactions.

vi) Precipitation of solid corrosion product in the inner canister. As anaerobic corrosion proceeds on the inner surface of the carbon steel, solid iron oxide will precipitate. This will affect the rate of increase of pressure of the hydrogen gas, by decreasing the available volume in the canister. It may also affect the corrosion rate, and this is discussed in the 'Corrosion Model' section below.

vii) Corrosion limited by diffusion of water vapour from the outer crack. When water has been completely removed from the canister by corrosion reactions, further corrosion of the annulus and canister will be limited by the diffusion of water vapour.

viii) Filling of void space in the inner canister and/or annulus with solid corrosion product. It is assumed that corrosion ceases when the solid product fills either the annulus, blocking the passage of water vapour to the inner canister, or both the annulus and canister, depending on the relative position of the cracks.

The model predicts the total amount of hydrogen produced by the canister and the length of time during which corrosion (and hence gas production) persist, as functions of the following parameters:-

i) Rate of anaerobic corrosion of steel.

ii) Positions and sizes of cracks in inner and outer canisters.

The mathematics of the model are summarised in Appendix A.

4.2 APPLICATION OF THE MODEL

4.2.1 'Base Case' Calculation

For the 'base case' calculation with the model, it is assumed that

- the corrosion current is 0.1μm/year
- there is no enhancement of the corrosion current due to galvanic contact between the carbon steel canister and the copper canister
- the widths of the cracks in the inner and outer canister, are w_1 = 1mm and w_2 = 1mm respectively
- two different scenarios are considered, in which the positions of the cracks are
  - Case 1 $h_1 = 4.3$m and $h_2 = 0.0$m
  - Case 2 $h_1 = 4.3$m and $h_2 = 4.3$m
- the outflow of hydrogen gas into the geology is given by

$$\frac{dB}{dt} = -K(p_o - p_i(t)) \qquad p_i > 5\text{MPa}$$

where B(t) is the volume of hydrogen gas external to the canister. The flow rate parameter K is a constant that depends on the permeability of the bentonite, and on the crack geometry. p_o is the hydroxatic pressure at the rock/bentonite interface, and p_i is the internal canister pressure.

Case 1: Cracks at Base of Outer Canister and Top of Inner Canister

After the outer copper canister has been breached, the following sequence of results are calculated.

1. Water flows into the canister, rapidly filling the annulus and then spilling over into the inner canister (Figure 11 and Figure 12).

2. Corrosion of the carbon steel initiates, releasing hydrogen gas. After 200 years, the pressure of the hydrogen gas inside the canister (Figure 13) becomes larger than the hydrostatic pressure and starts to force water from out of the annulus into the geology. The volume of water trapped in the inner canister is about 0.36 m^3.

3. The water within the annulus is consumed/expelled after 350 years.

4. The canister experiences a long period of corrosion as the water trapped in the inner canister is consumed. This takes about 80000 years (Figure 14), and results in the formation of 0.076 m^3 of magnetite (Figure 15).

5. Once the inner canister is empty of water, the annulus is able to fill with corrosion residue. This takes about 18000 years (Figure 16).

6. Hydrogen gas is produced by the corrosion of the carbon steel canister. The rate at which hydrogen gas is produced is uniform for the first 80000 years. It reduces when the inner surface of the carbon steel canister stops corroding, and falls to zero when the annulus blocks (Figure 17).

7. The hydrogen gas pressure rises rapidly to an equilibrium value, at which the rate of production equals the rate of outflow into the geology. After 80000 years the inner surface of the carbon steel canister stops corroding, and the hydrogen gas pressure decreases. After a further 18000 years the canister stops corroding, and the hydrogen gas pressure gradually reduces to the hydrostatic pressure (Figure 18).

Case 2: Cracks at Top of Outer Canister and Top of Inner Canister

After the outer copper canister has been breached, the following processes are predicted to occur:

1. Water flows into the canister, rapidly filling the annulus and then spilling over into the inner canister (Figure 19 and Figure 20).

2. Corrosion of the carbon steel initiates, releasing hydrogen gas. After 200 years, the pressure of the hydrogen gas inside the canister (Figure 21) becomes larger than the hydrostatic pressure and prevents any more water from flowing into the canister. The volume of water trapped in the inner canister is about 0.36 m^3.

3. The water trapped in the annulus is consumed by the corrosion of the carbon steel canister. After about 6000 years the annulus is empty of water (Figure 22), but corrosion continues at the same rate (Figure 23) as a result of the diffusion of water vapour into the annulus. The annulus starts to fill with corrosion residue, and after 24000 years is blocked (Figure 24).

4. The water trapped in the inner canister is consumed by the corrosion of the carbon steel canister. After 24000 years the consumption rate reduces, because water vapour is no longer able to diffuse from the inner canister into the annulus (Figure 25). After 110000 years the inner canister is empty of water (Figure 25), but corrosion continues at a similar rate (Figure 26) as a result of the diffusion of water vapour into the inner canister. The gas production rate actually increases slightly because the internal surface area of the carbon steel canister which is corroding increases. After 390,000 years, the inner canister is full of corrosion residue (Figure 27), and the canister stops corroding (Figure 26).

5. Hydrogen gas is produced by the corrosion of the carbon steel canister. The rate at which the hydrogen gas is produced is approximately uniform for the first 24,000 years etc, reduces when the annulus blocks, and falls to zero when the inner canister stops corroding.

6. The hydrogen gas pressure rises rapidly to an equilibrium value, at which the rate of production equals the rate of outflow into the geology. After 24000 years the outer surface of the carbon steel canister stops corroding, and the hydrogen gas pressure decreases. After 390,000 years the canister stops corroding, and the hydrogen gas pressure gradually reduces to the hydrostatic pressure (Figure 28).

4.3 SENSITIVITY CALCULATIONS

A number of sensitivity tests on the base case calculations were performed. In particular, these considered the effect of

- increasing the corrosion rate to 1.0 μm/year

- enhancing the corrosion current as a result of galvanic contact between the carbon steel canister and the copper canister
- increasing the widths of the cracks to $w_1 = 2mm$ and $w_2 = 2mm$
- changing the mechanism for the flow of hydrogen gas out of the canister and into the geology
- changing the dimensions of the canister to the latest SKB specification

4.3.1 Increased Corrosion Current

The corrosion rate in the model was increased to 1.0 μm/year.

After a breach of the copper canister, water flows into the canister rapidly filling the annulus and then spilling over into the inner canister. The enhanced corrosion rate results in the pressure of the hydrogen gas in the canister increasing more rapidly, reducing the volume of water that is able to enter the canister.

For Case 1, because the corrosion rate is increased and there is less water in the canister, the time taken for the water in the inner canister to be consumed is reduced to 4000 years. The annulus is then able to fill with corrosion residue, and after an additional 2000 years is blocked. The hydrogen gas production rate is shown in figure 29.

For Case 2, the hydrogen gas production rate is shown in figure 30. The annulus fills with corrosion residue after 2500 years, and the hydrogen gas production rate decreases. After 5000 years the water in the inner canister is consumed, and the hydrogen gas production rate decreases again. This is because continuing corrosion in the inner canister is limited by the diffusion of water vapour. After 48000 years the inner canister is full of corrosion residue and corrosion stops.

4.3.2 Galvanic Contact

The effect of increasing the corrosion current as a result of galvanic contact between the carbon steel canister and the copper canister is now considered.

This variant is not very different from the base case, because galvanic contact between the carbon steel canister and the copper canister results in only a small increase in the corrosion current for the relatively short time that there is water present in the annulus (figure 31 (Case 1) and figure 32 (Case 2)).

4.3.3 Increased Crack Widths

The effect of increasing the widths of the cracks in the canister to w_1 = 2mm and w_2 = 2mm is now considered. There is less resistance to the flow of water into the canister, and to the flow of hydrogen gas out into the geology. For crack widths of w_1 = 1 mm and w_2 = 1mm and a corrosion rate of 0.1μm/year, water vapour diffusion is not a limiting factor in controlling the corrosion of the canister. Therefore, increasing the crack widths can have no effect on the behaviour of the canister after it is empty of water.

For the above reasons this test gives similar results to the base case.

4.3.4 Episodic Hydrogen Gas Release

An alternative transport mechanism to describe the outflow of hydrogen gas into the surrounding geology has been suggested recently. The hydrogen gas is assumed to be trapped in the canister until p_i is comparable to the sum of the hydrostatic pressure and the swelling pressure of the bentonite. When p_i exceeds a critical value p_c deformation of the bentonite occurs, allowing a bubble of hydrogen gas to escape from the canister, and reducing the pressure in the canister.

As an example of this mechanism, it is assumed that

$$\frac{dB}{dt} = 0$$

until the pressure of the hydrogen gas exceeds the critical value p_c. B is then increased instantaneously in such a way that p_i is reduced to the hydrostatic pressure p_o. The critical pressure p_c is chosen arbitrarily to be

$$\begin{aligned} p_c &= \text{(hydrostatic pressure + swelling pressure)/2} \\ &= 7.5\text{MPa} \end{aligned}$$

This alternative mechanism for describing the outflow of hydrogen gas into the surrounding geology affects the calculation of B(t), the volume of hydrogen gas external to the canister, and $p_i(t)$, the internal canister pressure.

The processes associated with a failure of the ACPC are not sensitive to these variables, and so this variant is similar to the 'base case'.

For Case 1, B is shown in figure 33 and p_i is shown in figure 34.

It is possible that this transport mechanism could have a significant impact on the model, provided that the 'outgassing' of the canister disrupts the corrosion residue.

4.3.5 Canister Dimensions

SKB recently changed the specification of the ACPC dimensions.

- the inner radius of the ACPC was increased to 0.34m
- the radius of the annulus between the carbon steel and copper canisters was increased to 0.39m
- the outer radius of the ACPC was increased to 0.44m
- the void volume of the carbon steel canister was increased to

$$0.4 \times 1.22m^3 = 0.488m^3$$

This variant is similar to the 'Base Case', but is different in detail. The rate at which hydrogen gas is produced is shown in figure 35 for Case 1, and in figure 36 for Case 2. The differences are explained by noting that a crack of width 1mm has a larger area than the base case, and so a greater volume of water/water vapour is able to flow through the crack.

4.4 Comparison with Previous Calculations

The principal results of decreasing the corrosion rate from 6.5μm/year to 0.1μm/year are

- the rate of hydrogen gas production is reduced
- the maximum hydrogen gas pressure is lower
- corrosion of the ACPC canister takes place over a longer timescale

5 SUMMARY AND CONCLUSIONS

The conclusions of this study are as follows:-

1. It has been found that the long-term hydrogen evolution rate from carbon steel in a high humidity anaerobic atmosphere is approximately 0.5 dm^3 (STP) m^{-2} $year^{-1}$. This is identical to that found previously[8] from carbon samples completely submerged in artificial Swedish granitic groundwater. The time taken to reach this long-term rate is approximately the same in the high humidity conditions as found with completely submerged samples. However, if the carbon steel is partially-submerged in the groundwater, which may be a more realistic scenario for an ACPC with a penetrated

outer copper canister, the time taken to reach the equilibrium value is considerably longer, although the equilibrium values appears to be the same.

2. Magnetite has been shown to be more protective than iron carbonate, with a thickness of 0.5 - 1.0 μm being sufficient to reduce the rate of hydrogen production to around 0.5 dm^3 (STP) m^{-2} $year^{-1}$.

3. No link has been established between the rate of formation of a protective magnetite film and the concentration of soluble Fe^{2+} species in the groundwater.

4. Decreasing the pH of the groundwater to a buffered value of pH 7.3 (0.1M $FeSO_4$ experiment) increased the long-term rate at which hydrogen was generated as a result of the anaerobic corrosion of carbon steel by more than an order of magnitude.

5. It has been demonstrated that the concentrations of ammonia and nitrate species expected to be formed from radiolysis reactions should not affect the amount of hydrogen evolved from the ACPC.

6. A 10-fold increase in the ionic strength of the groundwater was found to increase the long-term hydrogen evolution rate by almost an order of magnitude, to approximately 2.5 dm^3 (STP) m^{-2} $year^{-1}$. Further increases in the ionic strength of the groundwater did not cause any additional increase in the hydrogen evolution rate.

7. The results presented in this report suggest that, in the unlikely event of a penetration of the outer copper canister of an ACPC, hydrogen gas production rates on the carbon steel inner container will not be sustained above 3.0 dm^3 (STP) m^{-2} $year^{-1}$ for more than the first 2000 hours after penetration.

8. The results of the experimental programme have been used to update calculations of the hydrogen production rate and corrosion behaviour from the ACPC, assuming that the outer copper canister is breached and that water can enter the inner canister through the gas seal at the top. The model considers the ingress of water into the canister, the subsequent corrosion of the inner steel canister and the production of hydrogen gas. The previous calculations assumed a much higher corrosion rate for the carbon steel inner canister, than those inferred from the measured gas production rates in the current programme, i.e. approximately 0.1 μm $year^{-1}$.

9. The new calculations predict that the maximum pressure of hydrogen will be approximately 5.2 MPa (compared to a value of about 9MPa, assuming a corrosion rate of 6.5 μm $year^{-1}$). The maximum rate of production of gas is slower with the new parameters, approximately 8×10^{-3} m^3 $year^{-1}$ at 0.1 MPa compared to 0.5 m^3 $year^{-1}$

from previous calculations. However, the corrosion process goes on for longer: 95,000 years as compared to 400 years for one scenario of crack positions; for an alternative scenario of crack positions, corrosion continues for 3.9×10^5 years.

10. A number of sensitivity studies of assumptions made in the model were performed. Assuming enhancement of the corrosion rate due to galvanic contact had little effect on the predictions, due to the relatively short time during which the copper and iron were electrically connected by water in the canister. Also, increasing the crack widths or changing the canister dimensions slightly to reflect the most recent SKB design had little effect on the predictions. The model assumes that gas is released through the bentonite 'smoothly'. More recent studies have suggested that such release might occur in 'bursts'. However, this will not have a significant effect on the predictions of the model unless there is an associated disruption of the corrosion product.

6 ACKNOWLEDGEMENTS

Financial support for this programme was provided by SKB of Sweden and TVO of Finland.

7 REFERENCES

1 L Werme, P Sellin and N Kjellbert, "Copper Canisters for Nuclear High Level Waste Disposal. Corrosion Aspects.", SKB Technical Report 92-26, 1992.

2 N de Zoubov, C Vanleugenhaghe and M Pourbaix, in "Atlas of Electrochemical Equilibria in Aqueous Solutions", Section 14.1 "Copper", Ed. M Pourbaix, 2nd edition, National Association of Corrosion Engineers, Houston, Texas, USA, 1974.

3 G P Marsh, "A Preliminary Assessment of the Advanced Cold Process Canister", AEA Technology Report, AEA-InTec-0011, 1990.

4 J Henshaw, A Hoch and S M Sharland, "Further Assessment Studies of the Advanced Cold Process Canister", AEA Technology Report, AEA-D&R-0060, 1990.

5 D M Drazic, in "Modern Aspects of Electrochemistry Vol. 19", Eds. B E Conway, J O'M. Bockris and R E White, Plenium Press, New York, 1989.

6 M Pourbaix and N de Zoubov., in reference 2, Section 12.1 "Iron".

7 M G Fontana, "Corrosion Engineering", 3rd edition, McGraw-Hill, New York, 1986.

8 D J Blackwood, C C Naish, N Platts, K J Taylor and M I Thomas., "The Anaerobic Corrosion of Carbon Steel in Granitic Groundwaters", AEA Technology Report, AEA-InTec-1414, 1993.

9 C C Naish, M I Thomas, D J Blackwood, and K J Taylor, "The Anaerobic Corrosion of Stainless Steels", AEA Technology Report for UK Nirex Ltd, NSS/R307, 1993.

10 J Rennerfelt, "Composition of Groundwater Deep Down in Granitic Bedrock", SKB Report KBS TR36, (1977)

11 K Nomura and Y Ujihira, J Mater. Sci. **19** (1984) 2664.

12 D W Shoesmith, T E Rummery, Woon Lee and D G Owen, Power Industry Research (1981) 43.

13 M Pourbaix and N de Zoubov., in reference 2, Section 18.1 "Nitrogen".

14 R S Wikramaratna, M Goodfield, W R Rodwell, P J Nash, and P J Agg, 1993, A Preliminary Assessment of Gas Migration from the Advanced Cold Process Canister AEA-D&W-0672

TABLE 1

STANDARD ARTIFICIAL GROUNDWATER FOR ALL EXPERIMENTS: - STANDARD WATER FOR SORPTION MEASUREMENTS ACCORDING TO KBS TR 36

	Concentration Mol dm^{-3}	Concentration ppm
$MgSO_4$	10^{-4}	12.6
$MgCl_2$	8×10^{-5}	8.6
KCl	10^{-4}	7.46
Na_4SiO_4	2×10^{-5}	37.84
HCl	8×10^{-4}	29.9
$CaCl_2$	4.5×10^{-4}	50.6
$NaHCO_3$	2×10^{-3}	169.2
pH*	8.1	8.1

*Adjusted where necessary with HCl or NaOH.

TABLE 2

APPROXIMATE HYDROGEN EVOLUTION RATE IN dm^3 (STP) m^{-2} $year^{-1}$

	Time (Hours)							
	100	500	1000	1500	2000	3000	4000	5000
Cell Type								
Standard Groundwater[8]	51.0	16.5	4.15	1.5	1.25	1.0	<0.5	<0.5
Task 1								
*Saturated Vapour No.1	70.0	4.15	3.8	1.5	1.0	0.75	0.5	<0.5
*Saturated Vapour No.2	19.5	16.5	15.2	6.7	5.4	1.6	1.0	0.75
Task 2								
Thin Magnetite	7.0	3.5	1.5	1.0	0.75	0.5	0.5	<0.5
Thick Magnetite	<0.5	0.75	1.0	0.75	0.5	<0.5	0.5	<0.5
Thin Carbonate	7.0	3.25	2.5	2.0	1.75	1.5	0.75	-
Thick Carbonate	8.0	3.0	1.5	0.75	0.5	<0.5	<0.5	<0.5
Powder	110.0	13.0	4.0	1.0	-	-	-	-
Powder (Control)	84.0	157.0	4.75	0.75	-	-	-	-
Task 3								
0.1 M $FeSO_4$	32.0	22.5	12.75	13.5	16.5	19.0	-	-
0.1 M K_2SO_4	16.0	5.0	1.75	3.75	2.5	3.25	4.0	-
Saturated $FeCO_3$	32.0	16.0	4.75	1.5	0.75	1.0	0.5	<0.5
Task 4								
9 mM NH_3	32.0	6.25	5.5	2.5	1.0	0.75	0.5	<0.5
3 mM HNO_3	32.0	16.0	4.0	1.0	0.75	0.5	<0.5	<0.5
10x strength**	16.0	3.25	4.0	4.0	3.25	3.25	2.5	2.0

*In the Saturated vapour cell number 1 the carbon steel was completely clear of the groundwater. Cell number 2 contains the partially-submerged carbon steel.

**After 7000 hours the 10x strength cell was still producing hydrogen at a rate of approximately 3 dm^3 (STP) m^{-2} $year^{-1}$.

TABLE 3

APPROXIMATE CORROSION RATE IN MICRONS PER YEAR

	Time (Hours)							
	100	500	1000	1500	2000	3000	4000	5000
Cell Type								
Standard Groundwater[8]	16.0	5.2	1.3	0.4	0.3	0.3	<0.1	<0.1
Task 1								
*Saturated Vapour No.1	22.0	1.3	1.2	0.4	0.3	0.2	0.1	<0.1
*Saturated Vapour No.2	6.1	5.2	4.8	2.1	1.7	0.5	0.3	0.2
Task 2								
Thin Magnetite	1.9	1.0	0.4	0.3	0.2	0.2	0.1	<0.1
Thick Magnetite	<0.1	0.2	0.4	0.2	0.1	<0.1	0.1	<0.1
Thin Carbonate	1.7	1.0	0.8	0.5	0.6	0.5	0.2	-
Thick Carbonate	2.5	0.9	0.4	0.2	0.1	<0.1	<0.1	<0.1
Powder	27	5.0	1.3	0.3	-	-	-	-
Powder (control)	50	3.5	1.0	0.3	-	-	-	-
Task 3								
0.1 M $FeSO_4$	10.0	7.0	4.0	4.1	5.2	5.0	-	-
0.1 M K_2SO_4	5.0	1.6	0.6	1.2	0.8	1.0	1.3	-
Saturated $FeCO_3$	10.0	5.0	1.5	0.5	0.2	0.4	0.2	0.1
Task 4								
9 mM NH_3	10.0	1.9	1.7	0.8	0.3	0.2	0.1	0.1
3 mM HNO_3	10.0	5.0	1.3	0.3	0.2	0.1	<0.1	<0.1
10x strength	5.0	1.0	1.3	1.3	1.0	1.0	0.8	0.7

*In the Saturated vapour cell number 1 the carbon steel was completely clear of the groundwater. Cell number 2 contains the partially-submerged carbon steel.

To convert from microns per year of carbon steel to dm^3 (STP) m^{-2} $year^{-1}$ of hydrogen gas multiply by 3.175.

TABLE 4

APPROXIMATE TOTAL VOLUMES OF HYDROGEN PRODUCED IN cm^3 (STP)
SURFACE AREA = 0.1 m^2

	Time (Hours)							
	100	500	1000	1500	2000	3000	4000	5000
Cell Type								
Standard Groundwater[8]#	75	160	201	206	216	220	221	222
Task 1								
*Saturated Vapour No.1	90	158	184	193	200	208	215	217
*Saturated Vapour No.2	25	65	140	165	200	210	230	240
Task 2								
Thin Magnetite	7	14	18	24	34	39	40	42
Thick Magnetite	<1	2	7	13	19	20	24	27
Thin Carbonate	7	10	18	30	44	61	72	-
Thick Carbonate	2	10	17	24	28	30	31	-
Powder	100	215	240	250	-	-	-	-
Powder (Control)	200	325	332	340	-	-	-	-
Task 3								
0.1 M $FeSO_4$	25	63	109	250	310	490	-	-
0.1 M K_2SO_4	15	29	48	68	89	124	158	-
Saturated $FeCO_3$	50	140	200	205	208	222	228	230
Task 4								
9 mM NH_3	19	80	140	155	164	169	174	176
3 mM HNO_3	26	107	133	135	139	142	143	145
10x strength##	18	30	50	75	95	110	150	175

#Total volume of hydrogen produced in standard artificial groundwater after 10 000 hrs was 222 cm^{-3}.

##Total volume of hydrogen produced 10x strength artificial groundwater after 7 000 hrs was 220 cm^{-3}

*In the Saturated vapour cell number 1 the carbon steel was completely clear of the groundwater. Cell number 2 contains the partially-submerged carbon steel.

TABLE 5

FINAL pH VALUES MEASURE IN EXPERIMENTAL CELLS

Cell Type	Final pH
Standard Groundwater[8]	8.7
Task 2	
Thin Magnetite	9.1
Thick Magnetite	9.2
Thin Carbonate	9.0
Thick Carbonate	8.2
Task 3	
0.1 M $FeSO_4$	7.3
0.1 M K_2SO_4	8.9
Saturated $FeCO_3$	9.0
Task 4	
9 mM NH_3	9.3
3 mM HNO_3	9.8
10x strength	9.2

APPENDIX A

Summary of Model of Hydrogen Production

In the model, the ACPC is represented by a 50 mm thick copper canister of height 4.5 m and radius 0.4 m covering a 50 mm thick carbon steel canister of height 4.4 m and radius 0.35 m (Figure 10). The canisters are separated by a 2 mm fitting gap. The inner steel canister is filled with packing materials, leaving a void volume of 0.4 m^3. It is intended that the ACPC will be placed in a hole drilled into the floor of a tunnel cut into granite rock. The hole will be backfilled with compacted sodium bentonite. After water saturation of the repository, the external pressure will reach a value of 15MPa, resulting from a hydrostatic pressure of 5MPa and a bentonite swelling pressure of 10MPa.

The following convention is adopted as a notational convenience. A subscript 1 is attached to any variable associated with the inner canister, while a subscript 2 is used for variables associated with the annulus.

It is assumed that the outer canister is penetrated by a single circumferential crack of width w_2 at a height h_2, and the inner canister is penetrated by a single circumferential crack of width w_1 at a height h_1. The model is characterised by the following variables

- $W_1(t)$ the volume of water in the inner canister
- $W_2(t)$ the volume of water in the annulus
- $Q_1(t)$ the volume of magnetite residue in the inner canister
- $Q_2(t)$ the volume of magnetite residue in the annulus
- $t_1(t)$ the thickness of the magnetite layer in the inner canister
- $t_2(t)$ the thickness of the magnetite layer in the annulus
- V(t) the volume of hydrogen gas at 1 atmosphere produced by the corrosion process
- B(t) the volume of hydrogen gas external to the canister

The processes associated with corrosion of the canister and hydrogen production separate naturally into two parts: the physics outside the canister which involves the transport of water to the canister and the transport of hydrogen gas away from the canister, and the processes inside the canister which involves modelling the way in which water enters the canister and causes corrosion.

A1 Processes Outside the Canister

A1.1 Water Ingress Through Breach in Outer Canister

External to the canister, the transport of water and water vapour to the canister, and the transport of hydrogen gas away from the canister are of concern. The canister is assumed to fail a long time after burial so that the repository is saturated and the groundwater has been deoxygenated by the external corrosion of the copper canisters. Also, the temperature is assumed to have decayed to 30°C. When the canister fails, groundwater enters the canister under the influence of the external hydrostatic pressure. It is a reasonable approximation[4] to assume that the influx of water to the canister is described by

$$\frac{d}{dt}(W_1 + W_2) = K\,(p_o - p_i(t)) \qquad (A1)$$

where K is a constant that depends on the permeability of the bentonite, and on the crack geometry. p_o is the hydrostatic pressure at the rock/bentonite interface, and p_i is the internal canister pressure.

A1.2 Hydrogen Transport

The ingress of groundwater to the canister causes anaerobic corrosion according to the chemical reaction

$$3Fe + 4H_2O \leftrightarrow Fe_3O_4 + 4H_2 \qquad (A2)$$

As the canister corrodes, it generates hydrogen gas, and the pressure inside the canister increases until it exceeds the external hydrostatic pressure. The hydrogen gas will then force the groundwater away from the canister. The transport mechanism which describes the outflow of hydrogen gas into the surrounding geology is complex.

In the previous application of the model[4], it was assumed that the equation which describes the ingress of groundwater to the canister also controls the outflow of hydrogen gas into the geology, i.e.

$$\frac{dB}{dt} = -K(p_o - p_i(t)) \qquad p_i > 5MPa \qquad (A3)$$

The pressure outside the canister is taken as 5MPa, and the hydrogen gas is trapped as a bubble in the vicinity of the canister.

Alternatively, it has been suggested that the hydrogen gas might be trapped in the canister until p_i is comparable to the sum of the hydrostatic pressure and the swelling pressure of the

bentonite. Deformation of the bentonite will then occur, allowing a bubble of hydrogen gas to escape from the canister, and reducing the pressure in the canister.

The diffusion of hydrogen gas away from the canister through the groundwater can be neglected[14].

A1.3 Diffusion of Water Vapour

The final process to be included is the diffusion of water vapour to the canister. Once the hydrogen gas has forced the groundwater away from the canister, then corrosion will continue only as a result of water vapour diffusing to the canister. This is a complicated diffusion problem, but if the crack in the canister is small then it is reasonable to assume that the hydrogen gas will be saturated with water vapour. At 30°C the vapour pressure of water is 25 mm Hg, which corresponds to a saturation concentration of 1.34 mols m^{-3}.

A2 Processes Inside the Canister

A2.1 Corrosion Rates

The steel canister is assumed to undergo uniform corrosion, and the corrosion rate is assumed to be the same for corrosion by water and water vapour. The current experiments also suggest that the maximum long term corrosion rate μ is 0.1μm $year^{-1}$ and this is independent of the presence of an oxide film. This corrosion rate can increase to 1.0μm $year^{-1}$ if the groundwater composition is changed.

If the inner surface area of the steel canister which undergoes corrosion is given by $A_1(t)$, then the rate of production of hydrogen from the inner canister is proportional to μA_1. The corrosion rate on the outer surface of the steel canister is possibly enhanced due to galvanic contact with the copper canister. Therefore, the rate of production of hydrogen in the annulus is proportional to $\mu(A_2 + \alpha A_w)$ where $A_2(t)$ is the outer surface area of the steel canister and $A_w(t)$ is the surface area of the water in the annulus in contact with the canister. α is a parameter that characterises the galvanic contact: $\alpha = 0$ corresponds to no galvanic enhancement, while $\alpha = 1$ corresponds to maximum galvanic enhancement.

A2.2 Water Vapour Transport Inside the Canister

A major factor influencing the way in which the canister corrodes is the presence or absence of water: a specific part of the canister surface will corrode only if water or water vapour is present. Therefore, it is necessary to model the transport of water and water vapour inside the canister. In this context, the following calculations are relevant.

1. Flux of Water Vapour into Canister

The small width w_i of the cracks in the canister limits the flux of water vapour. If the diffusion of the water vapour is assumed to be steady state, then the diffusion equation in cylindrical coordinates is

$$\frac{1}{r}\frac{\partial}{\partial r}\left(r\frac{\partial c}{\partial r}\right)=0 \tag{A4}$$

where c is the concentration of water vapour. This can be integrated to give

$$c = a \ln r + b \tag{A5}$$

The boundary conditions which give the greatest flux are

$$c(r = r_1) = 0 \text{ mols m}^{-3}$$

$$c(r = r_2) = 1.34 \text{ mols m}^{-3}$$

where r_1 and r_2 are the inner and outer radii of the copper canister. Then

$$c = 1.34\frac{\ln(r/r_1)}{\ln(r/r_2)} \tag{A6}$$

The corresponding flux of water vapour into the canister for a hydrogen gas pressure of 5 MPa is

$$2\pi w_i D\frac{1.34}{\ln(r_2/r_1)} = \frac{1.483}{\ln(r_2/r_1)} \text{ mols year}^{-1} \tag{A7}$$

where D is the diffusion coefficient of water vapour through hydrogen gas. These calculations lead to consideration of two canister failure scenarios. In Case 1, the copper canister has a circumferential crack at its base, and the carbon steel canister has a circumferential crack at its top. In Case 2, both the copper and carbon steel canisters have circumferential cracks near their tops.

2. Water Vapour Diffusion and Consumption in Annulus

The small width of the annulus limits the diffusion of water vapour into the canister. Assume that the annulus is filled with hydrogen gas at a pressure p_i, through which water vapour diffuses. The steady-state equation which describes the diffusion process along the length of the annulus z, is

$$D\frac{d^2c}{dz^2}+s=0 \qquad (A8)$$

where c is the number of moles of water vapour per unit length of the annulus, and s is the number of moles of water consumed by corrosion per unit length of the iron canister. D is the diffusion coefficient of water vapour through hydrogen gas, given by

$$D(p_i, T=30°C)=\frac{1}{p_i}D(1\ \text{atm}, T=30°C) \qquad (A9)$$

$$D(1\ \text{atm}, T=30°C)=0.9\times10^{-4}\ m^2s^{-1} \qquad (A10)$$

If the origin of the coordinate sytem is at the position of the crack in the outer canister, the boundary conditions are that c(z = 0) is given by the product of the cross-sectional area of the annulus and the saturation concentration of the water vapour

$$c(z=0)=2\pi r_1 w_a \times 1.34\ \text{mols}\ m^{-3} \qquad (A11)$$

and that

$$\frac{\partial c}{\partial z}(z=0)=0 \qquad (A12)$$

where w_a is the width of the annulus. If s is independent of height in the annulus, then equation (A8) can be integrated to give

$$c(z)=-\frac{s}{D}z^2+c(z=0) \qquad (A13)$$

It follows from this expression that for a hydrogen gas pressure of 5 MPa and a corrosion rate of 1μm/year

$$\left(\frac{D}{s}c(z=0)\right)^{0.5}=3.3\text{m} \qquad (A14)$$

is the maximum distance through which water vapour can diffuse in the annulus.

3. Water Vapour Transport Inside the Canister

A detailed description of the transport of water and water vapour inside the canister is not included. However, the following model seems reasonable.

- The inflow of water to the canister is limited by the permeability of the surrounding geology. Water inside the canister is distributed between the annulus and the inner canister in a way which depends only on the position of the cracks in the canister.

- If the annulus contains water, but the inner canister is empty, then the inner canister will corrode at a rate which is limited by the flux of water vapour from the annulus to the inner canister.

  If the annulus is empty, but the inner canister contains water, then the annulus will corrode at a rate which is limited by the flux of water vapour from both the inner canister and the surrounding geology to the annulus.

- If the canister is empty of water, then corrosion will continue at a rate which is limited by the flux of water vapour from the surrounding geology into the canister. For Case 1 the flux of water vapour into the annulus is

$$18.1\frac{w_2}{p_i} \text{ mols year}^{-1} \tag{A15}$$

  but there is no flux of water vapour into the inner canister, since the vapour would have to diffuse the length of the annulus. Similarly for Case 2, the flux of water vapour into the annulus can be found. A fraction of this will diffuse along the annulus, while the remainder will diffuse into the inner canister.

In addition to undergoing the above transport processes, water in the canister is consumed by the corrosion reaction. Water in the annulus is assumed to be consumed by the corrosion reaction in the annulus at a rate

$$\mu(A_2+\alpha A_w)\frac{4}{3}\frac{\rho z_{H_2O}}{z_{Fe}} \text{ cm}^3\text{year}^{-1} \tag{A16}$$

(where ρ is the density of iron, z_{Fe} is the molar weight of iron and z_{H_2O} is the molar weight of water) and water in the inner canister is consumed by the corrosion reaction in the inner canister at a rate

$$\mu A_1\frac{4}{3}\frac{\rho z_{H_2O}}{z_{Fe}} \tag{A17}$$

A2.3 Precipitation of Magnetite on Steel Canister

It is also necessary to model the growth of the magnetite layer on the surface of the carbon steel canister. For Case 1, it is assumed that the flows of hydrogen gas and water into and out of the canister will prevent corrosion residue from accumulating in the annulus until after the canister has emptied of water, and that the inner canister will corrode uniformly over its surface for the entire period in which water is present. Once the canister is empty of water, corrosion will take place only in the annulus at a rate which is limited by the diffusion of water vapour into the canister. Corrosion residue will build up at the rate

$$\frac{dt_2}{dt} = 1.1\mu \tag{A18}$$

until the annulus is plugged, and corrosion stops. The factor 1.1 derives from the relative densities of carbon steel and magnetite.

For Case 2, it is assumed that corrosion residue will not accumulate in the annulus until after the annulus has emptied of water, but that the inner canister will always corrode uniformly over its surface. Once the annulus is empty of water corrosion residue will build up in the annulus at the rate

$$\frac{dt_2}{dt} = 1.1\mu \tag{A19}$$

until the annulus is plugged. The inner canister will continue to corrode uniformly over its surface until it is full of corrosion residue.

A2.4 Hydrogen Production

Hydrogen is produced by the corrosion reaction at a rate

$$\frac{dV}{dt} = \frac{4}{3}\frac{\rho}{z_{Fe}} C\, 22.4\ dm^3\ year^{-1} \tag{A20}$$

where C is the total corrosion rate in the canister. The pressure of the hydrogen gas is given by

$$p_i(t) = 0.1\frac{V(t)}{0.4 + 0.02 + B(t) - Q_1(t) - Q_2(t) - W_1(t) - W_2(t)}\ MPa \tag{A21}$$

FIGURE LEGENDS

Figure 1 Schematic of the barometric cell design used to measure hydrogen production rates via a liquid displacement technique. The diameter of the precision bore tubing is 1.6mm and di-n-butyl phthalate was used as the low vapour pressure liquid. This arrangement allowed hydrogen gas evolution rates to be determined to within ±0.5 dm^3 (STP) m^{-2} $year^{-1}$ from a total carbon steel surface area of 0.1 m^2.

Figure 2 Rate of hydrogen evolution versus time for carbon steel in standard artificial SKB groundwater[8].

Figure 3 Rate of hydrogen evolution versus time for carbon steel suspended in a humid atmosphere above a solution of artificial SKB groundwater.

Figure 4 Rate of hydrogen evolution versus time for carbon steel partially-submerged in artificial SKB groundwater. Approximately 20% of the carbon steel was below the surface of the solution.

Figure 5 Rate of hydrogen evolution versus time for carbon steel in standard artificial SKB groundwater. The carbon steel was pre-coated with either a magnetite or iron(II) carbonate layer. Approximate thicknesses 50 nm or 500 nm.

Figure 6 Rate of hydrogen evolution from carbon steel wires buried under a mixture of powdered corrosion products versus time. The rate of hydrogen evolution from a control cell containing only the powdered corrosion product, i.e. no carbon steel, is also shown.

Figure 7 Rate of hydrogen evolution versus time for carbon steel in artificial SKB groundwater with either an additional 0.1M $FeSO_4$ or 0.1M K_2SO_4 or saturated with $FeCO_3$.

Figure 8 Rate of hydrogen evolution versus time for carbon steel in artificial SKB groundwater with either an additional 9 mM NH_3 or 3 mM HNO_3 to simulate the products of radiolysis reactions involving nitrogen and water.

Figure 9 Rate of hydrogen evolution versus time for carbon steel in artificial SKB groundwater which is either 10x the strength of the standard composition (Table 1) or contains an additional 0.1M K_2SO_4.

Figure 10 Schematic representation of ACPC with one circumferental crack in each canister.

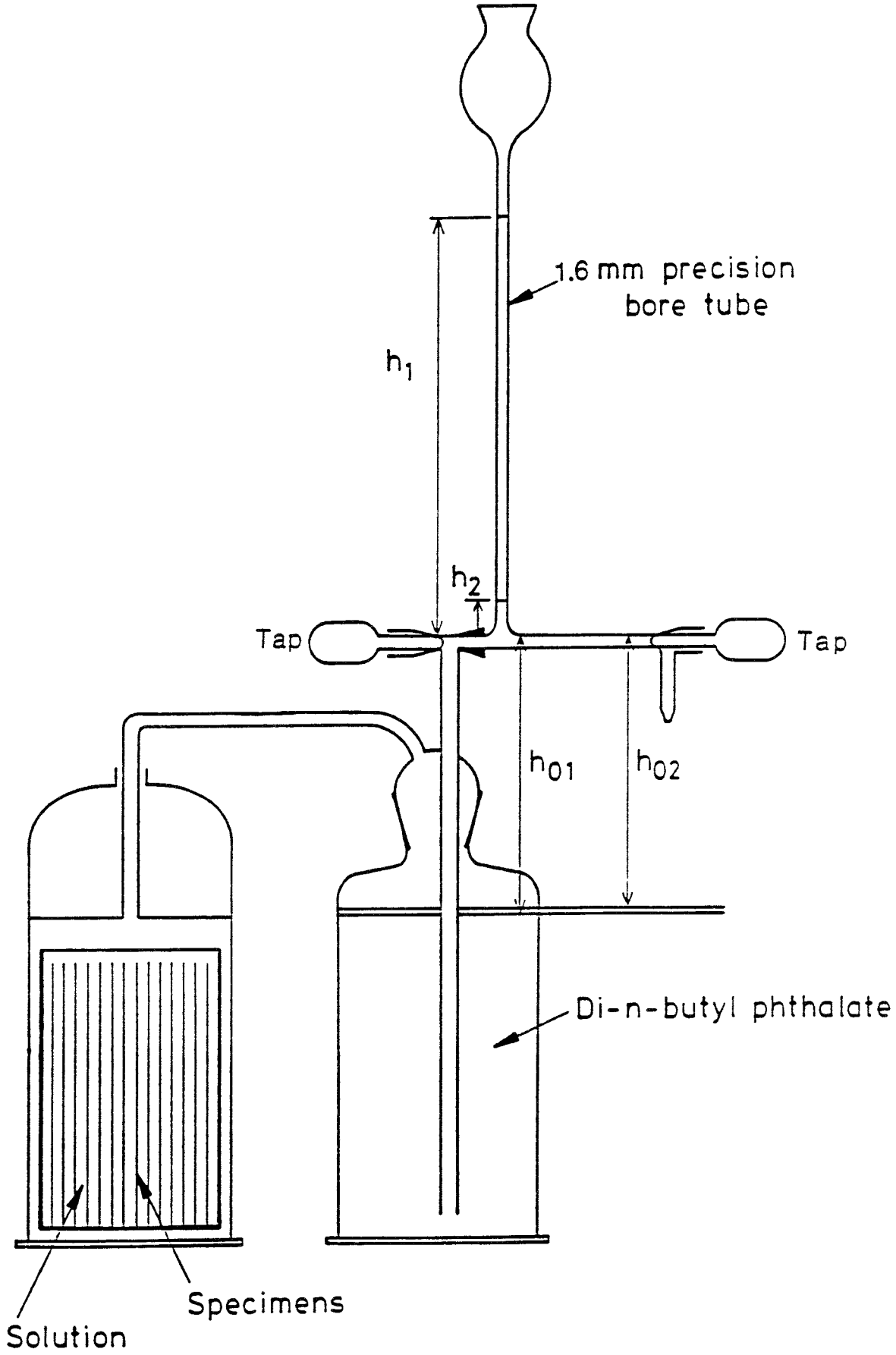

Figure 1. Schematic of the barometric cell design used to measure hydrogen production rates via a liquid displacement technique

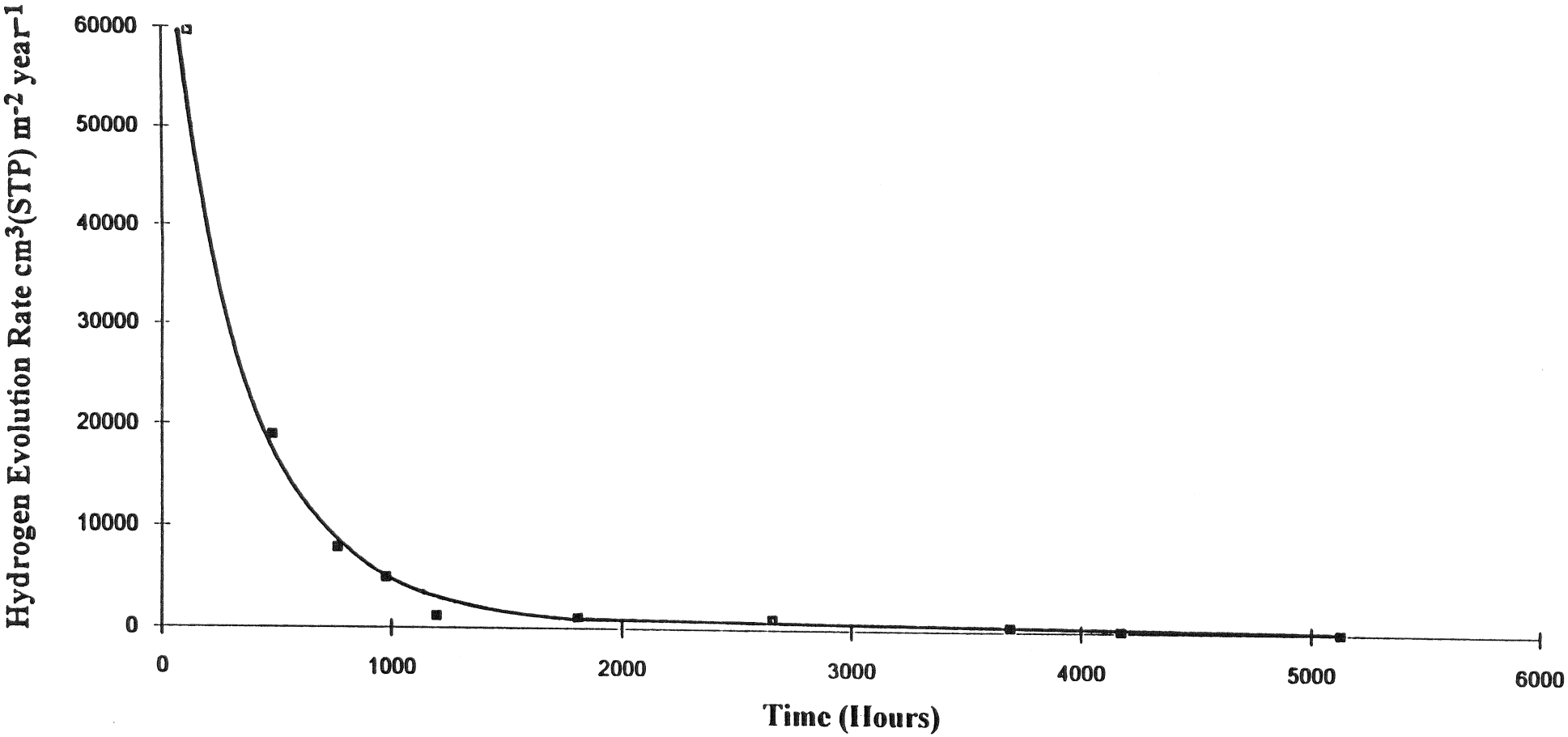

Figure 2. Rate of hydrogen evolution versus time for carbon steel in standard artificial SKB groundwater[8]

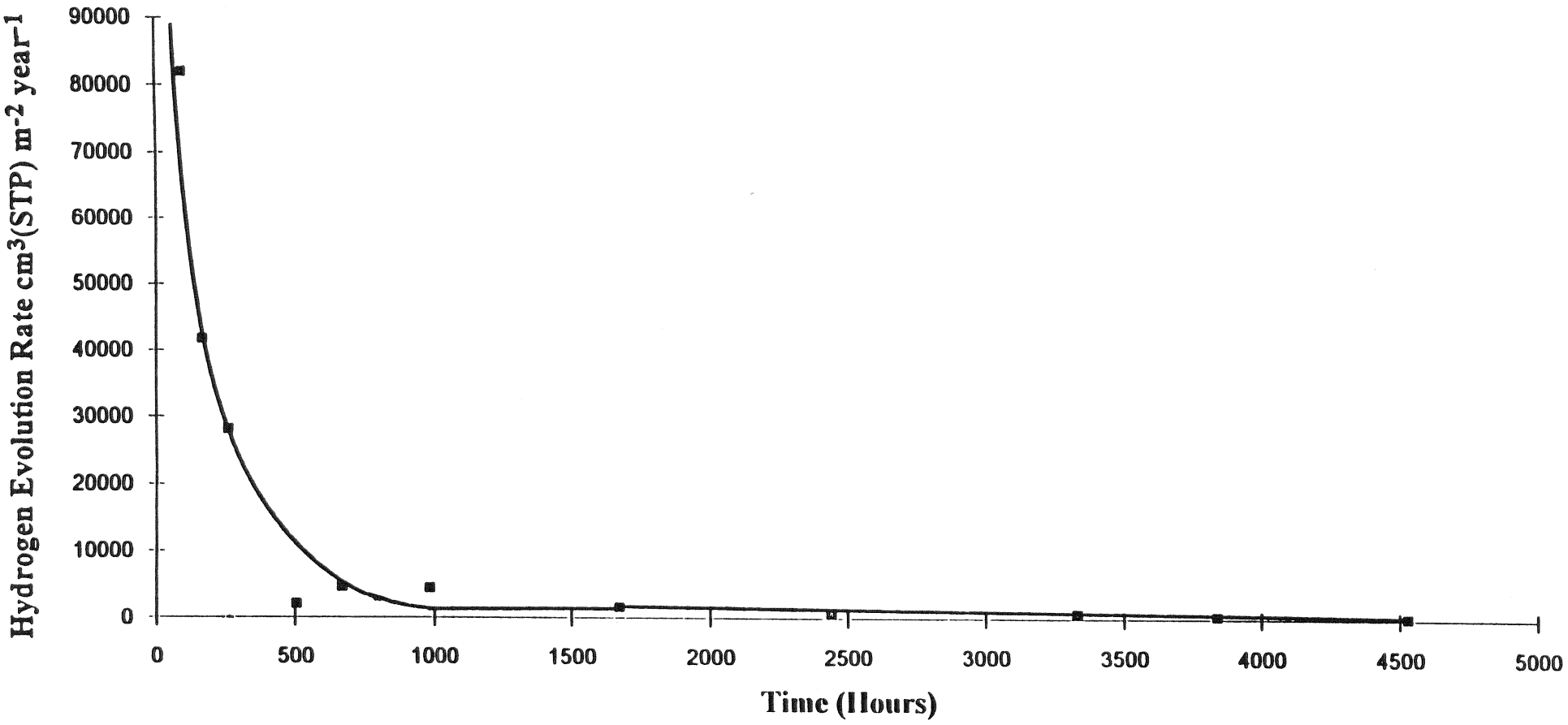

Figure 3. Rate of hydrogen evolution versus time for carbon steel suspended in a humid atmosphere above a solution of artificial SKB groundwater

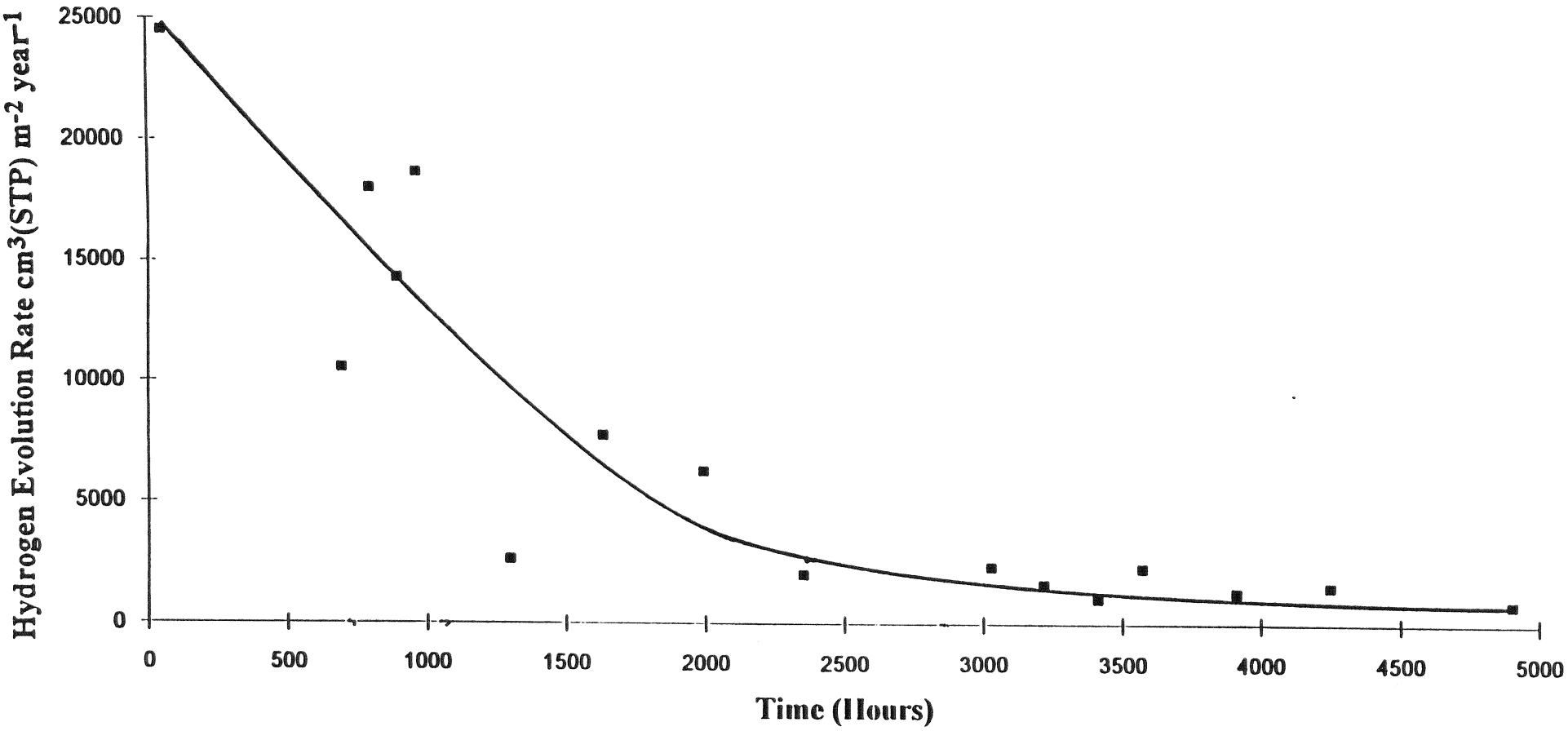

Figure 4. Rate of hydrogen evolution versus time for carbon steel partially-submerged in artificial SKB groundwater. Approximately 20% of the carbon steel was below the surface of the solution

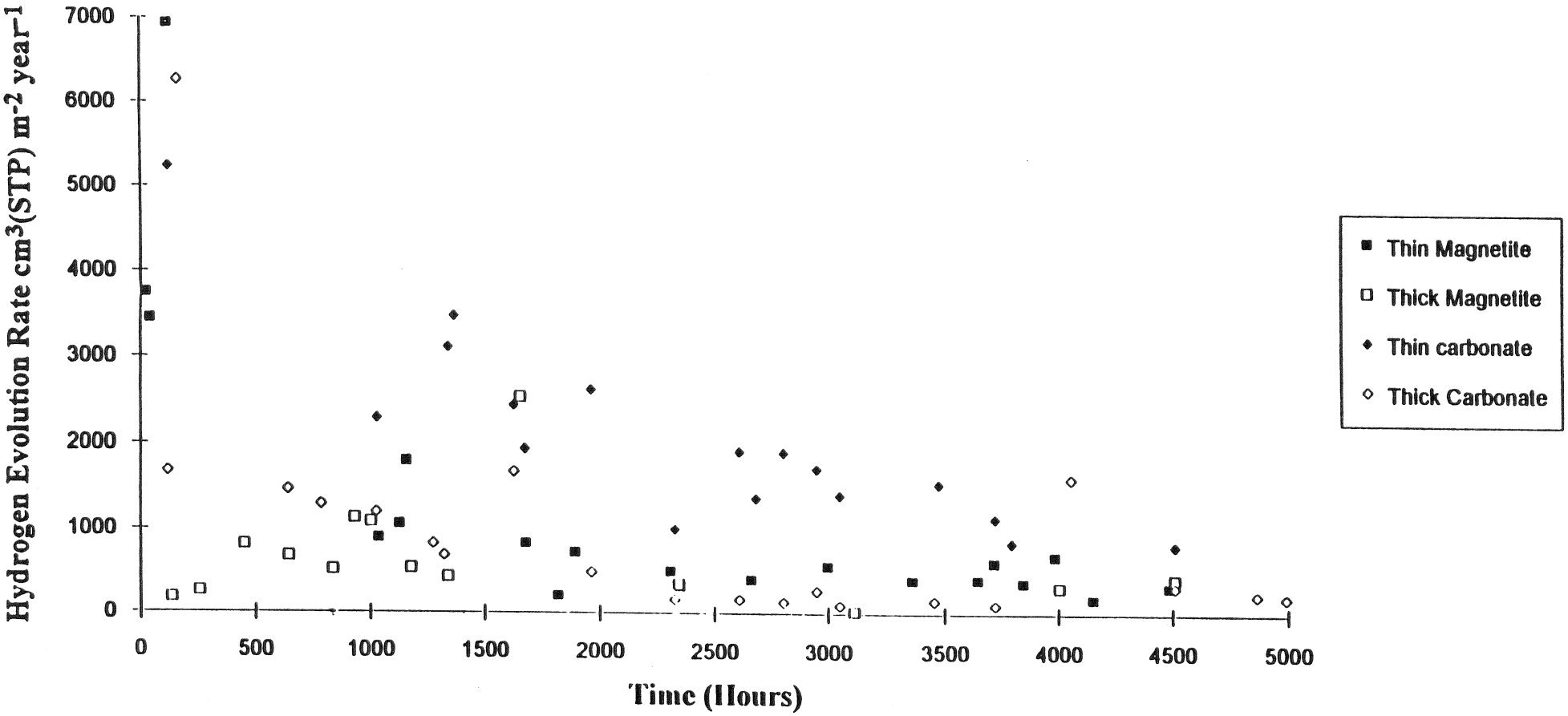

Figure 5. Rate of hydrogen evolution versus time for carbon steel in standard artificial SKB groundwater. The carbon steel was pre-coated with either a magnetite or iron(II) carbonate layer. Approximate thicknesses 50 nm or 500 nm

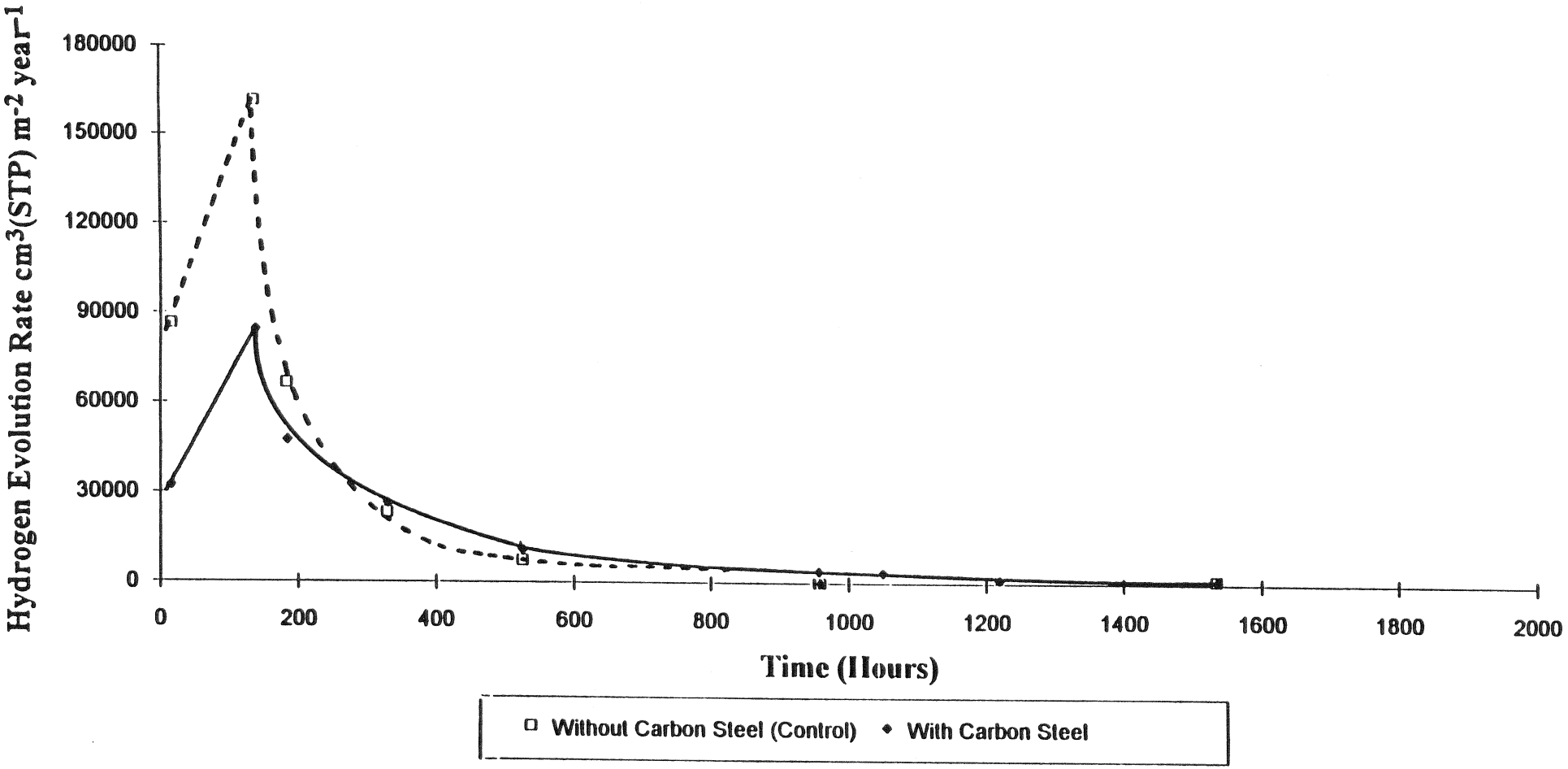

Figure 6. Rate of hydrogen evolution from carbon steel wires buried under a mixture of powdered corrosion products versus time. The rate of hydrogen evolution from a control cell containing only the powdered corrosion product, i.e. no carbon steel, is also shown

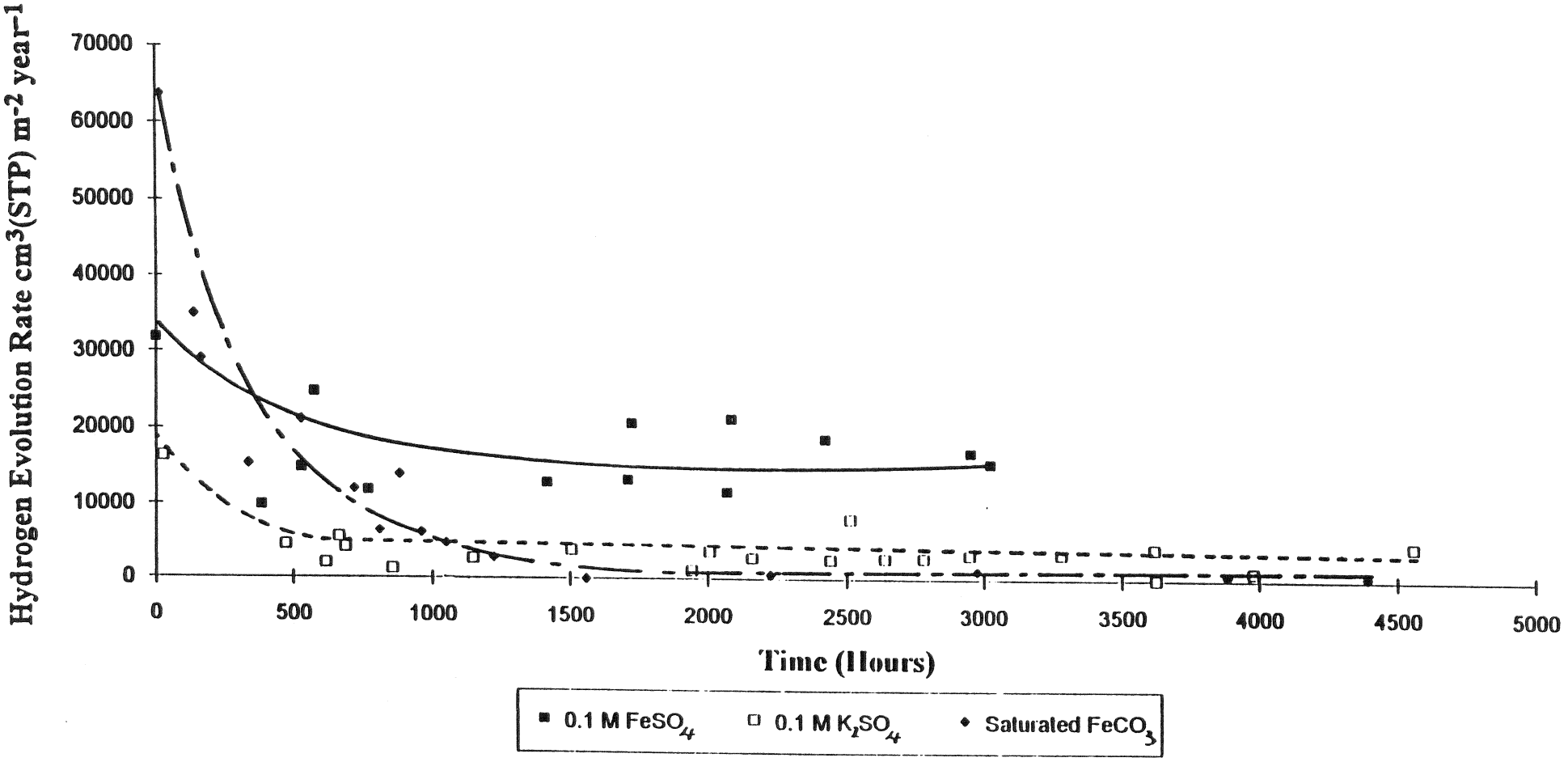

Figure 7. Rate of hydrogen evolution versus time for carbon steel in artificial SKB groundwater with either an additional 0.1M $FeSO_4$ or 0.1M K_2SO_4 or saturated with $FeCO_3$

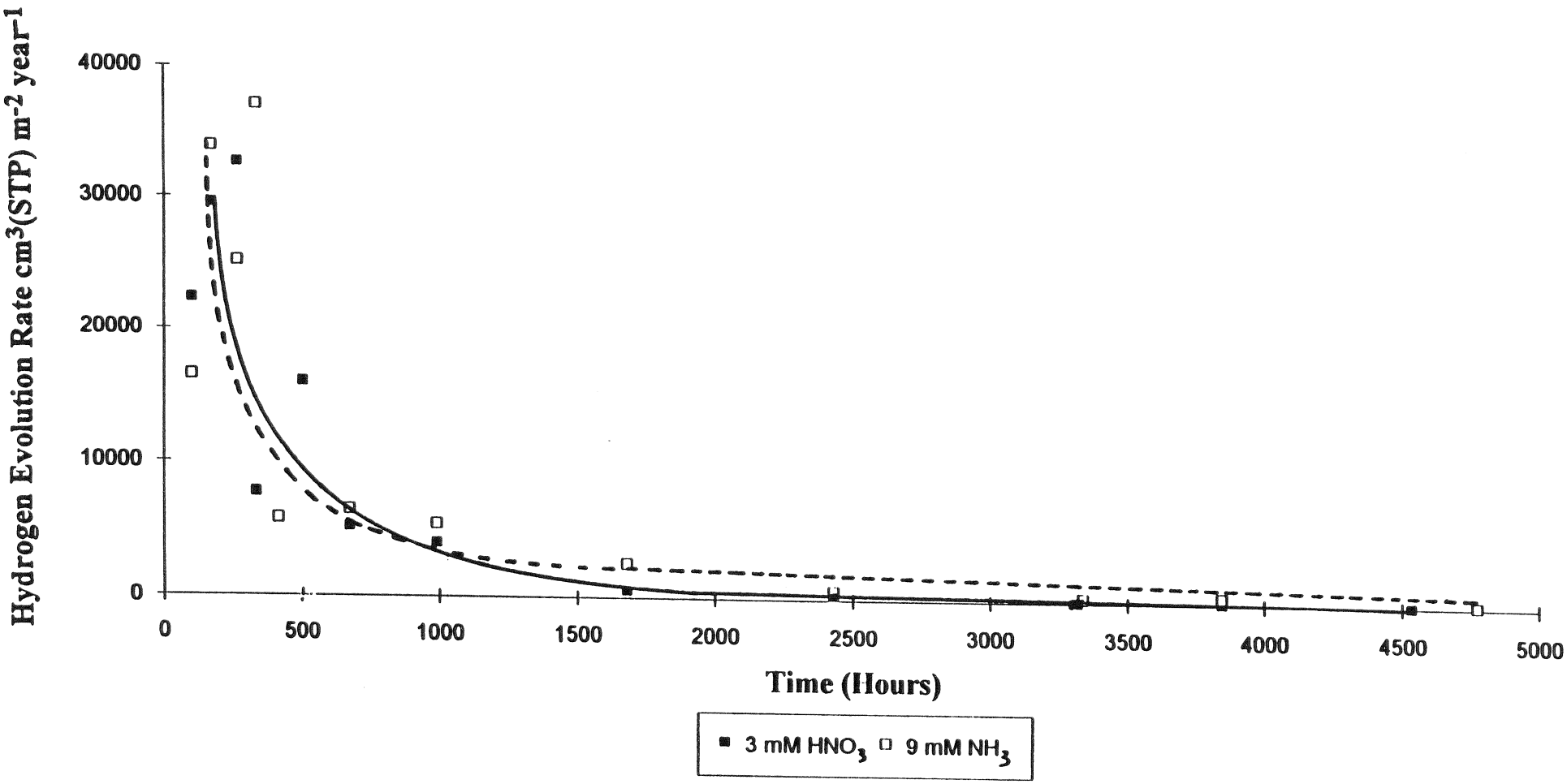

Figure 8. Rate of hydrogen evolution versus time for carbon steel in artificial SKB groundwater with either an additional 9 mM NH_3 or 3 mM HNO_3 to simulate the products of radiolysis reactions involving nitrogen and water

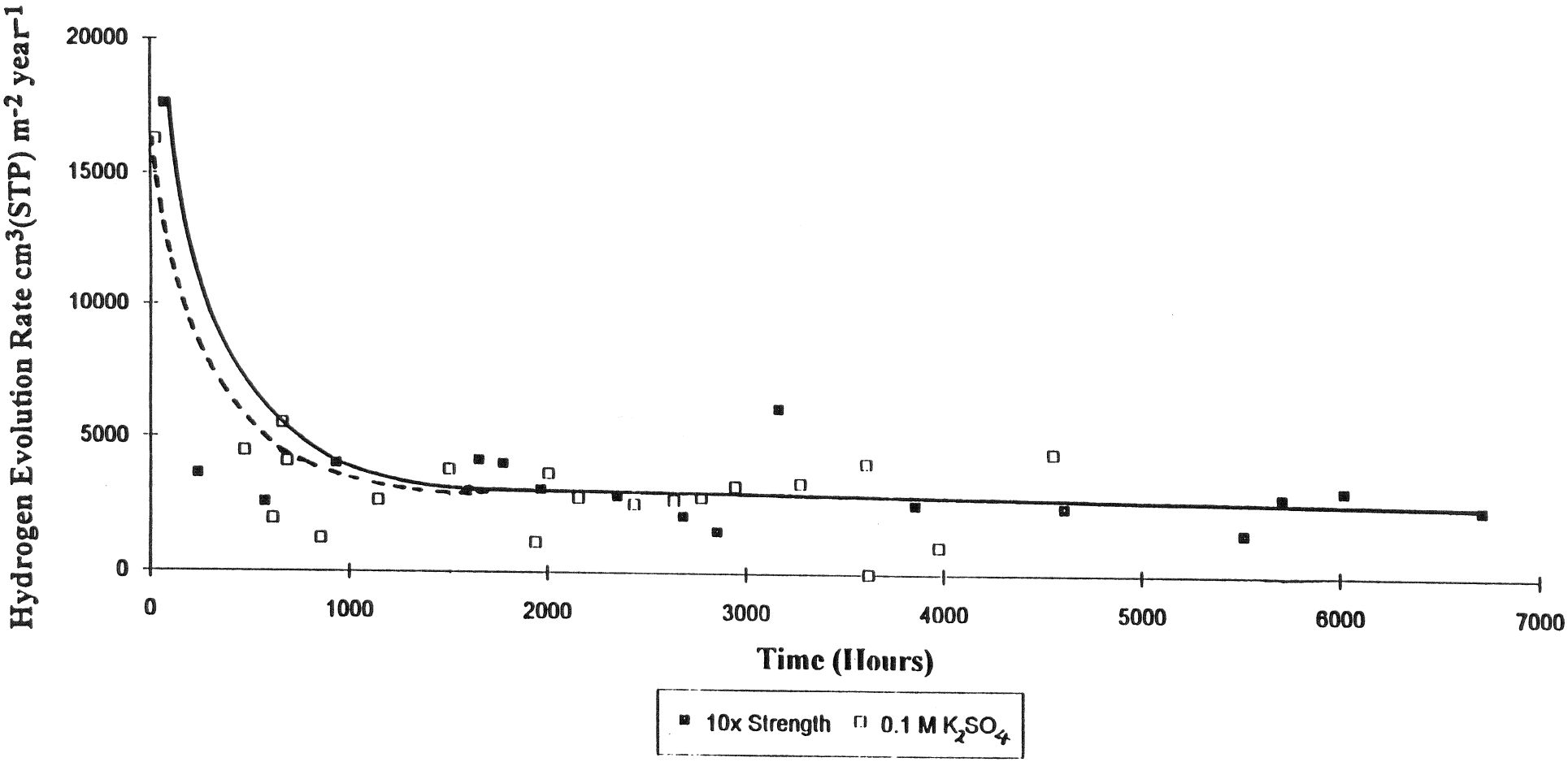

Figure 9. Rate of hydrogen evolution versus time for carbon steel in artificial SKB groundwater which is either 10x the strength of the standard composition (Table 1) or contains an additional 0.1M K_2SO_4

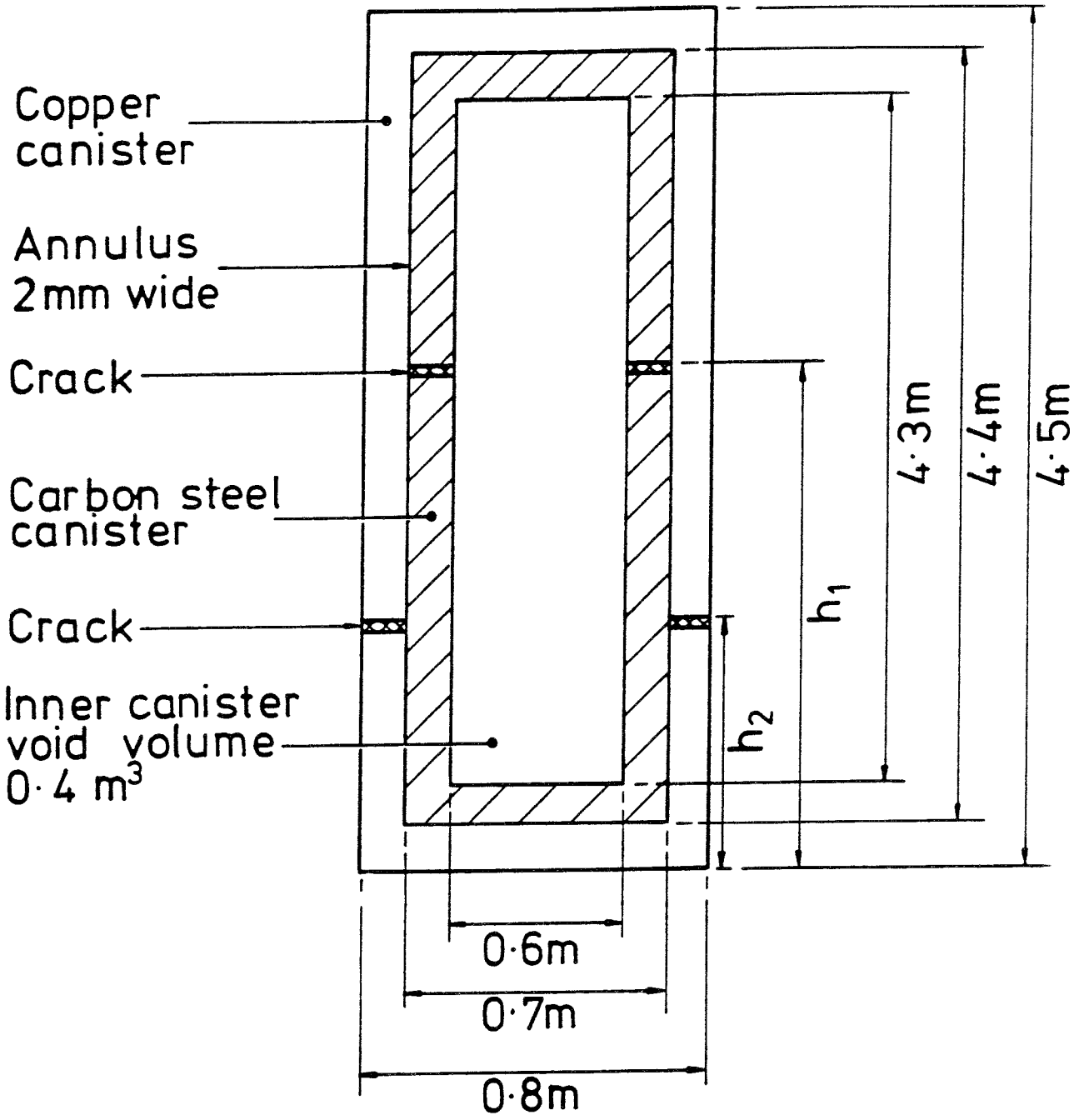

Figure 10. Schematic representation of ACPC with one circumferental crack in each canister

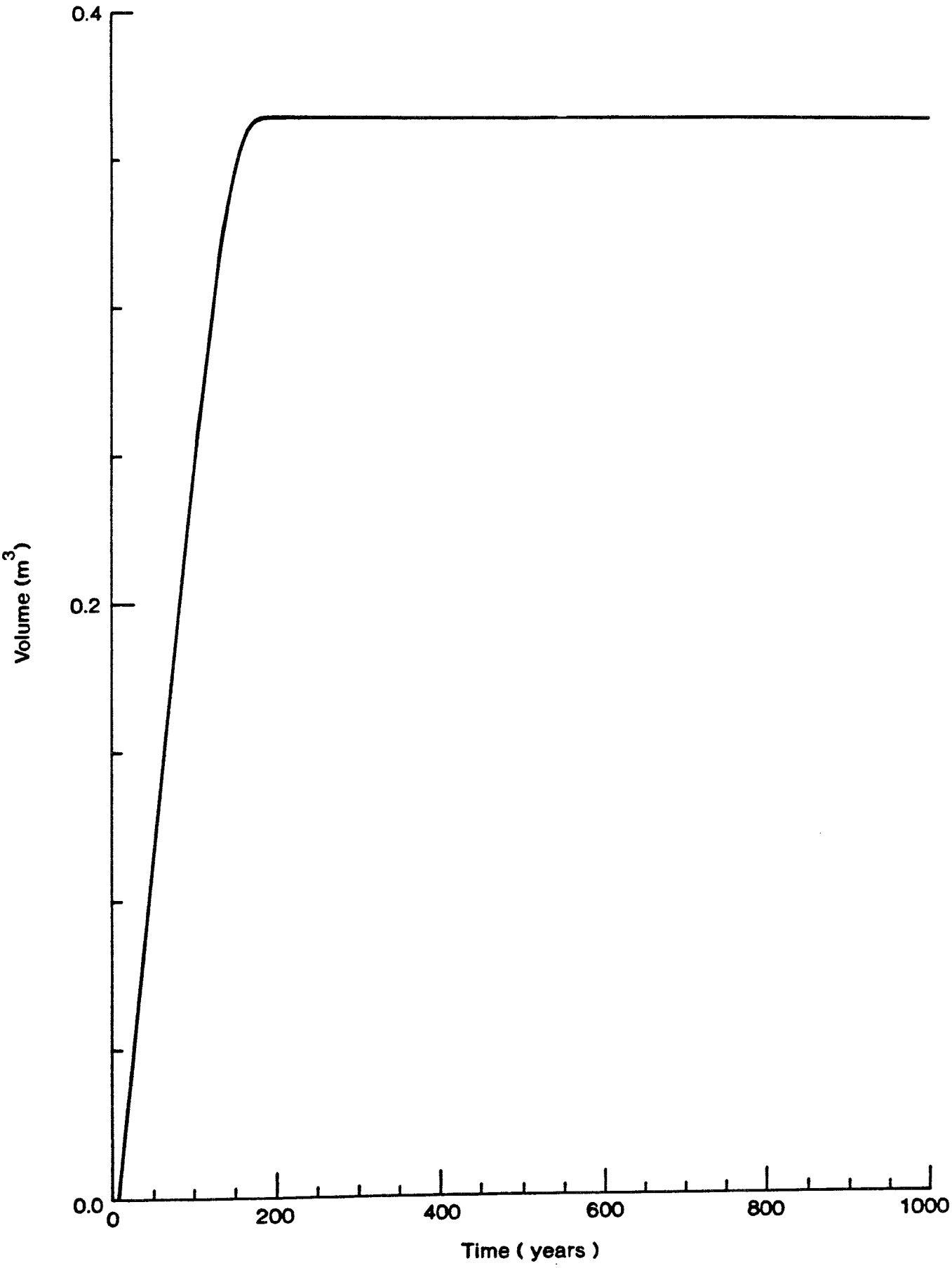

Figure 11. Predicted volume of water in inner canister for base case parameters and crack in outer canister at base (Case 1)

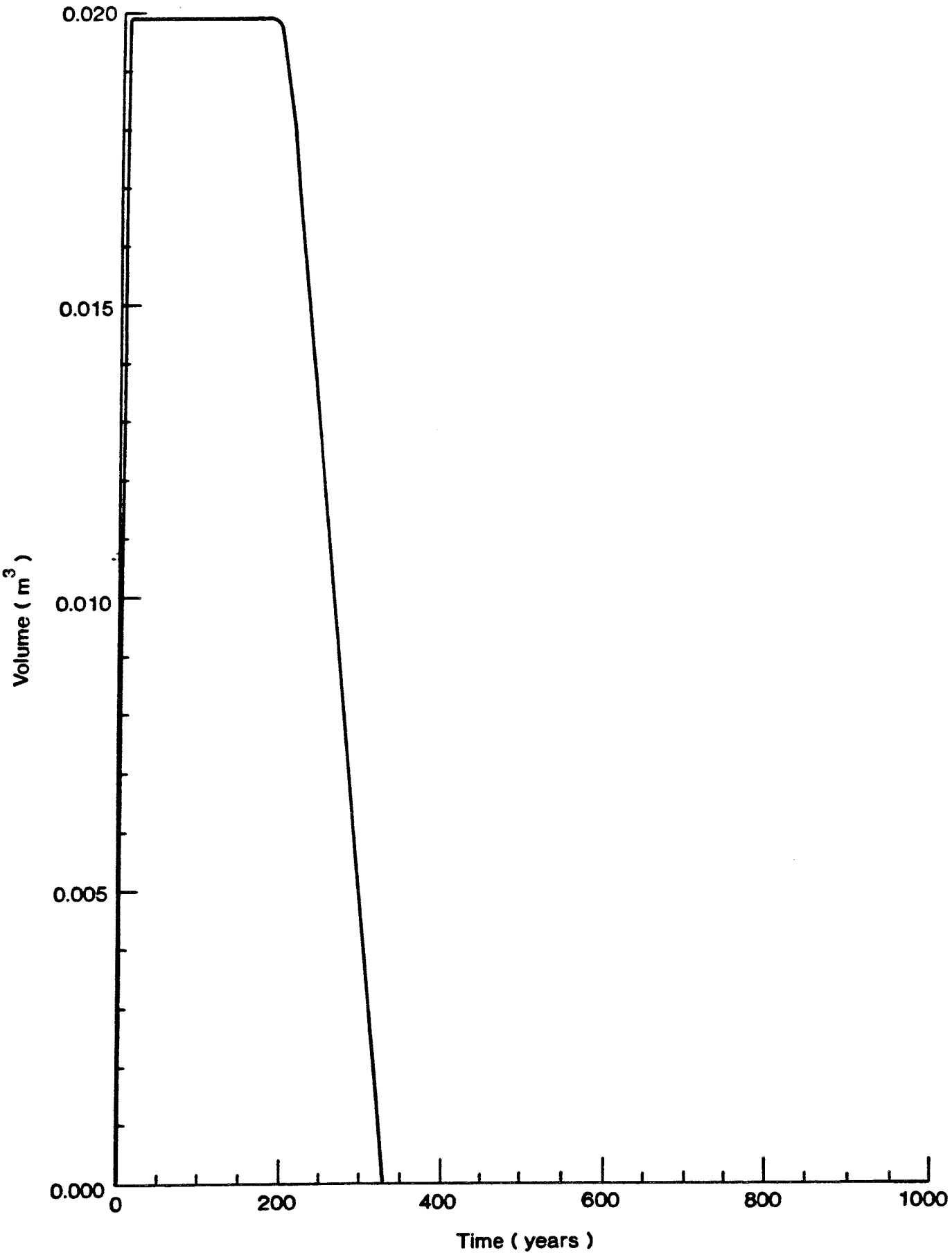

Figure 12. Predicted volume of water in annulus for base case parameters and crack in outer canister at base (Case 1)

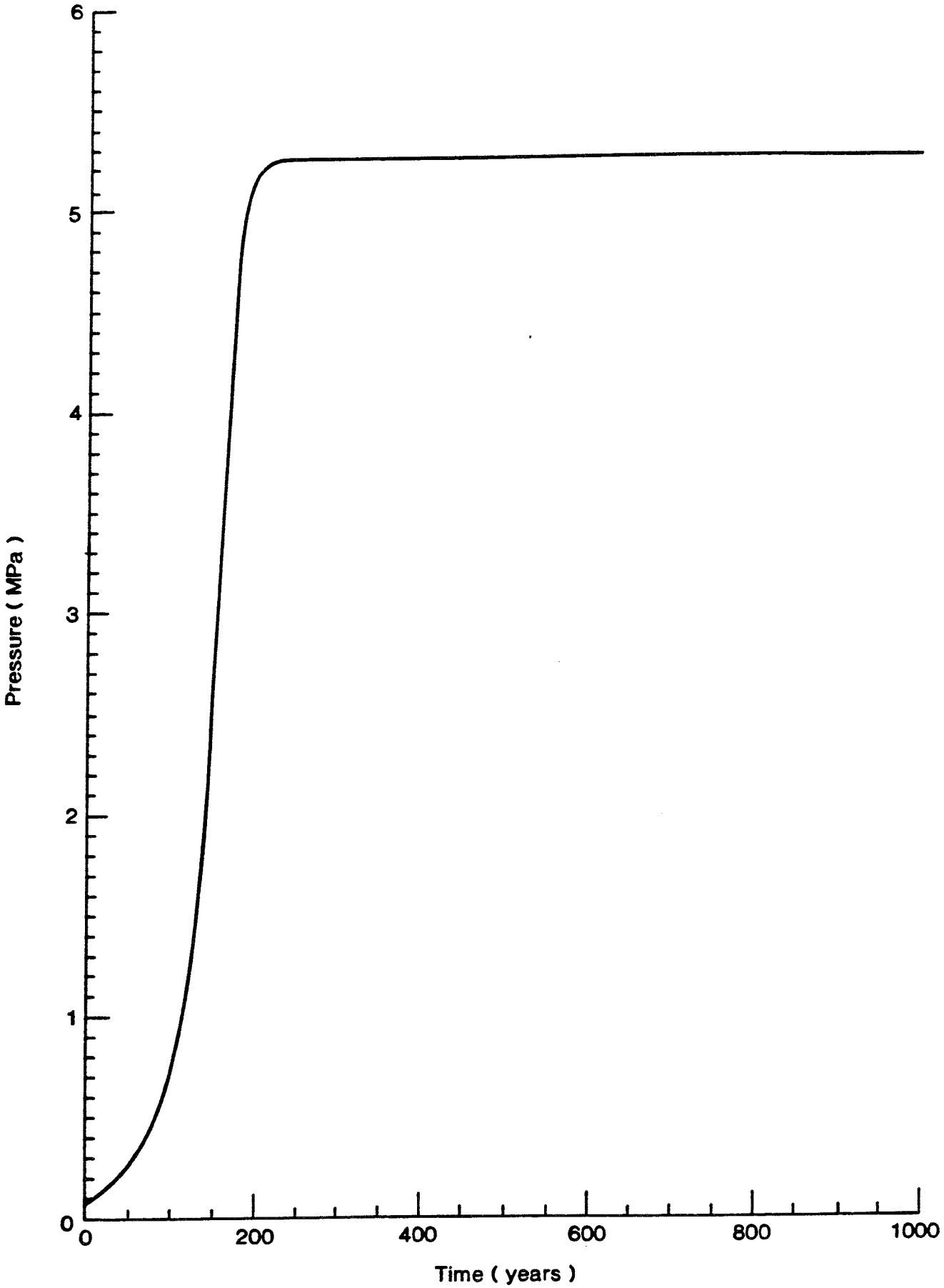

Figure 13. Predicted pressure of hydrogen gas in the canister for base case parameters and crack in outer canister at base (Case 1)

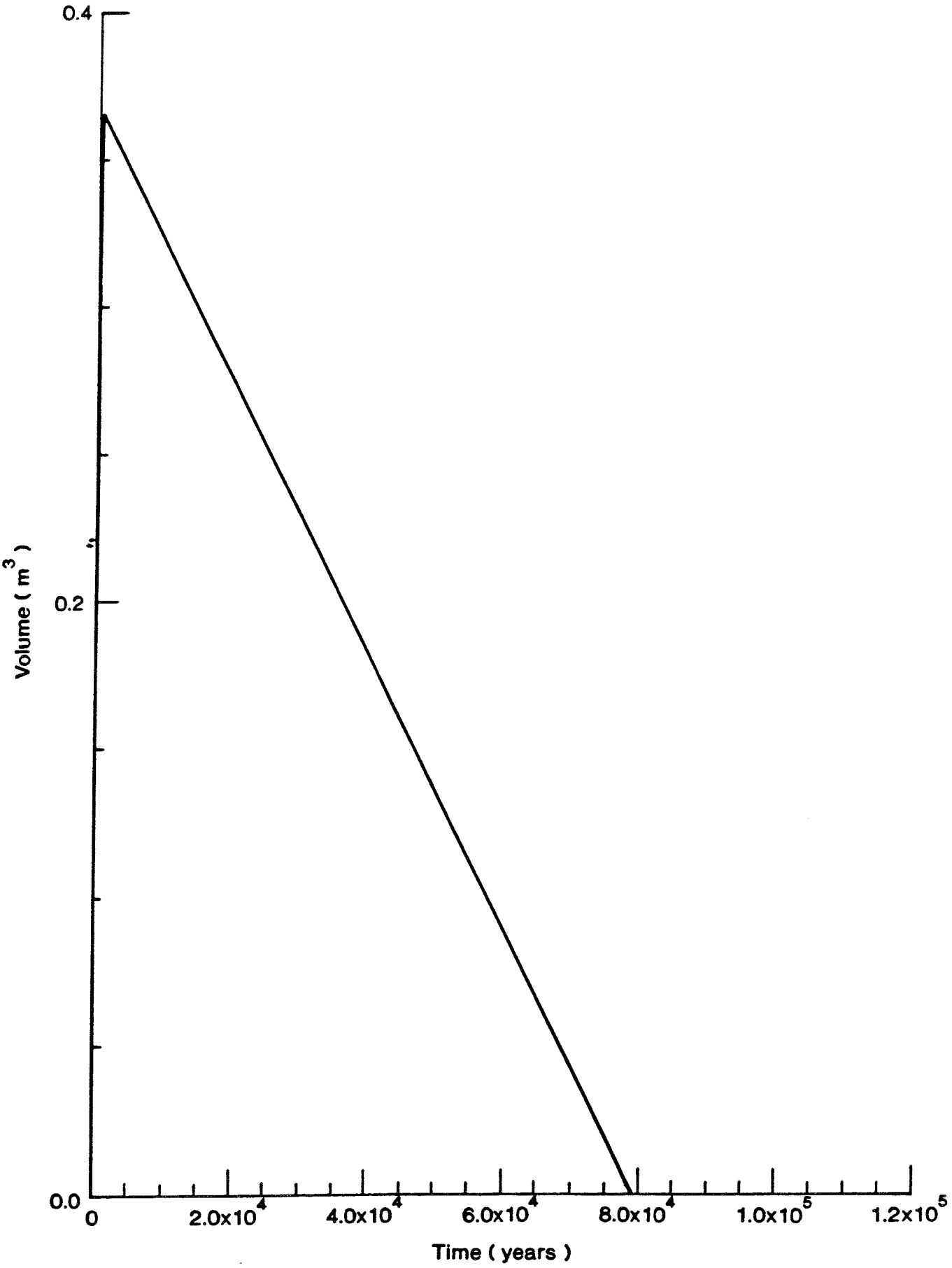

Figure 14. Predicted volume of water in inner canister for base case parameters and crack in outer canister at base (Case 1)

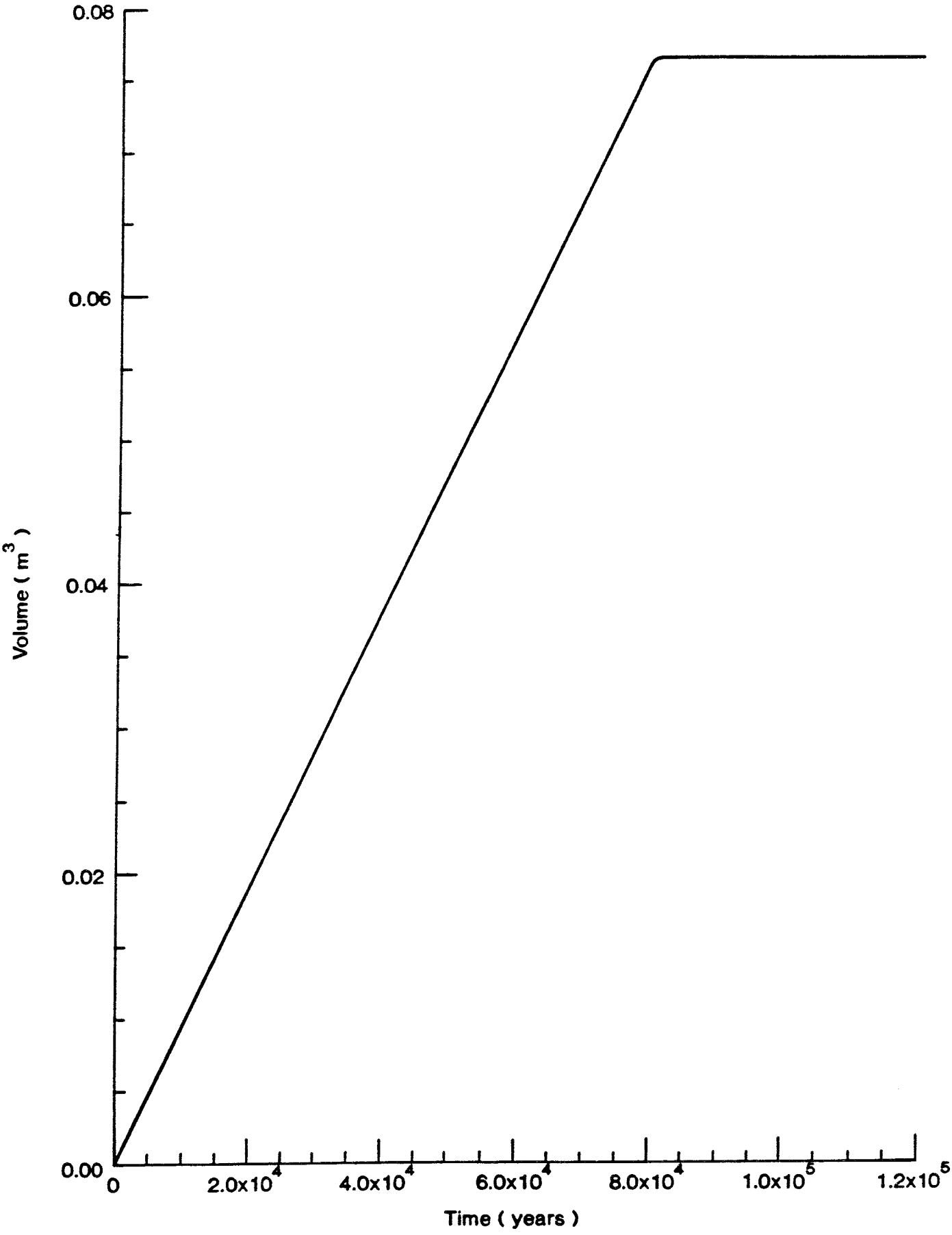

Figure 15. Predicted volume of magnetite in inner canister for base case parameters and crack in outer canister at base (Case 1)

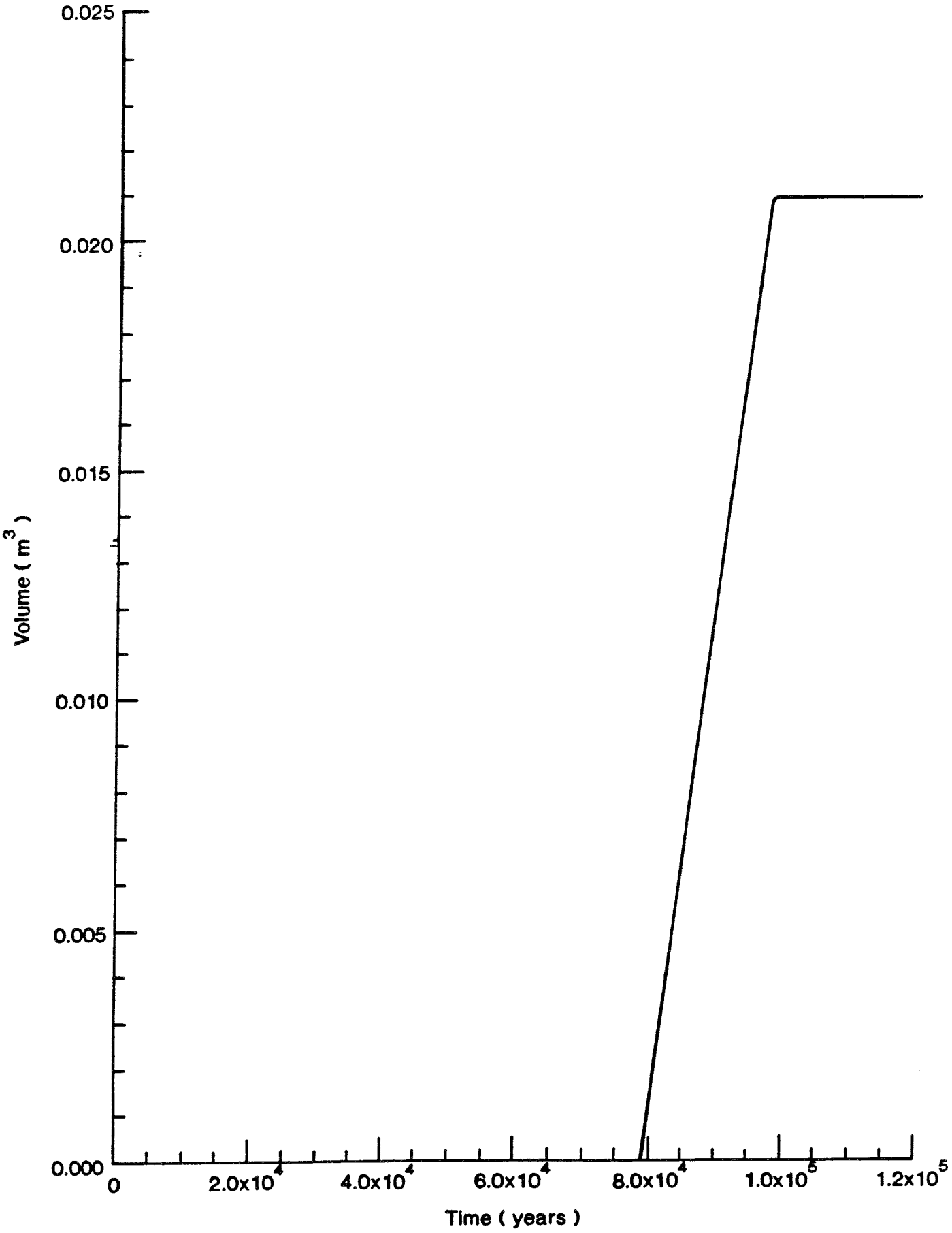

Figure 16. Predicted volume of magnetite in annulus for base case parameters and crack in outer canister at base (Case 1)

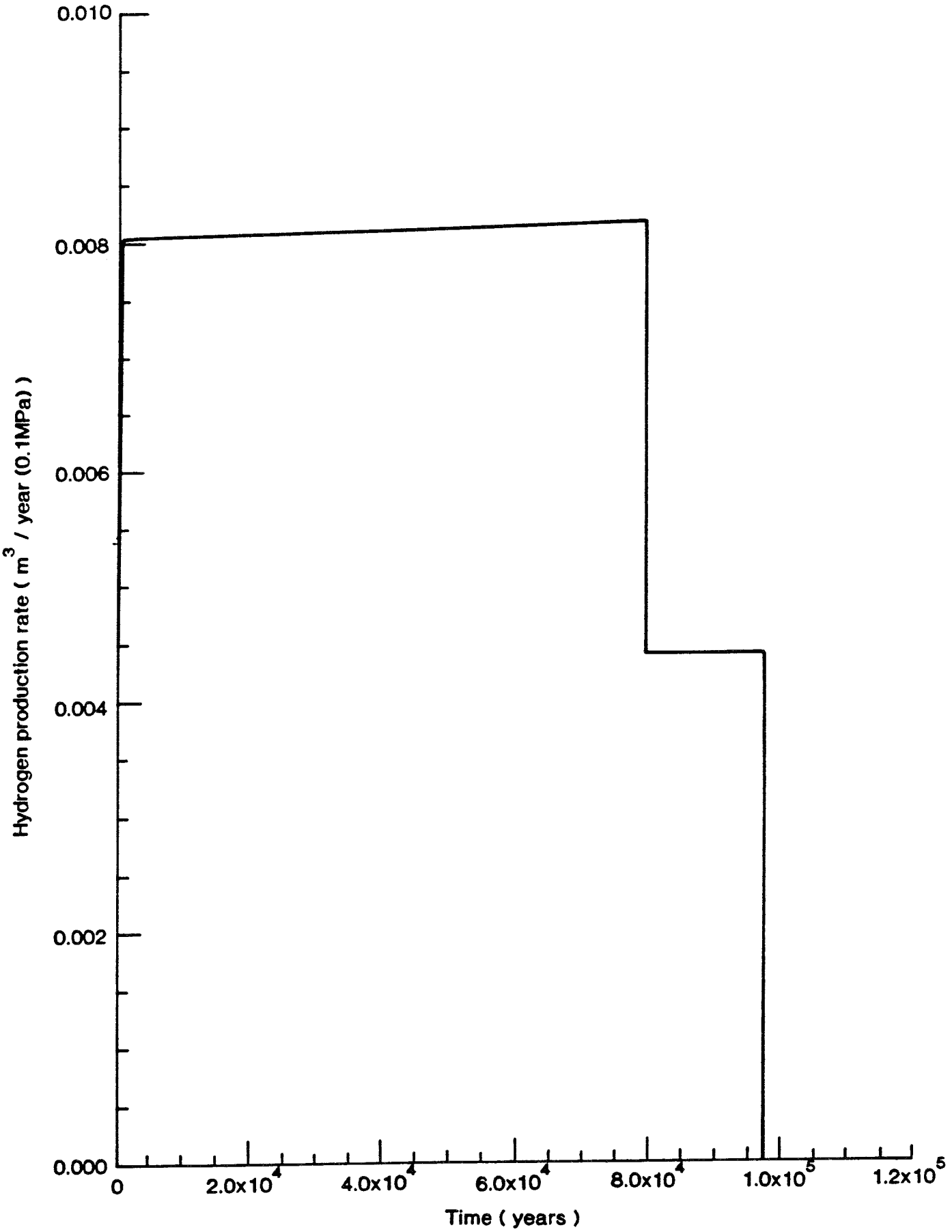

Figure 17. Predicted hydrogen production from canister for base case parameters and crack in outer canister at base (Case 1)

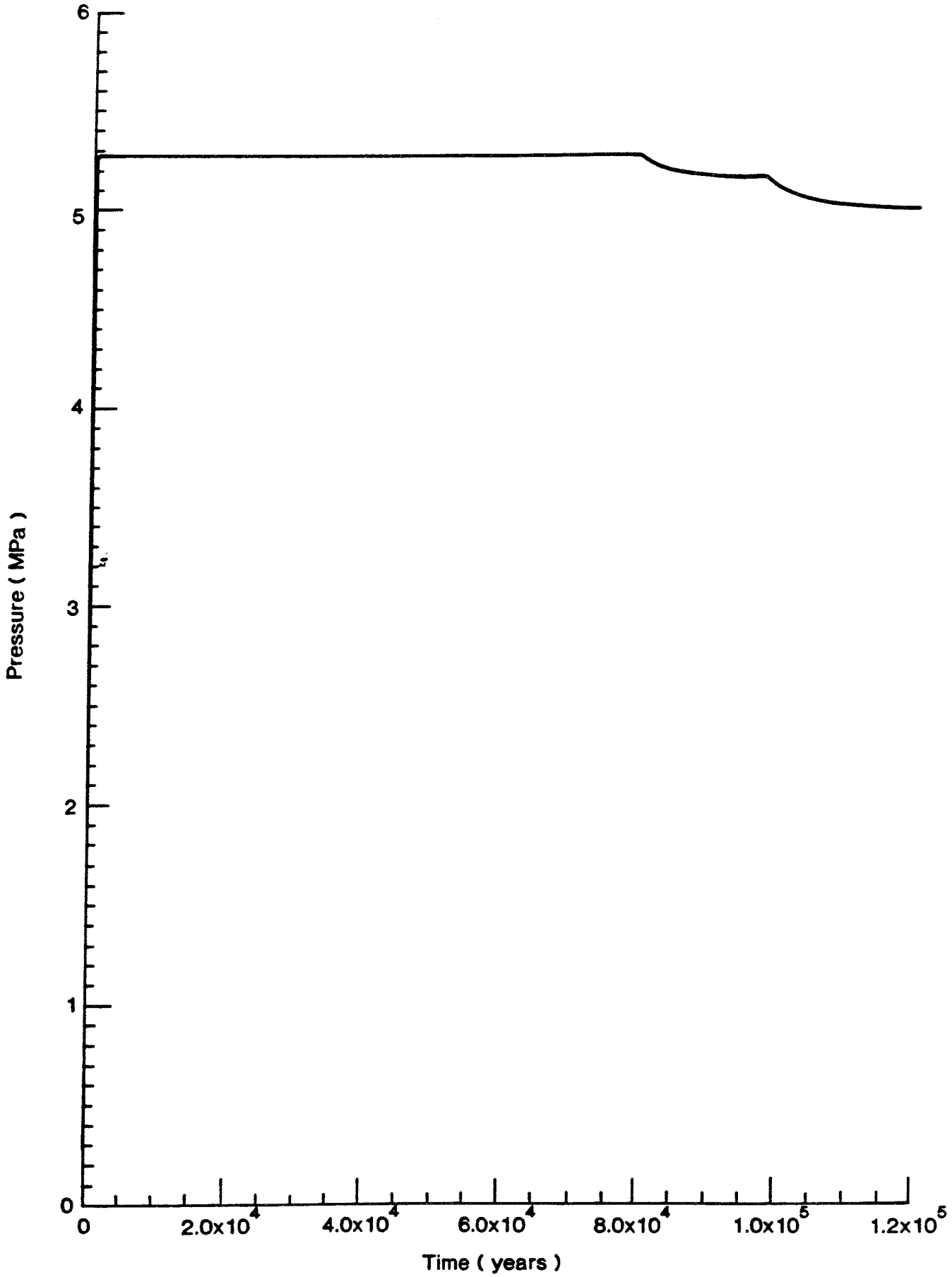

Figure 18. Predicted hydrogen gas pressure for base case parameters and crack in outer canister at base (Case 1)

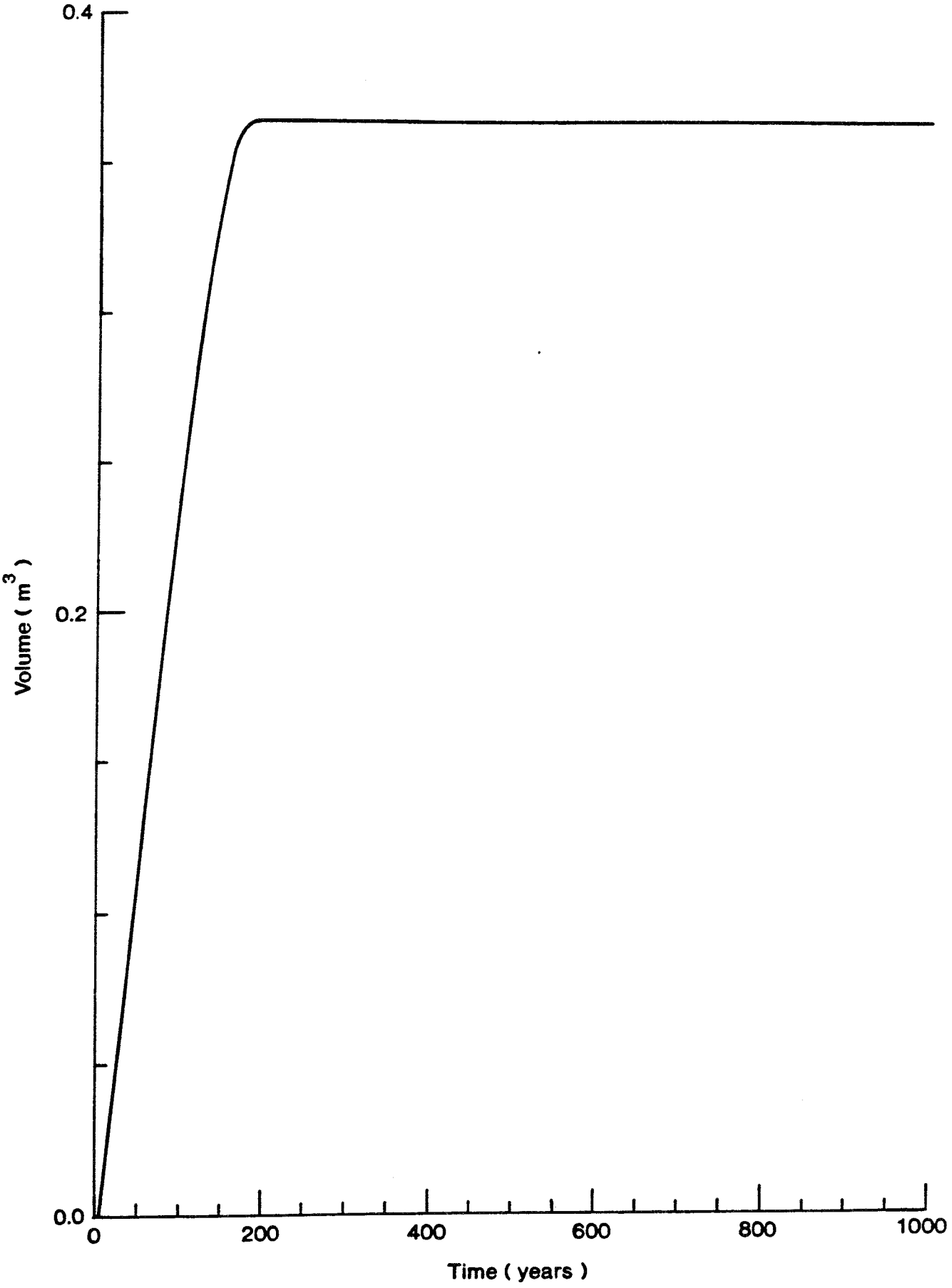

Figure 19. Predicted volume of water in inner canister for base case parameters and crack in outer canister at top (Case 2)

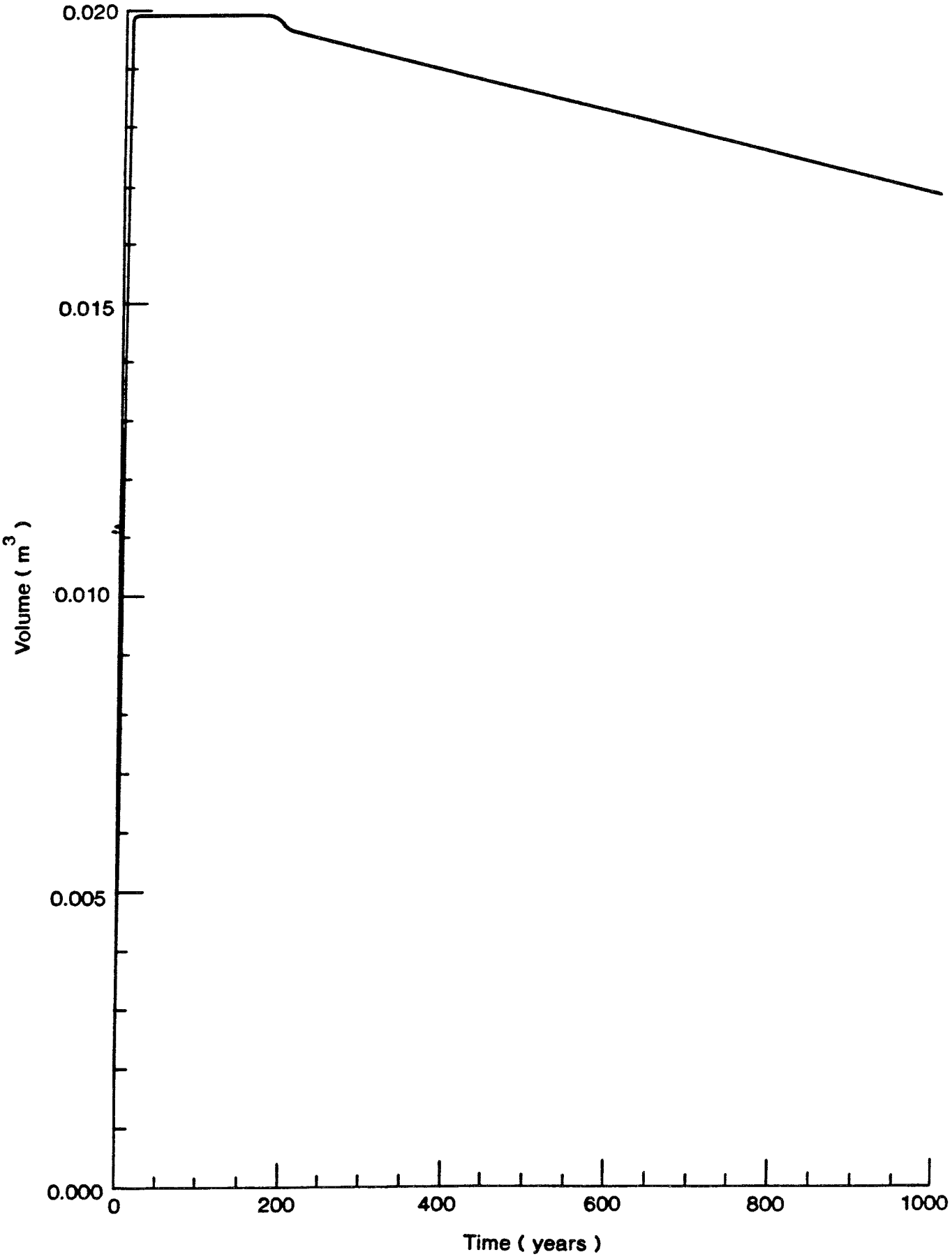

Figure 20. Predicted volume of water in annulus for base case parameters and crack in outer canister at top (Case 2)

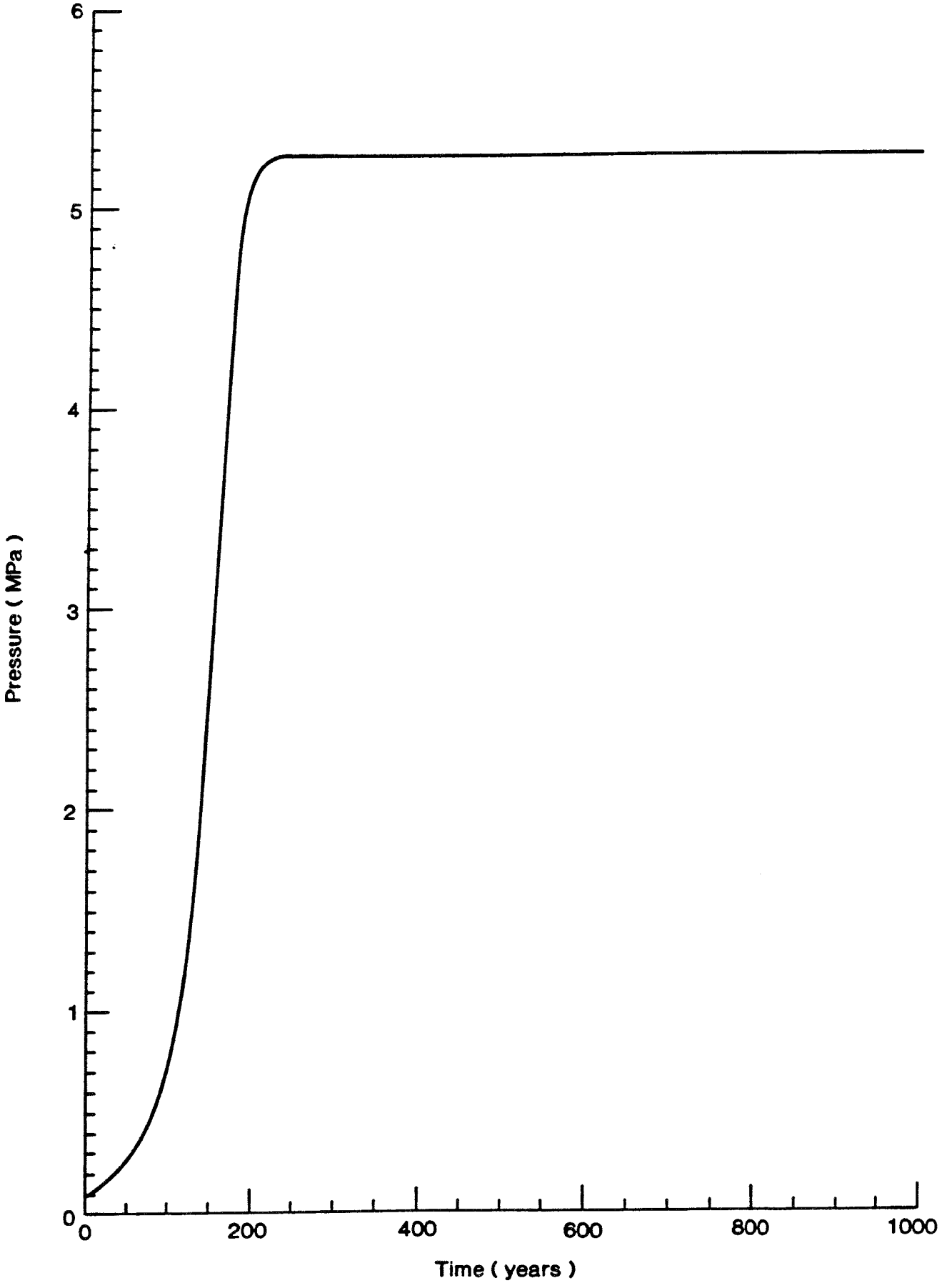

Figure 21. Predicted pressure of hydrogen gas in the canister for base case parameters and crack in outer canister at top (Case 2)

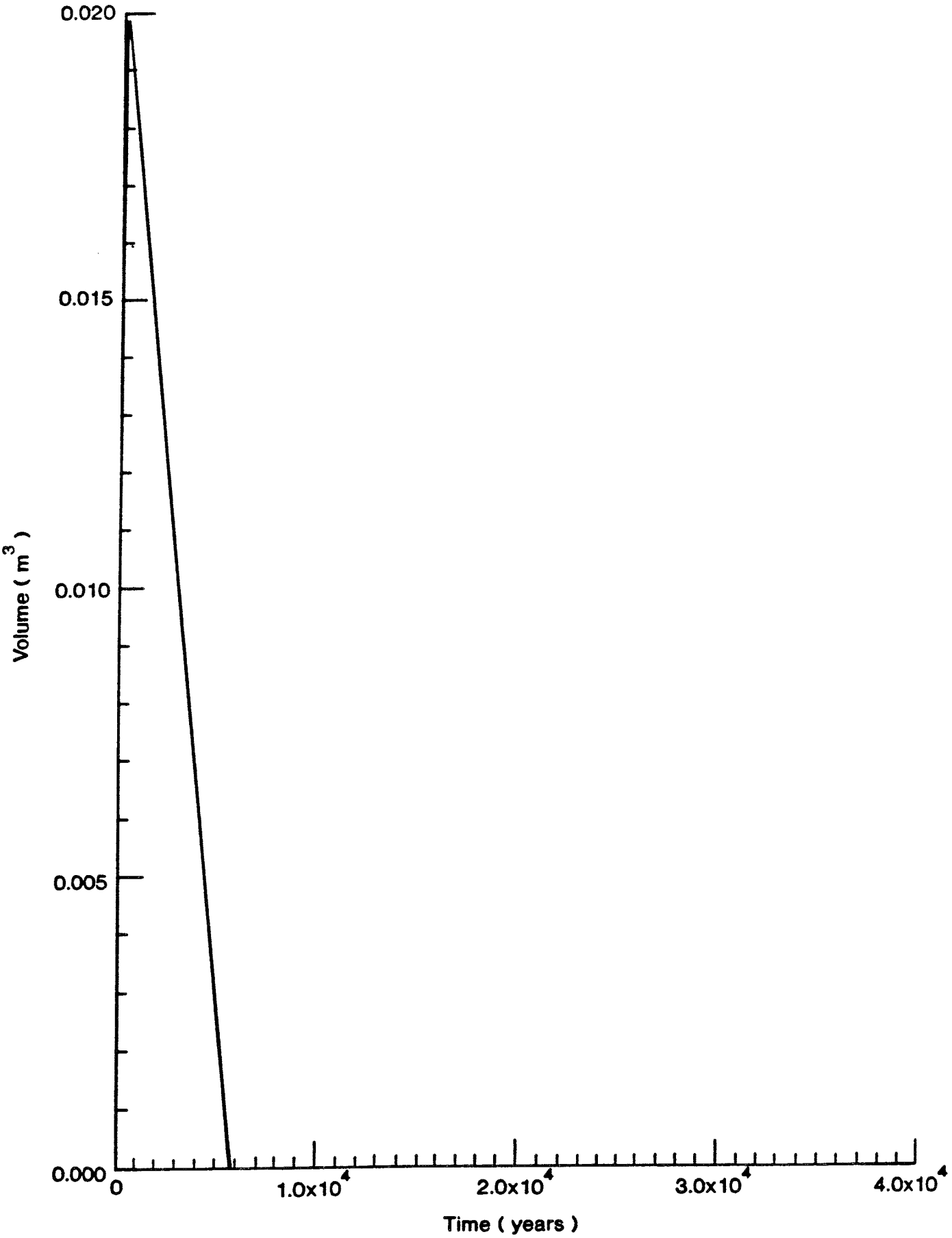

Figure 22. Predicted volume of water in annulus for base case parameters and crack in outer canister at top (Case 2)

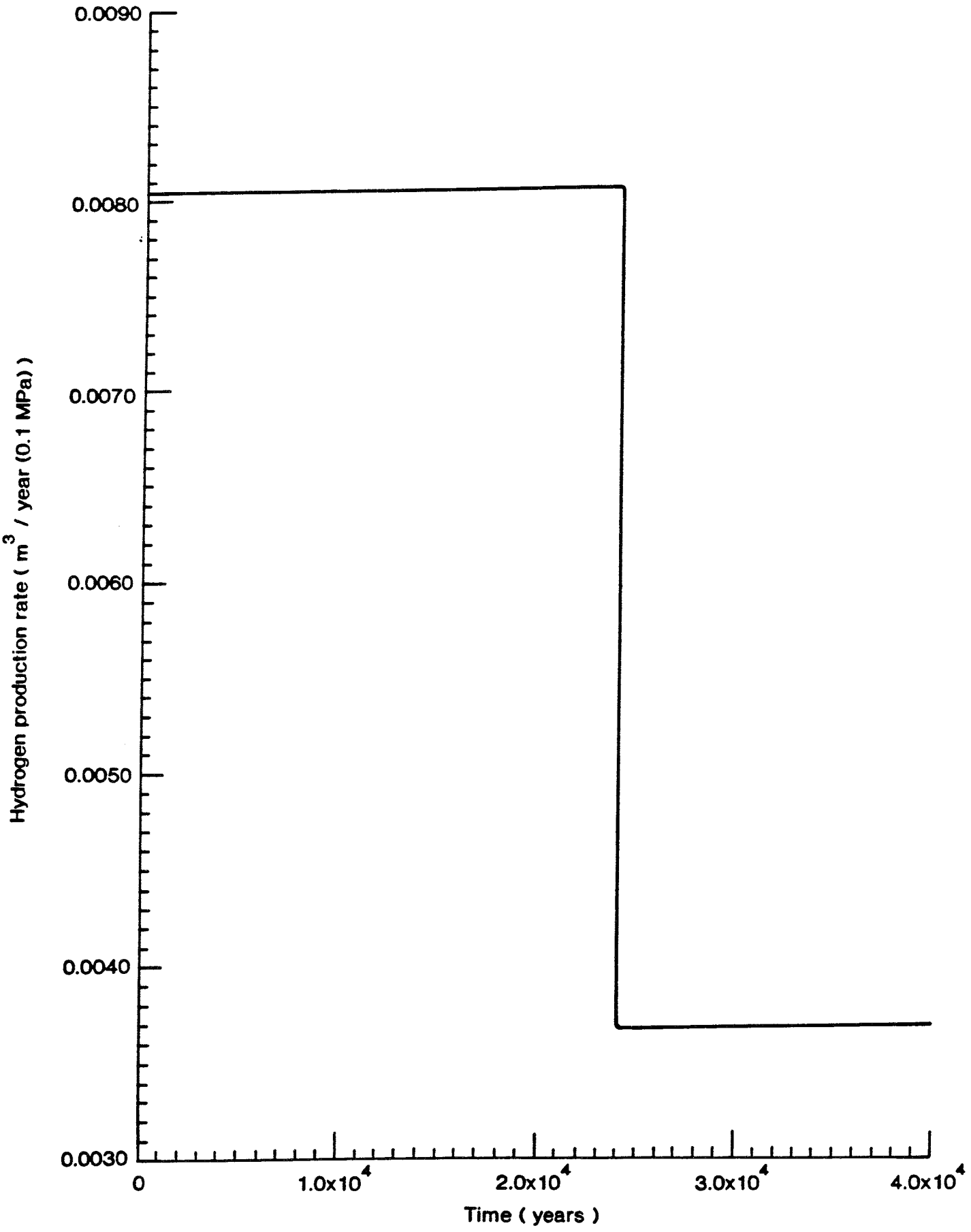

Figure 23. Predicted hydrogen production from canister for base case parameters and crack in outer canister at top (Case 2)

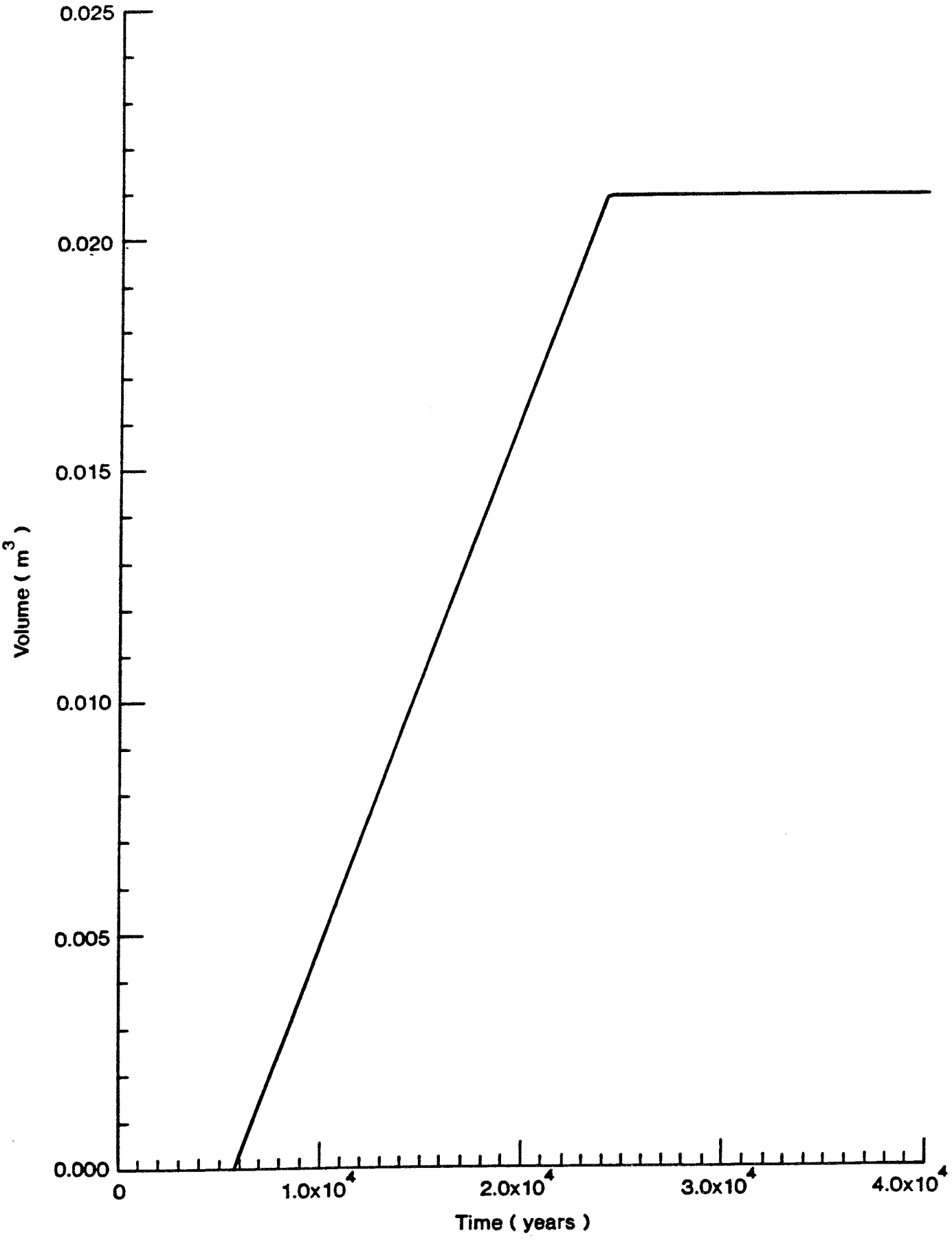

Figure 24. Predicted volume of magnetite in annulus for base case parameters and crack in outer canister at top (Case 2)

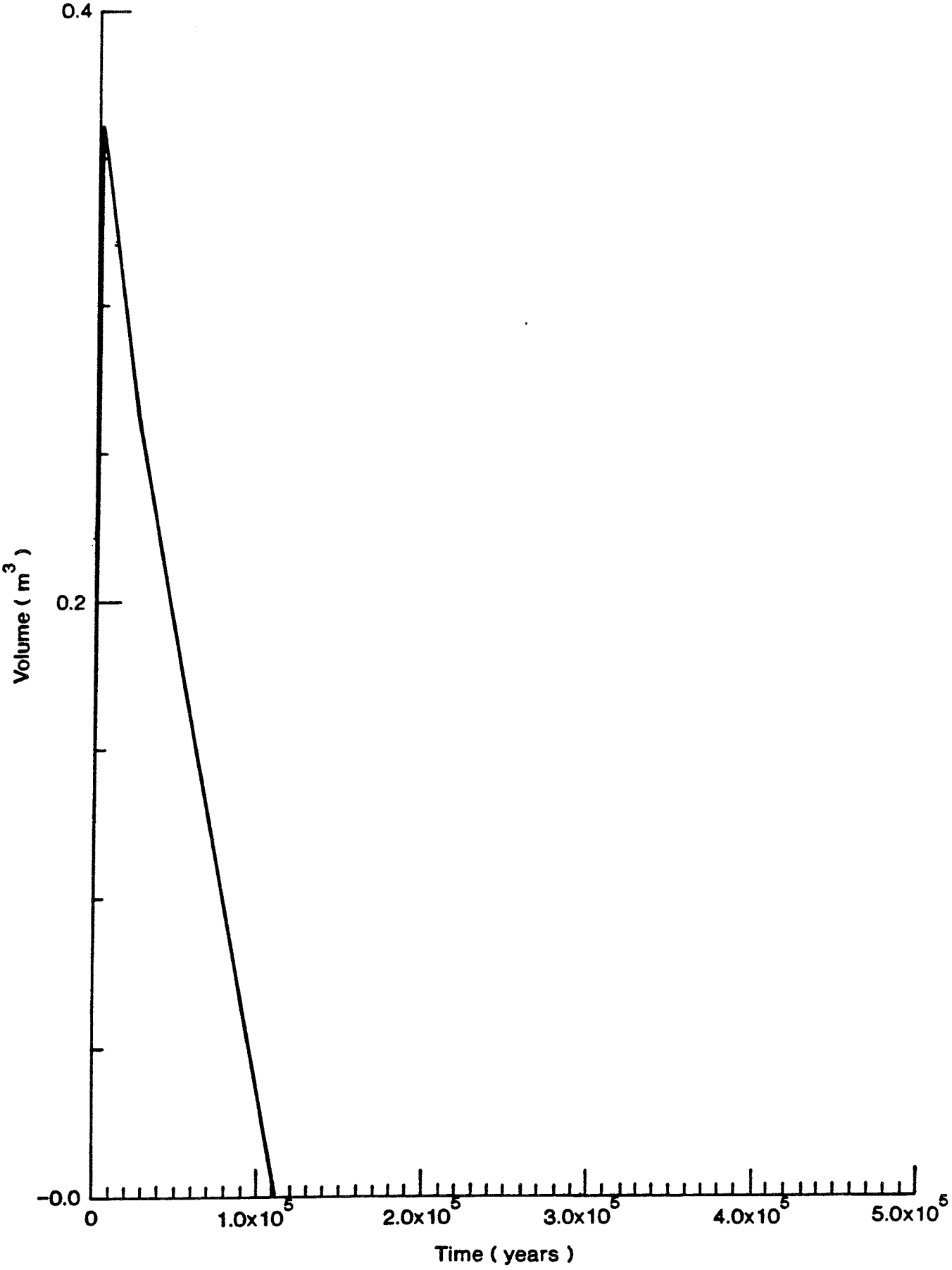

Figure 25. Predicted volume of water in inner canister for base case parameters and crack in outer canister at top (Case 2)

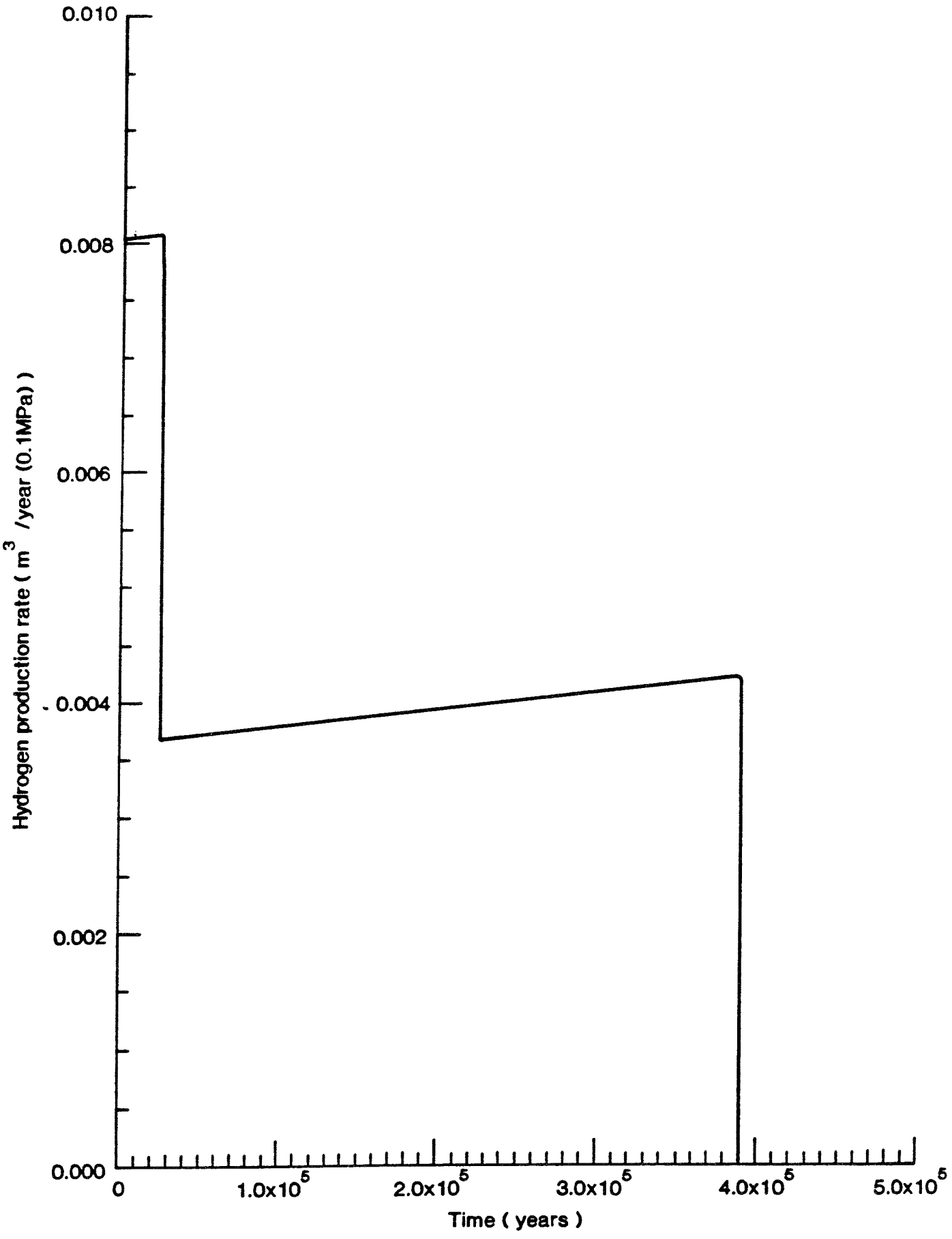

Figure 26. Predicted hydrogen production from canister for base case parameters and crack in outer canister at top (Case 2)

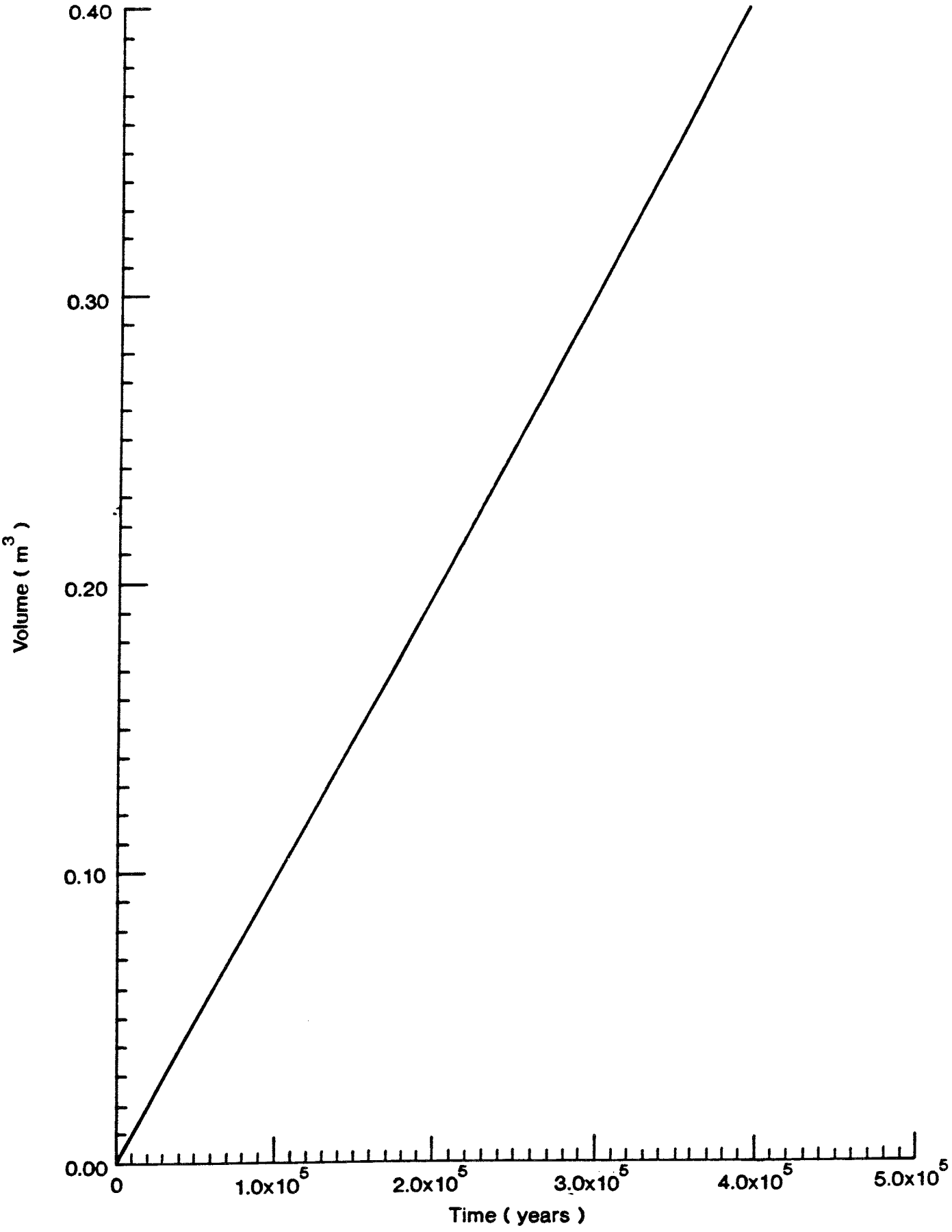

Figure 27. Predicted volume of magnetite in inner canister for base case parameters and crack in outer canister at top (Case 2)

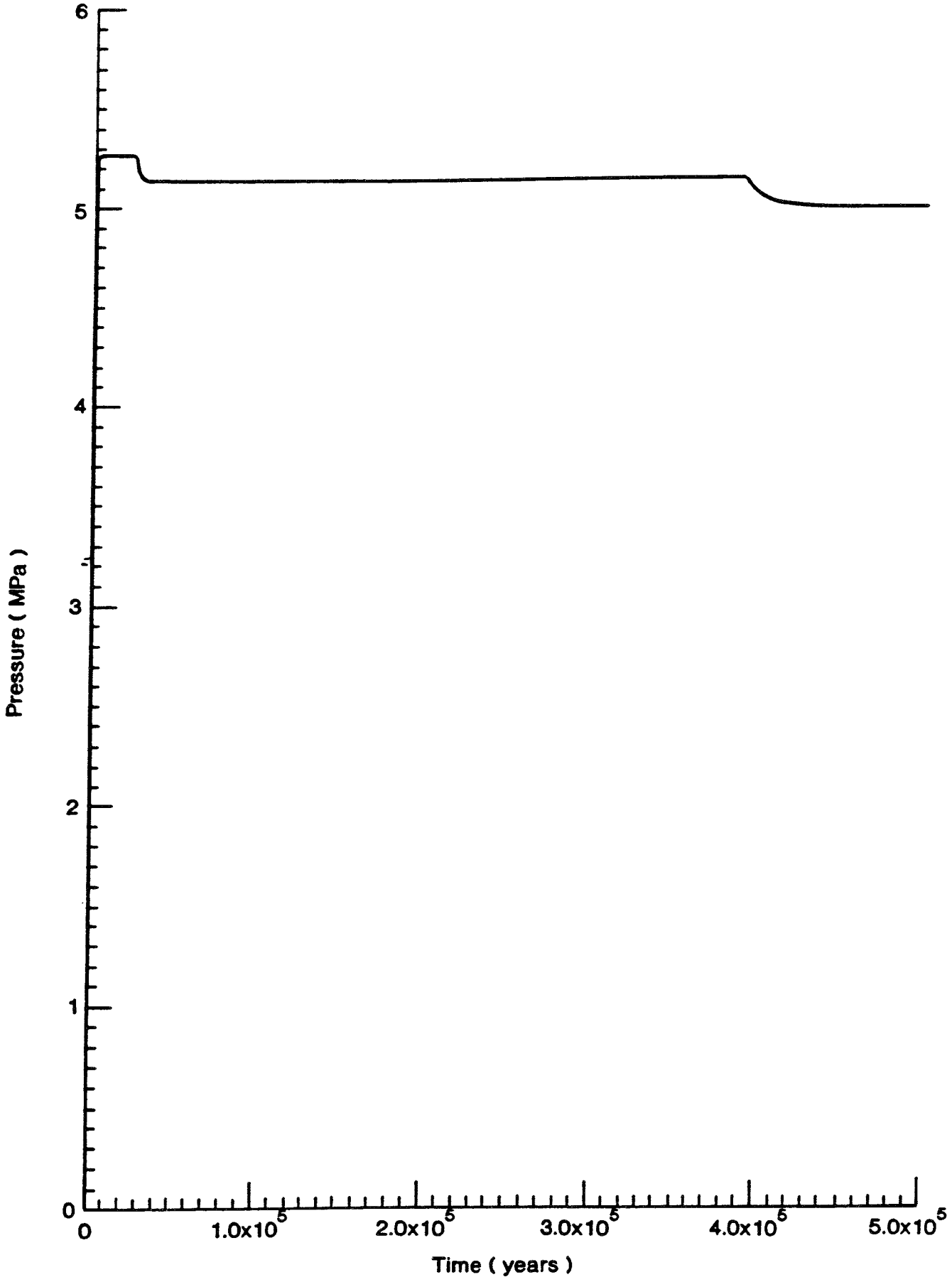

Figure 28. Predicted hydrogen gas pressure for base case parameters and crack in outer canister at top (Case 2)

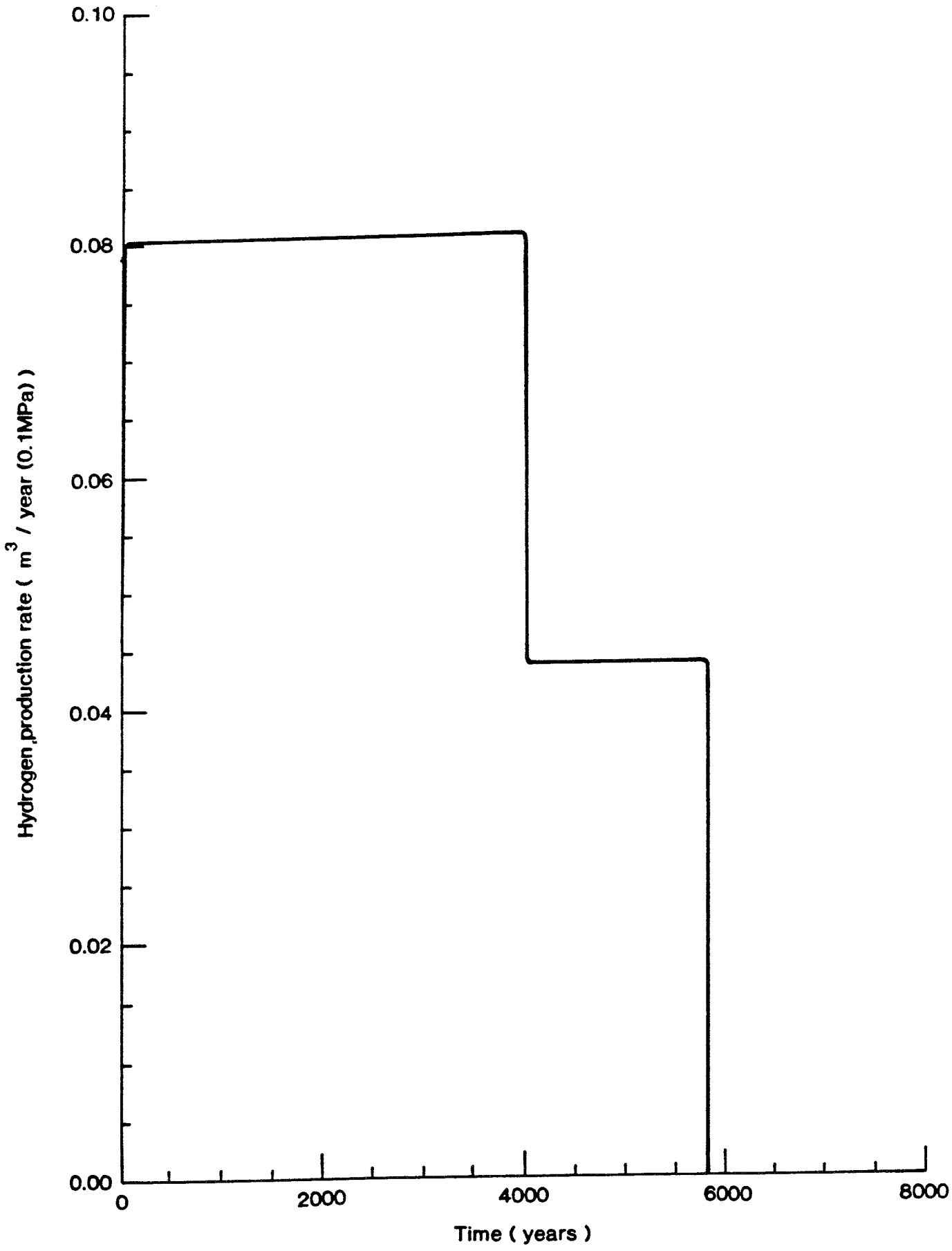

Figure 29. Sensitivity to corrosion rate. Predicted hydrogen production rate with corrosion current increased to 1 μm/yr and crack in outer canister at base (Case

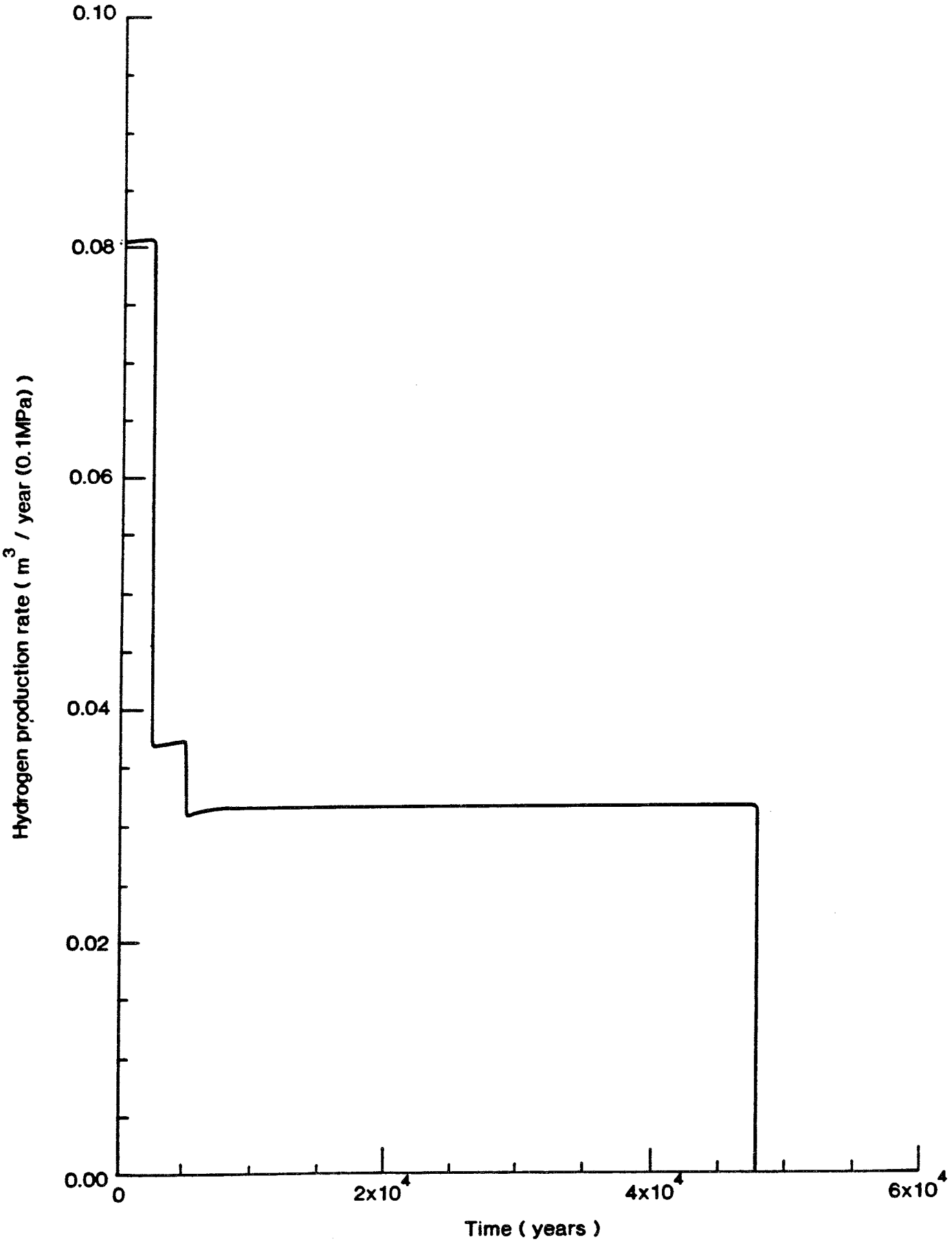

Figure 30. Sensitivity to corrosion rate. Predicted hydrogen production rate with corrosion current increased to 1 μm/yr and crack in outer canister at top (Case 2

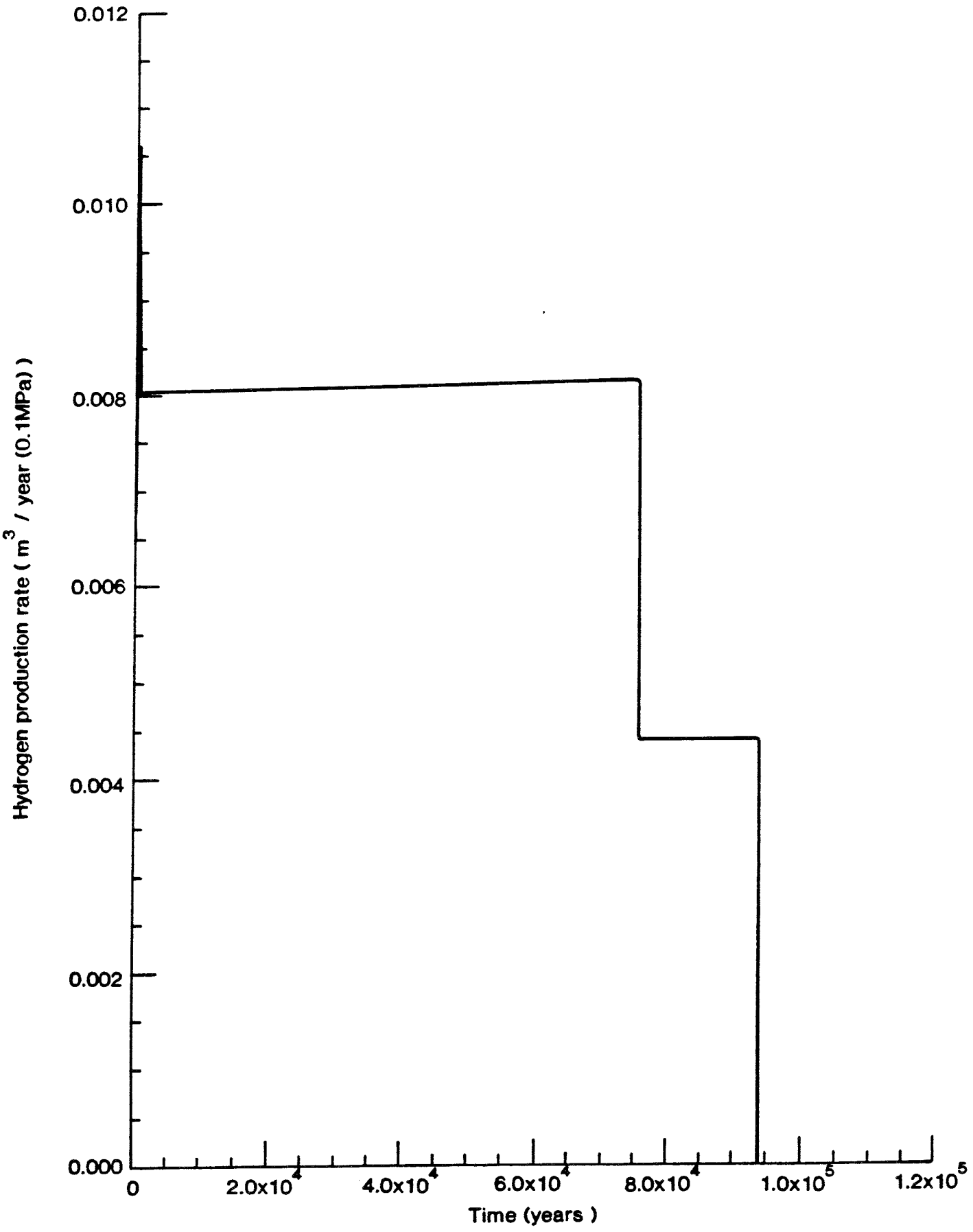

Figure 31. Sensitivity to galvanic contact. Predicted hydrogen production rate for crack in outer canister at base (Case 1)

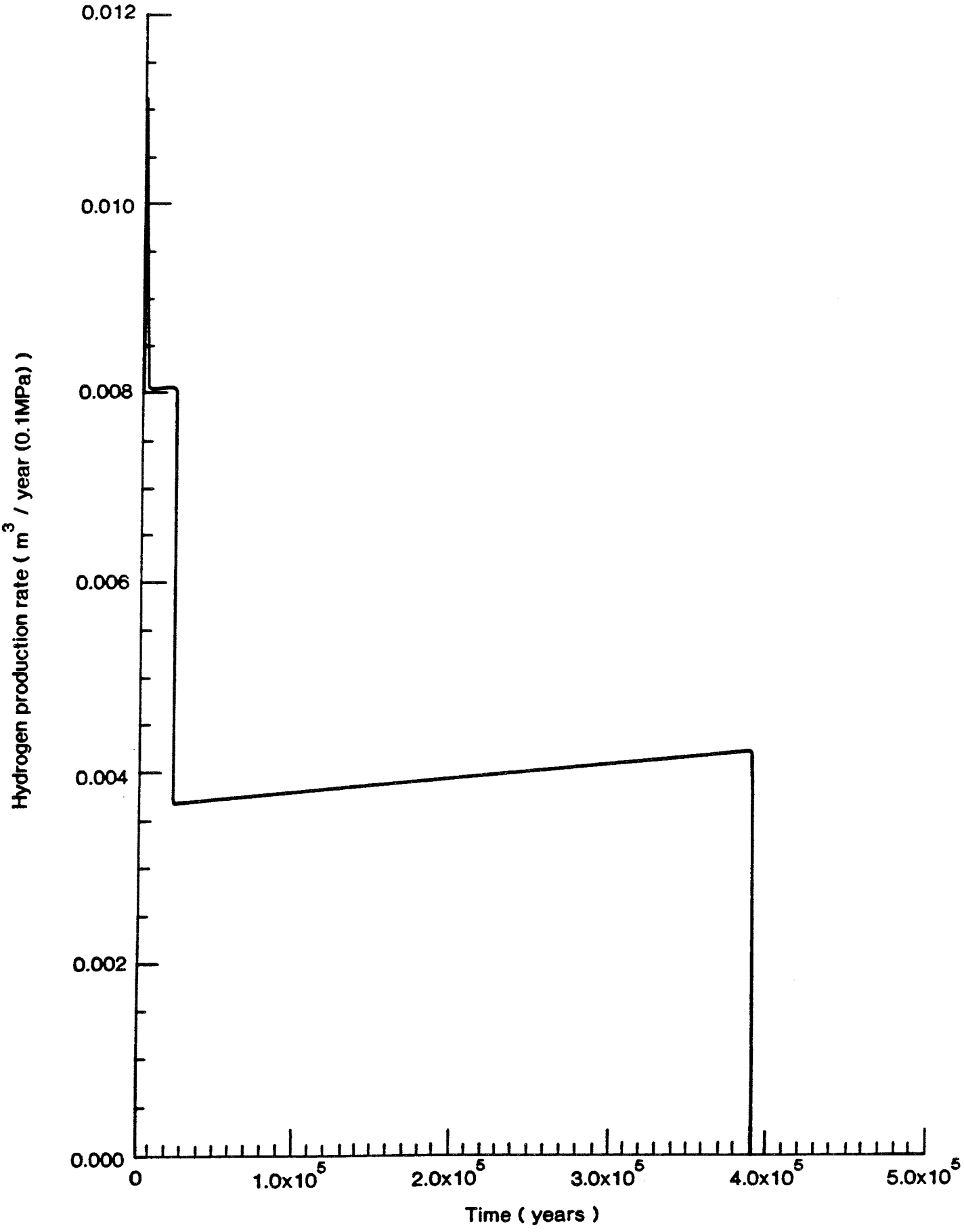

Figure 32. Sensitivity to galvanic contact. Predicted hydrogen production rate for crack in outer canister at top (Case 2)

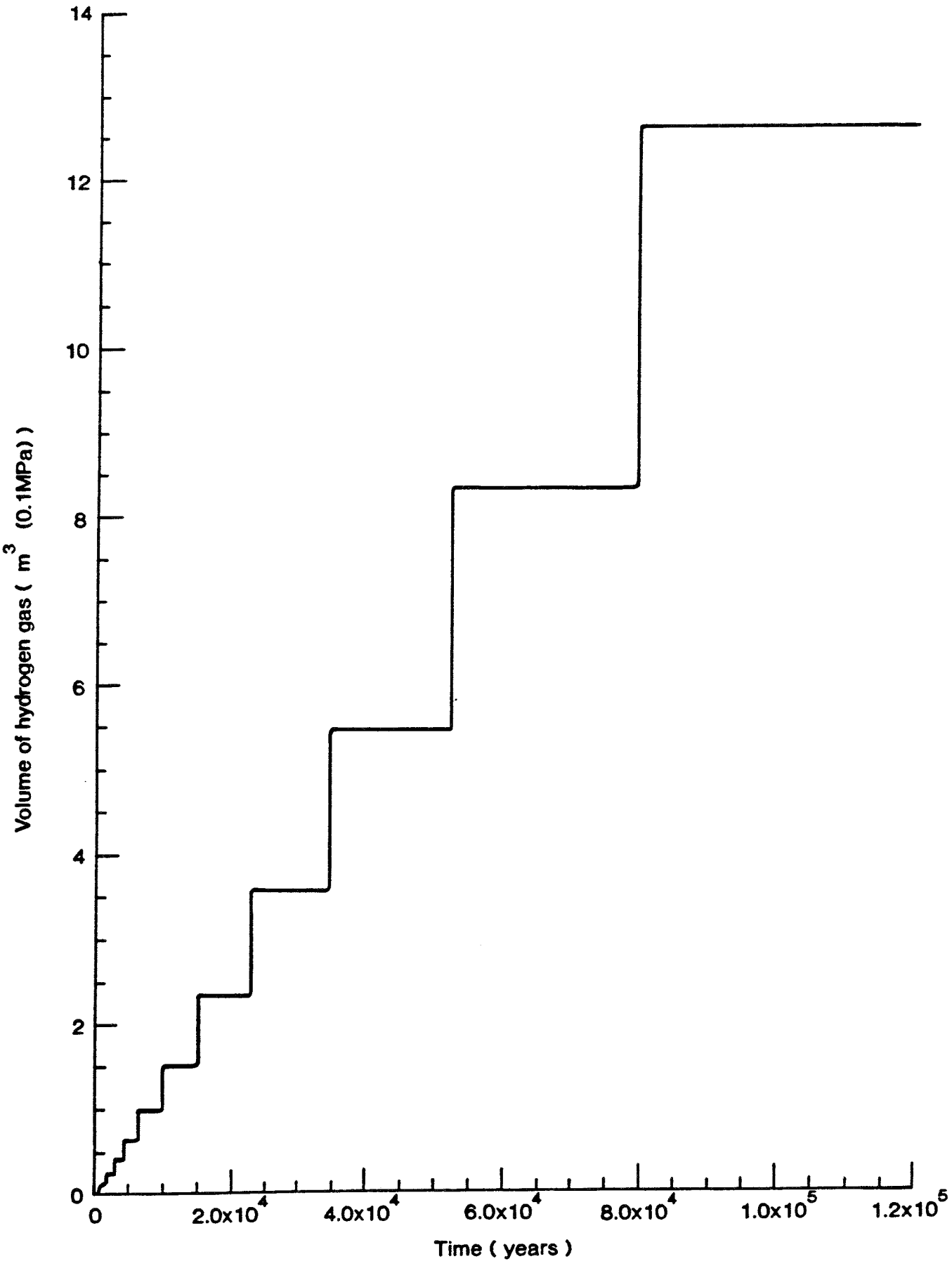

Figure 33. Sensitivity to hydrogen gas release . Predicted volume of hydrogen gas external to canister for crack in outer canister at base (Case 1)

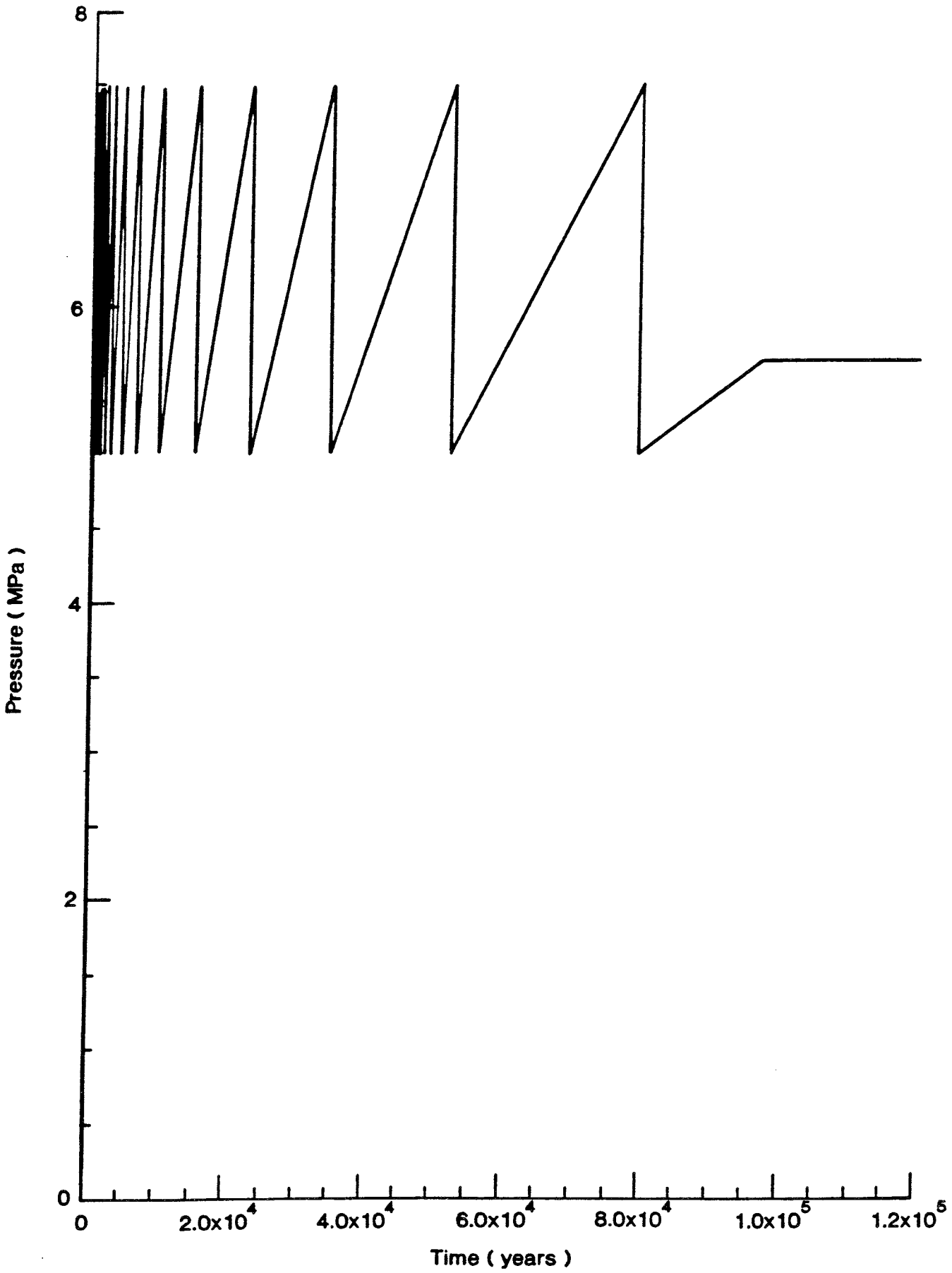

Figure 34. Sensitivity to hydrogen gas release. Predicted pressure of hydrogen gas in the canister for crack in outer canister at base (Case 1)

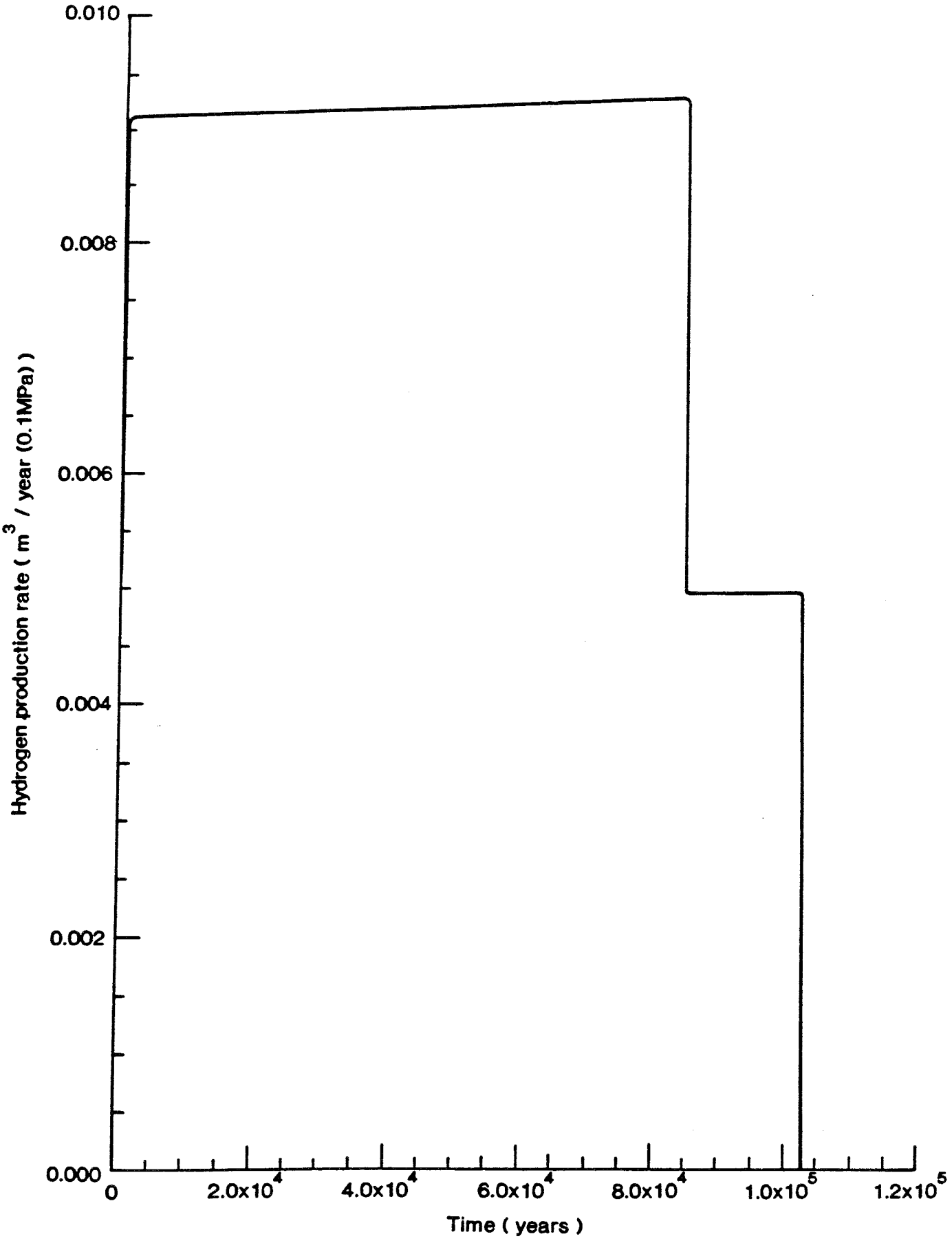

Figure 35. Sensitivity to canister dimensions. Predicted hydrogen production rate for SKB canister dimensions with crack in outer canister at base (Case 1)

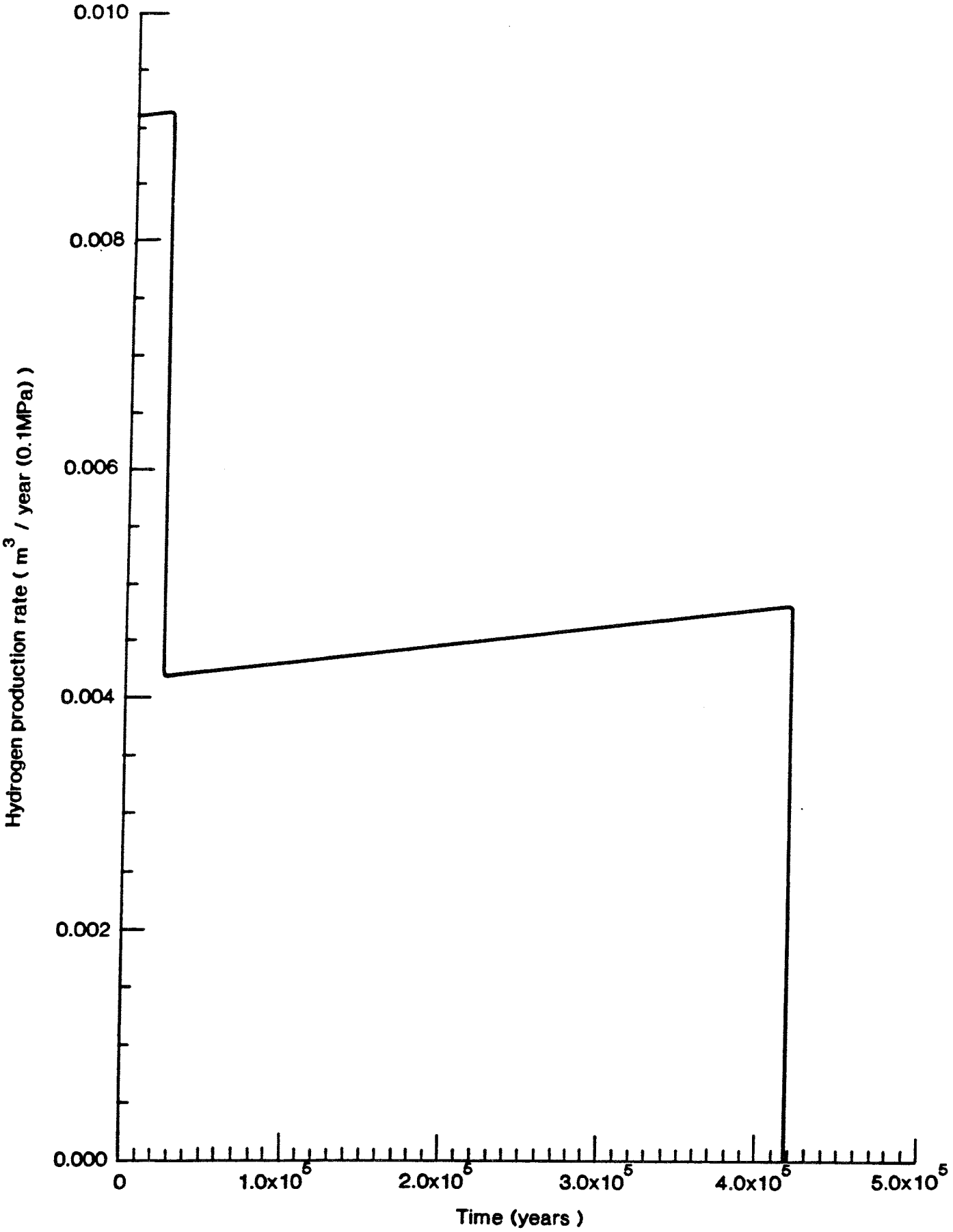

Figure 36. Sensitivity to canister dimensions. Predicted hydrogen production rate for SKB canister dimensions with crack in outer canister at top (Case 2)

List of SKB reports

Annual Reports

1977-78
TR 121
KBS Technical Reports 1 – 120
Summaries
Stockholm, May 1979

1979
TR 79-28
The KBS Annual Report 1979
KBS Technical Reports 79-01 – 79-27
Summaries
Stockholm, March 1980

1980
TR 80-26
The KBS Annual Report 1980
KBS Technical Reports 80-01 – 80-25
Summaries
Stockholm, March 1981

1981
TR 81-17
The KBS Annual Report 1981
KBS Technical Reports 81-01 – 81-16
Summaries
Stockholm, April 1982

1982
TR 82-28
The KBS Annual Report 1982
KBS Technical Reports 82-01 – 82-27
Summaries
Stockholm, July 1983

1983
TR 83-77
The KBS Annual Report 1983
KBS Technical Reports 83-01 – 83-76
Summaries
Stockholm, June 1984

1984
TR 85-01
Annual Research and Development Report 1984
Including Summaries of Technical Reports Issued during 1984. (Technical Reports 84-01 – 84-19)
Stockholm, June 1985

1985
TR 85-20
Annual Research and Development Report 1985
Including Summaries of Technical Reports Issued during 1985. (Technical Reports 85-01 – 85-19)
Stockholm, May 1986

1986
TR 86-31
SKB Annual Report 1986
Including Summaries of Technical Reports Issued during 1986
Stockholm, May 1987

1987
TR 87-33
SKB Annual Report 1987
Including Summaries of Technical Reports Issued during 1987
Stockholm, May 1988

1988
TR 88-32
SKB Annual Report 1988
Including Summaries of Technical Reports Issued during 1988
Stockholm, May 1989

1989
TR 89-40
SKB Annual Report 1989
Including Summaries of Technical Reports Issued during 1989
Stockholm, May 1990

1990
TR 90-46
SKB Annual Report 1990
Including Summaries of Technical Reports Issued during 1990
Stockholm, May 1991

1991
TR 91-64
SKB Annual Report 1991
Including Summaries of Technical Reports Issued during 1991
Stockholm, April 1992

1992
TR 92-46
SKB Annual Report 1992
Including Summaries of Technical Reports Issued during 1992
Stockholm, May 1993

Technical Reports
List of SKB Technical Reports 1994

TR 94-01
Anaerobic oxidation of carbon steel in granitic groundwaters: A review of the relevant literature
N Platts, D J Blackwood, C C Naish
AEA Technology, UK
February 1994

TR 94-02
Time evolution of dissolved oxygen and redox conditions in a HLW repository
Paul Wersin, Kastriot Spahiu, Jordi Bruno
MBT Technología Ambiental, Cerdanyola, Spain
February 1994

TR 94-03
Reassessment of seismic reflection data from the Finnsjön study site and prospectives for future surveys
Calin Cosma[1], Christopher Juhlin[2], Olle Olsson[3]
[1] Vibrometric Oy, Helsinki, Finland
[2] Section for Solid Earth Physics, Department of Geophysics, Uppsala University, Sweden
[3] Conterra AB, Uppsala, Sweden
February 1994

TR 94-04
Final report of the AECL/SKB Cigar Lake Analog Study
Jan Cramer (ed.)[1], John Smellie (ed.)[2]
[1] AECL, Canada
[2] Conterra AB, Uppsala, Sweden
May 1994

TR 94-05
Tectonic regimes in the Baltic Shield during the last 1200 Ma - A review
Sven Åke Larsson[1,2], Eva-Lena Tullborg[2]
[1] Department of Geology, Chalmers University of Technology/Göteborg University
[2] Terralogica AB
November 1993

TR 94-06
First workshop on design and construction of deep repositories - Theme: Excavation through water-conducting major fracture zones Såstaholm Sweden, March 30-31 1993
Göran Bäckblom (ed.), Christer Svemar (ed.)
Swedish Nuclear Fuel & Waste Management Co, SKB
January 1994

TR 94-07
INTRAVAL Working Group 2 summary report on Phase 2 analysis of the Finnsjön test case
Peter Andersson (ed.)[1], Anders Winberg (ed.)[2]
[1] GEOSIGMA, Uppsala, Sweden
[2] Conterra, Göteborg, Sweden
January 1994

TR 94-08
The structure of conceptual models with application to the Äspö HRL Project
Olle Olsson[1], Göran Bäckblom[2], Gunnar Gustafson[3], Ingvar Rhén[4], Roy Stanfors[5], Peter Wikberg[2]
1 Conterra AB
2 SKB
3 CTH
4 VBB/VIAK
5 RS Consulting
May 1994

TR 94-09
Tectonic framework of the Hanö Bay area, southern Baltic Sea
Kjell O Wannäs, Tom Flodén
Institutionen för geologi och geokemi, Stockholms universitet
June 1994

TR 94-10
Project Caesium–An ion exchange model for the prediction of distribution coefficients of caesium in bentonite
Hans Wanner[1], Yngve Albinsson[2], Erich Wieland[1]
[1] MBT Umwelttechnik AG, Zürich, Switzerland
[2] Chalmers University of Technology, Gothenburg, Sweden
June 1994

TR 94-11
Äspö Hard Rock Laboratory Annual Report 1993
SKB
June 1994